

## The Gemini NICI Planet-Finding Campaign: The Frequency of Giant Planets around Young B and A Stars

Eric L. Nielsen,<sup>1</sup> Michael C. Liu,<sup>1</sup> Zahed Wahhaj,<sup>2</sup> Beth A. Biller,<sup>3</sup> Thomas L. Hayward,<sup>4</sup> Laird M. Close,<sup>5</sup> Jared R. Males,<sup>6</sup> Andrew J. Skemer,<sup>7</sup> Mark Chun,<sup>1</sup> Christ Ftaclas,<sup>1</sup> Silvia H. P. Alencar,<sup>6</sup> Pawel Artymowicz,<sup>7</sup> Alan Boss,<sup>8</sup> Fraser Clarke,<sup>9</sup> Elisabete de Gouveia Dal Pino,<sup>10</sup> Jane Gregorio-Hetem,<sup>10</sup> Markus Hartung,<sup>4</sup> Shigeru Ida,<sup>11</sup> Marc Kuchner,<sup>12</sup> Douglas N. C. Lin,<sup>13</sup> I. Neill Reid,<sup>14</sup> Evgenya L. Shkolnik,<sup>15</sup> Matthias Tecza,<sup>9</sup> Nirranjan Thatte,<sup>9</sup> Douglas W. Toomey<sup>16</sup>

### ABSTRACT

We have carried out high contrast imaging of 70 young, nearby B and A stars to search for brown dwarf and planetary companions as part of the Gemini NICI Planet-Finding Campaign. Our survey represents the largest, deepest survey for planets around high-mass stars ( $\approx 1.5\text{--}2.5 M_{\odot}$ ) conducted to date and includes the planet hosts  $\beta$  Pic and Fomalhaut. We obtained follow-up astrometry of all candidate companions within 400 AU projected separation for stars in uncrowded fields and identified new low-mass

---

<sup>1</sup>Institute for Astronomy, University of Hawaii, 2680 Woodlawn Drive, Honolulu HI 96822, USA

<sup>2</sup>European Southern Observatory, Alonso de Córdova 3107, Vitacura, Santiago, Chile

<sup>3</sup>Max-Planck-Institut für Astronomie, Königstuhl 17, 69117 Heidelberg, Germany

<sup>4</sup>Gemini Observatory, Southern Operations Center, c/o AURA, Casilla 603, La Serena, Chile

<sup>5</sup>Steward Observatory, University of Arizona, 933 North Cherry Avenue, Tucson, AZ 85721, USA

<sup>6</sup>Departamento de Física - ICEX - Universidade Federal de Minas Gerais, Av. Antonio Carlos, 6627, 30270-901, Belo Horizonte, MG, Brazil

<sup>7</sup>University of Toronto at Scarborough, 1265 Military Trail, Toronto, Ontario M1C 1A4, Canada

<sup>8</sup>Department of Terrestrial Magnetism, Carnegie Institution of Washington, 5241 Broad Branch Road, N.W., Washington, DC 20015, USA

<sup>9</sup>Department of Astronomy, University of Oxford, DWB, Keble Road, Oxford OX1 3RH, UK

<sup>10</sup>Universidade de Sao Paulo, IAG/USP, Departamento de Astronomia, Rua do Matao, 1226, 05508-900, Sao Paulo, SP, Brazil

<sup>11</sup>Tokyo Institute of Technology, 2-12-1 Ookayama, Meguro-ku, Tokyo 152-8550, Japan

<sup>12</sup>NASA Goddard Space Flight Center, Exoplanets and Stellar Astrophysics Laboratory, Greenbelt, MD, 20771, USA

<sup>13</sup>Department of Astronomy and Astrophysics, University of California, Santa Cruz, CA, USA

<sup>14</sup>Space Telescope Science Institute, 3700 San Martin Drive, Baltimore, MD 21218, USA

<sup>15</sup>Lowell Observatory, 1400 West Mars Road, Flagstaff, AZ 86001, USA

<sup>16</sup>Mauna Kea Infrared, LLC, 21 Pookela St., Hilo, HI 96720, USA

companions to HD 1160 and HIP 79797. We have found that the previously known young brown dwarf companion to HIP 79797 is itself a tight (3 AU) binary, composed of brown dwarfs with masses  $58_{-20}^{+21} M_{Jup}$  and  $55_{-19}^{+20} M_{Jup}$ , making this system one of the rare substellar binaries in orbit around a star. Considering the contrast limits of our NICI data and the fact that we did not detect any planets, we use high-fidelity Monte Carlo simulations to show that fewer than 20% of  $2 M_{\odot}$  stars can have giant planets greater than  $4 M_{Jup}$  between 59 and 460 AU at 95% confidence, and fewer than 10% of these stars can have a planet more massive than  $10 M_{Jup}$  between 38 and 650 AU. Overall, we find that large-separation giant planets are not common around B and A stars: fewer than 10% of B and A stars can have an analog to the HR 8799 b ( $7 M_{Jup}$ , 68 AU) planet at 95% confidence. We also describe a new Bayesian technique for determining the ages of field B and A stars from photometry and theoretical isochrones. Our method produces more plausible ages for high-mass stars than previous age-dating techniques, which tend to underestimate stellar ages and their uncertainties.

*Subject headings:* brown dwarfs — instrumentation: adaptive optics — planetary systems — planets and satellites: detection — stars: individual (HIP 79797)

## 1. Introduction

In the last two decades, over 800 planets have been detected outside of our solar system, the vast majority found by the transit (e.g. Borucki et al. 2011) or radial velocity (RV, e.g. Marcy et al. 2008) methods. These planets tend to be close to their parent star,  $\lesssim 1$  AU for transits and  $\lesssim 5$  AU for RV, and obtaining spectra is difficult for transiting planets and impossible for non-transiting RV planets. Direct imaging of self-luminous planets, by contrast, is most sensitive to large-separation ( $\gtrsim 10$  AU) planets which can be followed up with spectroscopy. Thus far, however, only a handful of planetary mass companions have been detected by direct imaging (e.g. Kalas et al. 2008; Marois et al. 2008, 2010; Lagrange et al. 2010), despite several concerted efforts at large telescopes.

One unexpected result from these initial direct imaging planet detections is the apparent prevalence of planets around high-mass stars: Fomalhaut (1 planet, Kalas et al. 2008), HR 8799 (4 planets, Marois et al. 2008, 2010), and  $\beta$  Pic (1 planet, Lagrange et al. 2010) are all A stars. These stars also all harbor debris disks, though as yet there is no compelling evidence that debris disk hosts are more likely to harbor giant planets (Wahhaj et al. 2013b). Bryden et al. (2009) found no significant correlation between presence of RV planets (mainly giant planets) and debris disks. However, studies of hosts of lower-mass RV planets (less than the mass of Saturn) by Wyatt et al. (2012) and hosts of Kepler planet candidates by Lawler & Gladman (2012) suggest that stars hosting lower-mass planets are more likely to also host debris disks. High-mass stars are intrinsically brighter than later-type stars, so a faint planet is much harder to directly detect

around an A star than an M star. The planet detections to date suggest either that giant planets are more common around A stars, as is the case for close-in RV planets (e.g. Johnson et al. 2010), that wide-separation planets are more common around high mass stars, or both.

The planets around  $\beta$  Pic and Fomalhaut were found as part of targeted studies of these stars specifically, motivated primarily by their bright debris disks, making it difficult to place statistical constraints on exoplanet populations around high mass stars from these two detections. The four HR 8799 planets were found as part of the International Deep Planet Survey (IDPS), and an analysis of the frequency of giant planets around A stars was presented recently by Vigan et al. (2012). Based on their sample of 38 A stars and 4 early-F stars, they find that between 6 and 19% of A stars have a giant planet between 5 and 320 AU at 68% confidence. However, these statistical constraints are based on optimistically young ages for many stars in their sample (see Section 3).

The Gemini NICI Planet-Finding Campaign is a 4-year program to detect extrasolar giant planets, measure their frequency, determine how that frequency depends on stellar mass, and study the spectral energy distributions of young exoplanets (Liu et al. 2010). The Campaign has thus far detected three brown dwarf companions around the young stars PZ Tel (Biller et al. 2010), CD–35 2722 (Wahhaj et al. 2011), and HD 1160 (Nielsen et al. 2012) but no planetary-mass companions ( $\lesssim 13 M_{Jup}$ ). Here we present an analysis of the frequency of giant planets around high mass stars based on the 70 young B and A stars observed by the Campaign. In companion papers we present an analysis of the planet frequency around stars in young moving groups (Biller et al. 2013) and debris disk hosts (Wahhaj et al. 2013b).

## 2. Target Selection

Prior to the start of the Gemini NICI Planet-Finding Campaign in December 2008, we assembled a list of 1353 potential target stars. Among the many considerations used to construct this input list were the radial velocity results of Johnson et al. (2007), which pointed to a correlation between the frequency of short-period giant planets and stellar host mass. We sought to determine if this trend continues to longer-period planets by selecting target stars from a range of masses, so as to directly measure planet frequency as a function of spectral type. For the B and A stars in the sample, we selected stars from three sources: members of young moving groups, stars with debris disks, and other B and A stars from the *Hipparcos* catalog. We describe target selection for the first two categories in more detail in Biller et al. (2013) and Wahhaj et al. (2013b), but in general we selected all B and A stars in nearby young moving groups as well as all of those that host debris disks for our input target list.

In addition, we used two other methods to flag young B and A stars from the *Hipparcos* catalog: main-sequence lifetime and position on the color-magnitude diagram. (1) We chose stars with an early spectral type (earlier than  $\sim A5$ ) which have main-sequence lifetimes of only hundreds of Myrs, providing a constraint on their ages even in the absence of any other age information.

(2) We added stars that have relatively faint absolute magnitudes on the color-magnitude diagram, which suggested they were potentially young. (We discuss this technique in more detail in the next section.) For the *Hipparcos*-selected stars, we chose stars within 75 pc with B or A spectral types and removed any giants. There was no distance cut placed on debris disk hosts or moving group targets in our sample, which can be found up to 172 pc from the Sun, though most stars are within 100 pc. Stars with close binaries and those not observable from Gemini-South ( $\delta > +20^\circ$ ) were also removed from the sample. Two stars, the debris disk host HD 85672 and the nearby HIP 54872, were also kept on the target list despite having declinations between  $+20^\circ$  and  $+30^\circ$ .

To produce an observing list from this input catalog, we used a variation of the Monte Carlo simulations described in Section 5.5 to rank targets by the likelihood of imaging a young hot-start planet around them with NICI, given their age, distance, spectral type, and apparent magnitude (see Liu et al. 2010). An ensemble of simulated planets was placed around each target star, following an extrapolation of the distribution of giant planets found by the RV method, and these were then compared to the expected NICI contrast curve. Stars around which NICI could detect a larger fraction of these simulated planets were given higher priority compared to stars with a lower fraction of detectable planets. This approach maximizes the probability of detecting a planet, and also produces a sample that offers the most stringent statistical constraints on the underlying planet population properties. Our final observing list contains 4 B and A stars that were added as members of moving groups, 24 that were added as debris disk hosts, and a further 4 stars that belong to both categories. 15 stars were added to the observing list with spectral types earlier than A5, and 33 were added that had faint  $V$  magnitudes on the color-magnitude diagram. In this way we obtained our final observing list of 70 B and A stars for the Gemini NICI Planet-Finding Campaign.

### 3. Age Determination for Field B and A Stars

#### 3.1. Previous Methods

Because planets and brown dwarfs cool and become fainter throughout their lifetime, determining the age of a substellar companion’s host star is essential to determining the physical properties of the companion. Therefore, direct imaging surveys must be able to reliably age-date their target stars to understand both detected companions and overall survey sensitivities. Age-dating methods are typically most successful for solar-type (FGK) stars, where a variety of techniques are available, including lithium absorption, calcium emission, and gyrochronology (e.g. Mamajek 2009). For stars with higher mass the most robust method is to identify stars in young moving groups which share a common age and determine a consistent age for all the stars in the group (e.g. Zuckerman & Song 2004). Alternatively, if an A star is in a binary system with a solar-type star, age-dating the solar-type secondary can yield the age of the higher-mass primary. In cases where a high-mass star is single and does not belong to a kinematic group, however, we require an

age-dating method that only utilizes the properties of the star itself.

Previous work has typically addressed the need to age-date B and A stars by turning to the color-magnitude diagram (CMD). In order to estimate the mass of the brown dwarf companion HR 7329 B, Jura et al. (1995) and Lowrance et al. (2000) placed its primary star HR 7329 A on an  $[M_V, B - V]$  color-magnitude diagram, along with A stars from nearby clusters and in the field (see Figure 3 of Lowrance et al. 2000). They noted that young ( $\lesssim 100$  Myr) clusters such as the Pleiades, Alpha Per, and IC 2391 have A stars near the bottom of this color-magnitude diagram (i.e., at fainter absolute  $V$  magnitudes) compared to brighter A stars of the older ( $\sim 600$  Myr) Hyades and Praesepe clusters. They also noted that the famous young A stars  $\beta$  Pic, HD 141569, and HR 4796 all lie at the very bottom of this diagram along with HR 7329 A, thus arguing for a young ( $\lesssim 100$  Myr) age for HR 7329 system. Moór et al. (2006) and Rhee et al. (2007) expanded this method to other high mass stars with debris disks, noting that many of these stars also lay near the bottom of the color-magnitude diagram. Vigan et al. (2012) use a similar approach by defining the dereddened single-star sequence of high mass stars in the Pleiades on the same  $[M_V, B - V]$  color-magnitude diagram and then assigning the age of the Pleiades (125 Myr, Stauffer et al. 1998) to stars with similar color-magnitude positions as the Pleiades A stars. However, this common approach to flagging young A stars is likely too optimistic in many cases, due to two effects: (1) the degeneracy between the effects of age and metallicity, and (2) the increase of main-sequence lifetime with decreasing stellar mass.

In order to demonstrate the limitations of this approach, we construct a volume-limited sample of Hipparcos stars within 100 pc and with parallax uncertainties below 5%, spectral types earlier than F0, luminosity class IV or V,  $-0.2 < B - V < 0.4$ , and purged of known binaries, resulting in 776 stars. All stellar data are taken from the extended Hipparcos compilation of Anderson & Francis (2012). Figure 1 illustrates the difficulty in using color-magnitude diagram position as a youth indicator for this volume-limited sample of B and A stars. The Siess et al. (2000) isochrones show that the “low CMD” stars (defined here as lying below the young cluster fit of Lowrance et al. 2000, with all other B and A stars referred to as “high CMD” stars) can be equally explained as young solar-metallicity stars or older sub-solar metallicity stars. Therefore a low position on the color-magnitude diagram is not a unique indicator of youth, but rather suggests either youth or low metallicity.

The Siess et al. (2000) isochrones themselves provide a good fit to B and A stars, as we demonstrate in Figure 2 where we plot the Siess et al. (2000) 120 Myr isochrones for sub-solar, solar, and super-solar metallicities against Pleiades stars from Stauffer et al. (2007), finding a good match between the solar track and the Pleiades single-star sequence. A more detailed analysis of Pleiades stars and main-sequence binaries by Bell et al. (2012) supports the validity of these models, showing that the Siess et al. (2000) isochrones are a good fit to both main-sequence and pre-main sequence stars.

Metallicities between 0 and  $-0.3$  dex are not particularly rare for B and A stars as illustrated

by Figure 3, which shows B and A stars from the Hipparcos sample with literature metallicity measurements (again from the Anderson & Francis 2012 compilation), divided into “low CMD” and “high CMD” samples. No appreciable difference is seen between the two samples of stars, nor between these B and A stars and the Casagrande et al. (2011) metallicity measurements of young (<1 Gyr) F and G dwarfs. The lack of a trend between color-magnitude diagram position and metallicity means that while “low CMD” stars are not uniformly young, neither are they uniformly low metallicity. They instead seem to have a similar metallicity distribution to the solar neighborhood. Therefore there are young solar or supersolar metallicity stars in the sample of “low CMD” stars, mixed in with lower metallicity, older stars.

In addition to metallicity, another important consideration is that most of a main-sequence star’s evolution across the color-magnitude diagram occurs during the final two-thirds of a star’s main-sequence lifetime (e.g. Soderblom 2010). The Siess et al. (2000) models indicate that this trend holds for stellar masses between 1.5 and 4.5  $M_{\odot}$  (appropriate to our NICI sample), where stars show little change in  $B - V$  or  $V$  from the ZAMS to  $\sim 1/3$  of the main sequence lifetime, and then a brightening in  $V$  over the remainder of the star’s main sequence lifetime. This effect can be seen in Figure 1, where at  $B - V > 0.1$ , the 30 Myr and 100 Myr isochrones for a given metallicity overlap, while all isochrones between 30 and 300 Myr overlap for  $B - V > 0.2$ . Even if we were to (incorrectly) assume that all stars have solar metallicity, while all Pleiades-age stars would lie low on the color-magnitude diagram, not all “low CMD” stars would be Pleiades-age. In this uniform solar metallicity scenario, at best we would be constraining the ages of stars to be in the first third of their main-sequence lifetime, which is true for all Pleiades A stars. But the longer lifetimes for later-type A stars would make the default assigned age of 125 Myr increasingly inaccurate. For A9V stars, with an expected lifetime of 1.5 Gyr, “low CMD” stars would have ages up to  $\sim 500$  Myr, a factor of 4 older than the age of the Pleiades. Figure 4 demonstrates this by plotting the fraction of “low CMD” stars as a function of  $B - V$  from our Hipparcos volume-limited sample. For comparison, we also plot the expected fraction of stars younger than the Pleiades, which is the quotient of 125 Myr and the main-sequence lifetime for solar-metallicity stars from Siess et al. (2000), assuming a constant star formation rate in the solar neighborhood. While the fraction of “Pleiades-like” stars derived from the color-magnitude diagram appears to be relatively constant for all values of  $B - V$ , the expected fraction of Pleiades-aged stars drops by a factor of 8 over this range. In other words, the “low CMD” stars are expected to have an increasingly large age spread at lower masses simply from stellar evolution. This effect is missed by the common procedure of assigning Pleiades ages to all “low CMD” stars.

### 3.2. A Bayesian Approach to Estimating Ages from Isochrones

For a given location on a color-magnitude diagram, there are multiple combinations of age, mass, and metallicity that can reproduce the color and magnitude of a given star. We turn to Bayesian inference in order to determine the relative likelihoods of these combinations and to

incorporate prior knowledge about the distributions of these stellar parameters. Such a technique has been previously used for solar-type stars by Takeda et al. (2007), who determined the ages of target stars for RV planet searches through a Bayesian analysis of their spectroscopically-derived properties ( $T_{eff}$ ,  $[Fe/H]$ , and  $\log(g)$ ) combined with their  $V$  magnitude.

To determine the ages for B and A stars using photometry, we begin with Bayes' theorem:

$$P(model|data) \propto P(data|model)P(model). \quad (1)$$

That is, the probability of a model given a set of data ( $P(model|data)$ ) is proportional to the product of the probability of the data given the model ( $P(data|model)$ ) and the probability of the model itself ( $P(model)$ ). From left to right, the three terms above are referred to as the posterior probability density function (PDF), the likelihood, and the prior.

Our model is the set of three stellar parameters, age ( $\tau$ ), mass ( $M_*$ ), and metallicity ( $[Fe/H]$ ), and our data are the measured absolute magnitude  $M(V)$  and  $B - V$  color for a given star. At any combination of age, mass, and metallicity Siess et al. (2000) predict the  $M(V)$  and  $B - V$ . It is then straightforward to compute the chi-squared statistic for this model:

$$\chi^2(\tau, M_*, [Fe/H]) = \sum \frac{(O - E)^2}{\sigma^2} = \frac{((B - V)_O - (B - V)_E)^2}{\sigma_{B-V}^2} + \frac{(M(V)_O - M(V)_E)^2}{\sigma_{M(V)}^2} \quad (2)$$

where  $(B - V)_O$  and  $M(V)_O$  are the observed ( $O$ ) color and absolute magnitude, with observational errors  $\sigma_{B-V}$  and  $\sigma_{M(V)}$ , respectively.  $(B - V)_E$  and  $M(V)_E$  are the expected ( $E$ ) color and magnitude, predicted by Siess et al. (2000) for a given age, mass, and metallicity. The relative likelihood of a specific combination of three stellar parameters is then

$$P(data|model) = P(B - V, M(V)|\tau, M_*, [Fe/H]) \propto e^{-\frac{1}{2}\chi^2(\tau, M_*, [Fe/H])} \quad (3)$$

This formulation assumes Gaussian statistics, which is a reasonable assumption given that our errors are from photometry and parallax measurements.

Siess et al. (2000) provide pre-main sequence and main-sequence evolutionary tracks, which we interpolate to a regular 3-dimensional grid in age, mass, and metallicity. Age is logarithmically gridded between 1 Myr and 10 Gyr, with the predicted photometry becoming undefined when the star leaves the main sequence. Mass is uniformly gridded between 1 and 5  $M_\odot$ . Metallicity is uniformly gridded between  $-0.3 < [Fe/H] < +0.3$ , since a linear grid in  $[Fe/H]$  corresponds to a logarithmic grid in absolute metal abundance.

We adopt priors to incorporate knowledge of the solar neighborhood when deriving probability distributions of stellar parameters.

1. For metallicity, we turn to the Casagrande et al. (2011) metallicities for a magnitude-limited sample ( $V < 8.3$  mag) of 16000 F and G dwarfs in the solar neighborhood. In particular, we use their Figure 16 to provide a metallicity distribution for stars younger than 1 Gyr, an appropriate age range for field B and A stars. We model the Casagrande et al. (2011) metallicity histogram with a normal distribution with mean of  $-0.05$  and  $\sigma$  of 0.11 dex and use this as our metallicity prior. We note that the Casagrande et al. (2011) metallicity distribution of young F and G stars in the solar neighborhood is consistent with the Nieva & Przybilla (2012) metallicity results for 20 nearby ( $< 500$  pc) early-B stars ( $[\text{Fe}/\text{H}] = 0.0 \pm 0.1$  dex). This good match to the young F and G dwarf measurements occurs despite the fact that the lifetimes of early-B stars are over an order of magnitude younger than 1 Gyr. Further support for the near solar metallicity of young stars is given by Biazzo et al. (2012), who find  $[\text{Fe}/\text{H}] = 0.10 \pm 0.03$  dex for five solar-type stars in the AB Dor moving group (100 Myr). So all the evidence to date suggests that solar neighborhood B and A stars have a metallicity distribution similar to young F and G stars.
2. For our age prior, since the star formation rate is basically constant in the solar neighborhood over at least the last 2 Gyr (Cignoni et al. 2006), we adopt a prior that is uniform in linear age for B and A stars. Our gridding of the Siess et al. (2000) models is logarithmic in age, and so we weight each grid point such that equal linear age intervals have equal probability. The relative probability of age bin  $i$  is given by  $\delta\tau_i/T$ , where  $\delta\tau_i$  is the age range encompassed by the  $i$ -th bin, and  $T$  is the total age range for all bins. This prior has the effect of pushing the posterior PDF toward older ages, since older logarithmic age bins encompass a greater span of time than younger ones.
3. Finally, we apply a Salpeter IMF of the form  $dN/dM \propto M^{-2.35}$  (Salpeter 1955) as our mass prior. Each mass bin is weighted by this IMF, favoring lower masses over higher ones. We note that the effect of this prior is minimal, since each star has a narrow, well-defined mass posterior PDF. As a check, we computed the shift in the median of the mass and age posterior PDFs for all our target stars with and without the IMF prior. When the IMF prior is applied, the median shift is 0.2% toward lower masses and 1.4% to older ages. The standard deviation of the shift is 0.15% in mass and 1.4% in age.

Our final age probability distribution for each star is then given by marginalizing over all metallicities and masses. This is done after determining all likelihoods for each model (given by Equations 2 and 3), weighted by the metallicity and age priors (Equation 1). Figure 5 shows an example of our Bayesian age analysis for the A0V star HD 24966. Since the main-sequence lifetime for a  $2.1 M_{\odot}$  star is 600 Myr, a median age for HD 24966 of 128 Myr (and 68% confidence level between 51–227 Myr) suggests that this star is in the first third of its main-sequence lifetime.

Figure 6 shows the combined  $[\text{Fe}/\text{H}]$  posterior PDFs marginalized over age and mass from all 70 target stars compared to our adopted Casagrande et al. (2011) prior. The posterior and prior closely match each other for the “low CMD” stars, while there is a small 0.05 dex offset toward

higher metallicities for the “high CMD” stars. This is as expected, since “high CMD” stars are best fit by higher metallicity isochrones.

In addition to age, mass, and metallicity, we can also produce a posterior PDF of main-sequence lifetime for each star from the same likelihood and priors that produce posterior PDFs for age, mass and metallicity (though main-sequence lifetime is a function only of mass and metallicity and independent of age). We express the combined age PDFs for all stars in Figure 7 as a fraction of their main-sequence lifetime, using the lifetime PDF for each star. Despite allowing metallicity to vary (though following the Casagrande et al. 2011 prior), our Bayesian technique finds “low CMD” stars to be systematically younger than “high CMD” stars as expected.

In Figure 8, we display the same combined age PDF as a function of absolute age. The most common ages for our target stars are between 50 and 500 Myr, with low-probability tails extending below 10 Myr and above 1 Gyr. The median age, 68% confidence limit, and 95% confidence limit for each of our 70 target stars are given in Table 1. We also show the properties of our target stars in Figure 9. About a fifth (14 out of 70) of our stars have independent age measurements from moving group membership, as indicated in Table 1, which we adopt as the final ages for these stars. Also, we adopt the age of 5 Myr for HD 141569 from Weinberger et al. (2000), based on their study of its two M-star companions. These independent ages are often significantly younger than the ages derived by our Bayesian analysis, which at best can only place a star within the first third of its main sequence lifetime.

### 3.3. Comparison with Previous Ages

Stars with debris disks are generally well-studied and have literature age measurements that are widely cited (e.g. Moór et al. 2006, Rhee et al. 2007). Nevertheless, for most of the debris disk stars in our B and A star sample, we do not use these literature ages and instead use our Bayesian ages. Of the 28 stars in our sample with debris disks, 10 belong to well-known moving groups, and we adopt that moving group age for these stars. Also, we use the 5 Myr age for HD 141569 from Weinberger et al. (2000). Of the remaining 17 stars, 3 (HIP 85340,  $\gamma$  Oph, and Fomalhaut) have ages taken from isochrones, while 14 (HD 10939, HD 17848, HD 24966, HD 31295, HD 32297, HD 54341, HD 71155, HD 85672, HD 110411, HD 131835, HD 138965, HD 176638, HD 182681, and HD 196544) are flagged as young for their low position on the color-magnitude diagram. For these our Bayesian analysis provides more accurate representations of the ages than isochrones or color-magnitude diagram position alone, so we override the literature ages for these 17 stars with our Bayesian ages.

Figure 10 compares our ages to stars that we have in common with Su et al. (2006). For the ages derived by our Bayesian analysis, we find good agreement for stars which Su et al. (2006) determine to be older than 100 Myr. Stars that Su et al. (2006) find to be younger than 100 Myr show a systematic disagreement, with the median of our Bayesian age distribution significantly older than

the single age found by Su et al. (2006). This is as we would expect, since most movement across the color-magnitude diagram happens in the final two-thirds of a star’s main-sequence lifetime, so older stars can be age-dated more definitively while younger stars can be anywhere in the first third of their main-sequence lifetimes. Our Bayesian method takes this uncertainty into account, rather than assigning very young ages ( $\lesssim 100$  Myr) for “low CMD” stars. Also, stars that belong to a well-known moving group (as well as HD 141569) have adopted ages that are uniformly younger than the Bayesian distributions. This is not surprising, as nearby moving groups are significantly younger than the field population.

Finally, we consider the ages derived by Vigan et al. (2012) for their sample of young A stars. We apply our Bayesian analysis to their sample and compare the histogram of our derived ages to theirs in Figure 11. Out of the 39 stars from their sample, 11 belong to moving groups, and we adopt the same moving group ages for these stars. For the remaining 28 stars, we derive ages from our Bayesian analysis and populate each bin of our histogram with the appropriate contribution from the posterior age PDF. As expected, the Bayesian approach results in a significant tail at large ages ( $> 200$  Myr). By contrast, almost half of the Vigan et al. (2012) ages (17/39) are incorrectly assumed to be 125 Myr, the age of the Pleiades. For stars not in young moving groups, we compute the offset from the Vigan et al. (2012) ages to the median age from our Bayesian analysis. The median of this offset for these 28 stars is 135 Myr, an increase in age of 55%, which significantly increases the minimum detectable mass around these stars. The typical contrast achieved at 2” in Vigan et al. (2012) is 14.2 mags, which for 26 of these 28 stars corresponds to planetary masses using their ages and the Baraffe et al. (2003) evolutionary models for companion luminosity. When we instead adopt the median of our Bayesian age distributions for these stars, only 18 stars reach planetary masses at 2”, and the median increase in detectable mass at 2” for these 18 stars is 22%. The magnitude of this increase in detectable mass ranges from 0 to  $9 M_{Jup}$ , with a median of  $2.2 M_{Jup}$ . Therefore, if our older ages were to be used, the constraints on exoplanets from the Vigan et al. (2012) dataset would become weaker.

In Figure 12 we examine how this age uncertainty for “low CMD” stars depends on  $B - V$  color. We divide “low CMD” stars in our volume-limited sample of *Hipparcos* stars into 9 color bins, and combine the marginalized PDFs for age for the stars in that bin. As expected, the median age in each color bin increases with redder color. Assuming a Pleiades age for “low CMD” stars is a fair representation of stars bluer than  $B - V$  of  $-0.05$ , but for redder stars such an assumption significantly underestimates the age.

To summarize the results of our age analysis, the standard practice of assigning an age of 125 Myr to stars in the Pleiades locus on the color-magnitude diagram produces systematically younger ages than we find with our Bayesian method. Figure 8 shows that these Pleiades-like stars in the NICI Campaign sample have a median age of 200 Myr with a 68% confidence level between 160 and 840 Myr. This is expected since identifying a star as similar to a Pleiades A star only places it within the first third of its main-sequence lifetime, which for late-type A stars can imply ages much larger than 125 Myr.

## 4. Observations

Observations for this work were carried out as part of the Gemini NICI Planet-Finding Campaign between 2008 and 2012, using the NICI instrument at Gemini-South. We describe the performance of NICI and the observing process in greater detail in Wahhaj et al. (2013a). Briefly, we utilize two observing modes to optimize our sensitivity to all types of planetary companions over a wide range of angular separations: Angular Differential Imaging (ADI) and Angular and Spectral Differential Imaging (ASDI). In ADI mode, we observe in the broadband  $H$  filter through a partially transparent focal plane mask with the telescope rotator off. This provides the highest sensitivity at large separations ( $\gtrsim 1.5''$ ), where sensitivity to faint companions is limited by background noise. Large-separation companions also move the most as the field rotates.

In ASDI mode, we again observe with the focal plane mask in place and the rotator off, but a 50/50 beamsplitter sends light to two cameras simultaneously, which contain methane-on ( $CH_4L$ , central wavelength  $1.652 \mu\text{m}$ ) and methane-off ( $CH_4S$ , central wavelength  $1.578 \mu\text{m}$ ) 4% narrow-band filters in the  $H$  band. These two simultaneous images are scaled and then subtracted to remove speckle noise and the stellar halo and leave behind the flux from a real companion. ASDI is most sensitive to methanated companions (which will have greater flux in the methane-off filter than the methane-on filter) but can detect companions of all spectral types, and produces higher contrasts  $\lesssim 1.5''$  than ADI alone. Typically we observe targets with both observing modes. We note that observations of planets around HR 8799 suggest that the methane absorption in the spectra of these planets is significantly weaker than predicted by theoretical models (e.g. Bowler et al. 2010; Barman et al. 2011; Skemer et al. 2012). If this is a general feature of young giant planets it could indicate that our expected sensitivity to these planets in the ASDI mode is overly optimistic. It will not, however, impact our expected sensitivity in the ADI mode, or at larger separations in ASDI mode where self-subtraction is not an issue (see Section 5.5).

For each target star, Table 2 gives the observing epoch, observing mode, number of images, total exposure time, and amount of sky rotation. The typical exposure time for ADI observations was 1200 s, and 2700 s for ASDI. In addition, we obtained  $\sim 2$ – $3$  times deeper exposures of Fomalhaut and  $\beta$  Pic, given the existence of their planetary companions.

## 5. Results

### 5.1. Candidates and Follow-up

Given NICI’s ability to achieve very high contrasts (median of  $\sim 15$  magnitudes—a flux ratio of  $10^6$ —at  $1''$ ) and its  $18'' \times 18''$  field of view, it is expected that our images will contain a large number of background objects in addition to any common proper motion (CPM) companions. The Campaign data were reduced and checked for candidate companions by both an automated procedure and visual inspection of the images as described in Wahhaj et al. (2013a). Stars with

candidate companions were flagged, and archival high contrast imaging data (from the VLT, HST, Gemini-North, or Keck) were retrieved and analyzed to see if the candidates could be recovered. If archival data were insufficient to determine whether the candidates were background or CPM, an additional NICI observation was typically obtained to measure the astrometry of the companion(s) at a second epoch. In a few cases multiple additional epochs were required to definitively classify each candidate. We followed up all candidates within 400 AU except for most stars with large numbers ( $\gtrsim 10$ ) of candidates due to these stars being in the foreground of the galactic bulge or at galactic latitude close to  $0^\circ$ .

A candidate companion observed at multiple epochs with sufficient astrometric precision will either be in the same location as in the first epoch (CPM, with the possibility of a small amount of orbital motion) or displaced from the first epoch position, following the expected motion of a background object. A distant ( $\gtrsim 500$  pc) background object will have negligible proper motion ( $\lesssim 2$  mas/yr) and thus appear to move with respect to the target star in the opposite direction indicated by the target star’s (much larger) proper and parallactic motion. To quantitatively classify stars as background (bg) or CPM, we compute the chi-square statistic for the two scenarios:

$$\chi_{bg}^2 = \sum_i \left( \frac{(\rho_{obs,i} - \rho_{bg,i})^2}{\sigma_{\rho,i}^2} + \frac{(PA_{obs,i} - PA_{bg,i})^2}{\sigma_{PA,i}^2} \right) \quad (4)$$

$$\chi_{CPM}^2 = \sum_i \left( \frac{(\rho_{obs,i} - \rho_0)^2}{\sigma_{\rho,i}^2} + \frac{(PA_{obs,i} - PA_0)^2}{\sigma_{PA,i}^2} \right) \quad (5)$$

where the summation is over all epochs except the reference epoch;  $\rho_{obs,i}$  and  $PA_{obs,i}$  are the observed separation and position angle at the  $i$ -th epoch;  $\rho_{bg,i}$  and  $PA_{bg,i}$  are the separation and position angle predicted for a background object given the position at the reference epoch;  $\rho_0$  and  $PA_0$  are the separation and position angle at the reference epoch; and  $\sigma_{\rho,i}$  and  $\sigma_{PA,i}$  are the uncertainties in separation and position angle at the  $i$ -th epoch. We convert chi-square to reduced chi-square ( $\chi_\nu^2$ ) using the number of degrees of freedom (dof), which is  $(N_{epochs} - 1) \times 2$ , where  $N_{epochs}$  is the total number of epochs. The number of epochs in the dof calculation is reduced by one, since the background and CPM predictions are tied to the reference epoch, and then multiplied by 2, because there is a separation and PA measurement at each epoch. The result for each of our candidates is unambiguous, with  $\chi_\nu^2$  for background close to one and  $\chi_\nu^2$  for CPM much larger than one, or vice-versa.

Table 3 lists the properties of each candidate companion for which we have more than one epoch. For each of these companions we then give the astrometry at each epoch in Table 4. Errors in the background track are computed using a Monte Carlo method, combining astrometric errors at the reference epoch for the candidate and errors in the proper motion and parallax of the target star. All proper motion and parallax measurements for our targets are from van Leeuwen (2007). We typically choose the reference epoch to be the first NICI epoch for that candidate. We also show

the motion of each companion on the sky with respect to the background track in Figures 13–17.

## 5.2. Detected Companions: HD 1160 BC, HR 7329 B, and HIP 79797 Bab

Of the candidate companions imaged around our target stars, there are five that are CPM companions, found around HD 1160, HR 7329, and HIP 79797. HD 1160 B is a brown dwarf with mass  $33_{-9}^{+12} M_{Jup}$ , and HD 1160 C is an M3.5 star with mass  $0.22_{-0.04}^{+0.03} M_{\odot}$  (Nielsen et al. 2012). We also detect the known substellar companion to HR 7329 B (Lowrance et al. 2000), which is a brown dwarf with mass between 20 and 50  $M_{Jup}$  (Neuhäuser et al. 2011). The companion to HIP 79797 (also known as HR 6037) was independently discovered as a single object by Huélamo et al. (2010) who determined a mass of  $62 \pm 20 M_{Jup}$  for the  $6.7''$  companion.

NICI observations of HIP 79797 not only further confirm that HIP 79797 B is a CPM companion but reveal that the companion is in fact a binary, with a separation of  $0.06''$  and a near-unity flux ratio at  $JHK_S$ . We have retrieved the archival 2004 and 2006 VLT data used by Huélamo et al. (2010) but are unable to split the binary in these images, given the low S/N of the data. In five NICI epochs (2010-2012), however, we are able to resolve the binary (Figure 18) and determine relative astrometry for the two components (Table 5). We summarize the properties of the HIP 79797 system in Table 6.

We estimate the masses of the now-resolved brown dwarf binary companions using our measurement of the difference in the  $K_S$  magnitudes of the combined two components with respect to the primary ( $7.31 \pm 0.17$  mags), the  $K_S$ -band flux ratio of the two components ( $0.20 \pm 0.06$  mags), and our Bayesian age distribution for HIP 79797 (median 203 Myr, 68% confidence interval between 71–372 Myr). We also assume the spectral type of M9 measured by Huélamo et al. (2010) applies to both objects (which is reasonable given the nearly identical colors of the two components), and use a  $K$ -band bolometric correction from Golimowski et al. (2004) to determine the luminosity of each component, which we then convert to mass using the Lyon/DUSTY evolutionary models (Chabrier et al. 2000). We determine uncertainties through a Monte Carlo method, assuming Gaussian photometric and astrometric errors and using our posterior PDF for age. We find similar masses for the two components (as expected given their small flux ratio) of  $58_{-20}^{+21} M_{Jup}$  and  $55_{-19}^{+20} M_{Jup}$ , with a mass ratio of  $0.93 \pm 0.03$ . These are similar values to the mass estimated by Huélamo et al. (2010) based on their  $K_S$ -band photometry assuming the system was only a single object, meaning our mass estimates are discrepant with theirs. While our median age for the system of 203 Myr is slightly younger than their age of 300 Myr, we also find a brighter  $K_S$ -band flux for the combined Bab system of  $13.0 \pm 0.17$  mag, compared to the  $13.9 \pm 0.1$  mag and  $14.4 \pm 0.2$  mag measured by Huélamo et al. (2010) in their two VLT/NACO datasets. We note that the NACO data were taken with a neutral density filter to avoid saturation, and so HIP 79797 Ba/Bb is detected at low signal-to-noise in these images.

To assess the orbital properties, we have performed a preliminary Markov Chain Monte Carlo

(MCMC) analysis on our 2 years of astrometric data for HIP 79797 Ba and Bb. Any orbital motion over our short time baseline is less than half a NICI pixel, so we do not attempt to measure a dynamical mass for HIP 79797 Ba and Bb. Instead, we fix the combined mass of the brown dwarfs to  $113 M_{Jup}$  and attempt to constrain the possible orbital parameters. Our MCMC fit favors an edge-on orbit ( $i = 87 \pm 5^\circ$ ) with semi-major axis of  $0.48_{-0.37}^{+1.87''}$  ( $25_{-19}^{+97}$  AU). This preference for inclined orbits is understandable given the change in the separation from the first to the last epoch (17 mas) is only slightly larger than the mean error on a single epoch (12 mas), while the PA of the binary does not appear to change (within errors). That is, our data suggest, at low confidence, that the projected sky motion of HIP 79797 Bb is directly away from HIP 79797 Ba, as would be expected in an edge-on orbit. Similarly, the semi-major axis must be large enough for there to be such a small amount of motion over two years. The corresponding orbital period is then  $380_{-330}^{+3700}$  years. We stress that these are preliminary results, based on a short time baseline with very little on-sky motion, and so the 68% confidence interval for orbital periods spans almost two orders of magnitude. If the orbital period is on the shorter side of the estimated period range, future astrometric monitoring could plausibly yield a precise orbit and dynamical masses, as  $\sim 30\%$  coverage of an astrometric orbit is sufficient to yield these results (e.g. Liu et al. 2008; Dupuy & Liu 2011). In particular, a dynamical mass would be of immense value since the only other brown dwarf binary with a dynamical mass and an independent age estimate is the L4+L4 binary HD 130948 (Dupuy et al. 2009). Such benchmark brown dwarf binaries are key to testing models of brown dwarf atmospheres and evolution.

### 5.3. Single Epoch Candidates

For 20 of our 70 B and A stars, there are candidate companions that only appear in one epoch of NICI data and have no detections in archival observations. These candidates fall into three categories. (1) The most common case was that follow-up of these companions was given low priority, as we focused our observing time on candidates with the smallest projected physical separations ( $< 400$  AU). (2) In the second case follow-up was attempted but the second epoch observation was unable to recover the candidate, because the candidate was especially faint or close to the target star. In some cases with multiple candidates around a single star, we were able to confirm the nature of some candidates but not others. (3) Finally, since the target star is not centered on the NICI detector, the orientation of the detector on the sky depends on the parallactic angle of the observation. For wide-separation candidates ( $\gtrsim 6.3''$ ) this can mean a candidate is on the detector in one epoch and off the detector in another. While we typically tried to schedule our second epoch observations to detect these wide candidates, it was not always possible to do this so some remain unvalidated.

For the candidates around these 20 stars, we are unable to confirm whether these are background sources or co-moving companions. Given that only 4 of the 78 candidate companions in Table 3 are not background objects, it is likely that few, if any, of these single-epoch candidates are

co-moving companions, especially given that most of them are at wider separations. Nevertheless, we present the astrometry for these candidates in Table 7 as a reference for future observations of these stars.

## 5.4. Notes on Individual Stars

### 5.4.1. $\beta$ Pic

We assign the planet-host  $\beta$  Pic an age of 12 Myr, given its membership in the  $\beta$  Pic moving group (Zuckerman et al. 2001). Our Bayesian age analysis would suggest a significantly older age with a median of 109 Myr and 68% confidence between 82 and 134 Myr. While  $\beta$  Pic does lie “low” on the CMD (lower than any other star at that  $B - V$  in Figure 1), its spectral type of A5 and  $B - V$  color of 0.17 correspond to a main sequence lifetime about 10 times longer than 12 Myr. From CMD position alone it would only be possible to place  $\beta$  Pic near the beginning of its main sequence lifetime. The additional information of its membership in a moving group provides a more accurate age. Indeed, Barrado y Navascués et al. (1999) note the spread in isochronal ages found by different authors for  $\beta$  Pic, with previous ages ranging from the zero-age main sequence to 100 Myr to 300 Myr, thus providing motivation to instead determine the age of other (lower-mass) stars in the same moving group.

In our initial NICI epoch (UT 2008-11-22) using our standard campaign observing strategy we did not detect the faint planet  $\beta$  Pic b. Subsequent NICI observations beginning in 2009 did detect the planet, as a result of longer exposure times and the planet’s orbit leading to a larger angular separation from its star. Since these special observations were conducted separate from the NICI Campaign, we do not consider them here when deriving upper limits on the fraction of B and A stars that harbor planets. For this work, we only consider the 2008-11-22 contrast curve for  $\beta$  Pic and treat our survey as having detected zero planets, since in this observation  $\beta$  Pic b was not detectable.

### 5.4.2. Fomalhaut

From our Bayesian analysis, the planet-host Fomalhaut is assigned a median of 515 Myr and 68% confidence interval between 418 and 623 Myr. Fomalhaut has a similar  $B - V$  color to  $\beta$  Pic but is 0.6 magnitudes brighter on the CMD, placing it significantly above the Pleiades sequence. Being beyond the first third of its main sequence lifetime allows the age of Fomalhaut to be more accurately estimated from its CMD position compared to younger stars. Indeed, an analysis by Mamajek (2012) notes that Fomalhaut has a very wide (57000 AU) K-dwarf companion, TW PsA, with an estimated age of  $440 \pm 40$  Myr, consistent with the 68% confidence interval from our Bayesian age analysis. We note that this age is twice as old as the  $200 \pm 100$  Myr age estimated

for the Fomalhaut/TW PsA system by Barrado y Navascues et al. (1997).

#### 5.4.3. $\gamma$ Oph

$\gamma$  Oph is an A0 star with a resolved debris disk that extends out to 260 and 520 AU at 24 and 70  $\mu\text{m}$ , respectively (Su et al. 2008). Song et al. (2001) assign an age of 184 Myr to  $\gamma$  Oph with a range between 50 and 277 Myr, based on Strömberg photometry and isochrones. This is significantly younger than our Bayesian age, which has median 342 Myr and a 68% confidence interval between 285 and 388 Myr. As with other stars with literature ages based on isochrones or CMD position we adopt our Bayesian age distribution for this star.  $\gamma$  Oph is high on the color-magnitude diagram compared to Pleiades stars of the same color. We detect 8 candidate companions to  $\gamma$  Oph, the 7 innermost of which are determined to be background objects from two epochs of NICI data. The final candidate, at a separation of 9.2", is only visible in one epoch of NICI data and so we are unable to definitively determine if it is background or CPM. Given its large separation and the large number of background objects in the field, this eighth candidate is most likely also a background object.

#### 5.4.4. 49 Cet

49 Cet is an A1 star hosting a disk with significant amounts of molecular gas (Zuckerman & Song 2012). For its color 49 Cet is relatively low on the CMD, comparable to Pleiades A stars; as a result, we derive a Bayesian age of 225 Myr with 68% confidence interval between 91 and 377 Myr. This wide range is again a consequence of 49 Cet's location in the CMD being consistent with it being in the first third of its main sequence lifetime. Zuckerman & Song (2012) determine 49 Cet to be a member of the Argus association, allowing them to derive a much younger age of 40 Myr. We adopt this moving group age of 40 Myr.

#### 5.4.5. $\zeta$ Lep

$\zeta$  Lep has a small debris disk that has only been resolved at 18.3  $\mu\text{m}$ , with an extent of only 3 AU (Moerchen et al. 2007). Our Bayesian analysis finds an age of 330 Myr with 68% confidence interval between 224 and 410 Myr, consistent with its position on the CMD in the midst of Pleiades A stars. Nakajima & Morino (2012) find  $\zeta$  Lep to be a member of the  $\beta$  Pic moving group, and so we assign it an age of 12 Myr. We find a single candidate companion to  $\zeta$  Lep at 5.3" which we determine to be background based on two epochs of NICI data.

#### 5.4.6. HD 31295

HD 31295 has been shown to have an IR excess with MIPS 24 and 70  $\mu\text{m}$  data by Rhee et al. (2007), who estimate an age of 100 Myr based on its low position on the CMD. As expected, our Bayesian analysis shows an older age, with a median of 241 Myr and a 68% confidence interval that extends from 119 to 355 Myr. We note that HD 31295 is listed in CCDM (Dommangeat & Nys 2002) as having a 40" M-star companion (BD+09 683B). We have examined the 1975 DSS image and the 2000 2MASS image of HD 31295, and found that BD+09 683B is in fact a background object ( $\chi_{\nu,bg}^2=0.21$ ,  $\chi_{\nu,CPM}^2=2.94$ ). In addition, from our NICI images we have detected four candidate companions to this star, two of which we rule out as background objects. The remaining two (at 7.8" and 8.7") were only visible in one NICI epoch, leaving us unable to determine if they are background objects or CPM companions.

#### 5.4.7. HD 1160

HD 1160 is an infrared photometric standard from Elias et al. (1982) and has been observed numerous times at the VLT to calibrate observations of nearby stars. Nielsen et al. (2012) combined these archival data with new NICI data to show that HD 1160 is a triple system consisting of an A0 star, an  $\sim$ L0 brown dwarf at 80 AU, and an M3.5 star at 530 AU. Our Bayesian age for HD 1160 of 92 Myr, with 68% confidence between 36 and 178 Myr, is consistent with the Nielsen et al. (2012) age range of  $50_{-40}^{+50}$  Myr, derived by comparing the CMD positions of all three objects to young clusters of various ages.

#### 5.4.8. HR 7329

HR 7329 is an A0 star that hosts a debris disk (Backman & Paresce 1993), which Smith et al. (2009) find to be edge-on at 18.3  $\mu\text{m}$ . In addition, it hosts the brown dwarf companion HR 7329 B at 4.2" (Lowrance et al. 2000), whose mass is estimated by Neuhäuser et al. (2011) to be between 20 and 50  $M_{Jup}$ . We confirm that HR 7329 B is a CPM companion with our NICI observations, but find no other candidate companions in our NICI images. Like other members of young moving groups our Bayesian method only places HR 7329 in the beginning of its main sequence lifetime: our median age for HR 7329 is 182 Myr, with 68% confidence between 101 and 268 Myr. HR 7329 is a member of the  $\beta$  Pic moving group (Zuckerman et al. 2001), and so we adopt an age of 12 Myr for the star.

#### 5.4.9. *HR 4796*

HR 4796 is an A0 star that hosts a resolved narrow ring of debris with a sharp inner and outer edge (Jayawardhana et al. 1998; Koerner et al. 1998; Wahhaj et al. 2005; Thalmann et al. 2011). We assign the star an age of 10 Myr as Zuckerman & Song (2004) identify HR 4796 as a member of the TW Hydra Association (TWA). We designed our NICI observations to place the known M2 companion HR 4796 B (Jura et al. 1995) off the detector so that its light would not limit the dynamic range we could reach. We detect scattered light at the position angle HR 4796 B would appear, as it should have been less than 1" from the edge of the detector. We also detect a background star at 4.47" which is referred to as HR 4796 D by Mouillet et al. (1997) who identify it as a background object based on its colors. With 8 years of astrometry, including the initial Mouillet et al. (1997) detection, we confirm that this object is unambiguously a background star. We detect no other objects around HR 4796.

#### 5.4.10. *HD 141569*

HD 141569 is a B9 star that hosts a resolved disk (Weinberger et al. 1999) containing both gas and dust (Merín et al. 2004). Our Bayesian method find a median age of 318 Myr with a 68% confidence interval between 163 and 440 Myr. Weinberger et al. (2000) note that the two M-dwarf companions to HD 141569 show lithium absorption and X-ray flux consistent with youth, and find an age for the system of 5 Myr. Merín et al. (2004) examined high-resolution spectra of HD 141569 and confirm that it is a pre-main sequence star with low metallicity ( $[\text{Fe}/\text{H}] = -0.5$ ). As with other very young B and A stars additional information beyond photometry (in this case the ages of the two M-dwarf companions) helps refine the age. The two M-dwarf companions are off the detector in our NICI images. We detect two additional candidate companions at 6.40" and 7.85" and find them both to be background objects.

#### 5.4.11. *HD 71155*

HD 71155 is an A0 star with a debris disk detectable as an IR excess with MIPS 24 and 70  $\mu\text{m}$  data (Rhee et al. 2007). The disk of HD 71155 is barely resolvable at 10  $\mu\text{m}$ , with a radius of  $\sim 2$  AU (Moerchen et al. 2010). We find a median age for the star of 273 Myr, with a 68% confidence interval between 237 and 313 Myr. We detected 3 candidate companions to HD 71155, all of which were determined to be background, as well as a one-epoch candidate companion at 9.93" that we are unable to classify as CPM or background at this time.

#### 5.4.12. *HD 172555*

HD 172555 is a member of the  $\beta$  Pic moving group and so has an estimated age of 12 Myr (Zuckerman et al. 2001). It also has a wide K5 companion, CD-64 1208, with a separation of 71.3'' (2040 AU, Feigelson et al. 2006). The disk of HD 172555 contains both dust and gas (Riviere-Marichalar et al. 2012), possibly resulting from a recent impact event during planet formation (Johnson et al. 2012). Our age for HD 172555 is 276 Myr, with a 68% confidence interval between 83 and 462 Myr. As with other later-type A stars in young moving groups we find an age range that corresponds to the first third of the main sequence lifetime, rather than the much younger age for the group itself. We do not detect any closer components to this binary system, finding only a background object at 7.7'' separation.

### 5.5. Upper Limits on Planet Fraction

Given the non-detection of planets from the NICI Campaign survey of B and A stars, we can set an upper limit on the fraction of stars with planets using the measured contrast curves for each star and Monte Carlo simulations of completeness to planets.

#### 5.5.1. *Contrast Curves*

For every observed star contrast curves are produced for each observing mode (ADI or ASDI) and give the 95% completeness to companions as described in detail by Wahhaj et al. (2013a). Briefly, simulated planets at a grid of flux ratios and separations are inserted into the raw data from each star, which are then reduced with the Campaign pipeline and the candidates are recovered with an automated detection method. The resulting contrast curves give the flux ratio as a function of separation where 95% of the simulated companions can be recovered. These 95% completeness contrast curves are shown in Figures 19–25, grouped by apparent  $H$  magnitude of the target star, and tabulated in Table 8.

As described in Wahhaj et al. (2013a), contrast curves for both ADI and ASDI datasets must be corrected for four effects to account for the true flux of the companions after emerging from the data reduction pipeline. (1) Light from a close companion passes through the partially transparent coronagraphic mask, and the companion’s flux is diminished. (2) Over a single ADI exposure, as the sky rotates with respect to the detector, a companion can be smeared over multiple pixels, especially at larger angular separations. (3) ADI self-subtraction occurs for small-separation companions when the total amount of rotation for the companion is small, because some companion flux ends up in the combined PSF image and is then subtracted from the companion. (4) Finally, SDI reduction leads to self-subtraction of the companion flux, when subtracting the on-methane narrowband image from the off-methane image.

The first three effects (mask attenuation, smearing, and ADI self-subtraction) are functions of radius alone and are applied as corrections to the contrast curve itself (see Wahhaj et al. 2013a). The final effect, SDI self-subtraction, is a function of both radius and the flux ratio of the companion between the two narrowband filters, and so is dealt with in the Monte Carlo simulations, as described in the next section.

For stars with unconfirmed candidates due to having only one epoch of astrometric data (Section 5.3 and Table 7), we adjust the contrast curves to reflect the fact that we have not completely ruled out the presence of companions that are detectable by NICI. For each star with such candidates we make the following changes to the measured contrast curves:

(1) If there are unconfirmed candidate companions outside the radius with 100% angular coverage (i.e., where some position angles at that radius are off the edge of the NICI detector, typically  $>6.3''$ ) and brighter than the contrast curves at any of the observation epochs, then all contrast curves for that star are truncated at the angular separation of the innermost companion in the region with less than 100% coverage. For example, HD 31295 has two candidate companions at  $7.77''$  and  $8.66''$  seen only at epoch 2009-01-14, so all contrast curves at all epochs for this star are stopped at  $7.77''$ , i.e. we assume we have zero data at larger separations.

(2) If candidates are within the 100% angular coverage region and lie between the contrast curves from different epochs, then any contrast curve that is more sensitive than the brightest of these candidates is replaced with the best contrast curve that could not have detected the brightest of these candidates. For example, the target star HIP 50191 has a candidate at  $4.11''$  that was detected in the 2010-01-05 ADI dataset but was undetected in the 2008-12-16 ASDI dataset. As a result, we use the 2008-12-16 ASDI contrast curve to compute completeness to planets at both epochs.

In principle, both changes could be applicable to a single star, but that scenario never arose for our NICI B and A stars. In cases where candidate companions are within the 100% coverage region, brighter than the contrast curve, and there is only one NICI epoch, the star is dropped from our analysis altogether. This is the case for 7 of our 70 target stars, all of which have a large number of candidate companions, galactic latitude within  $20^\circ$  of the galactic plane and galactic longitude within  $30^\circ$  of the galactic center. The last column of Table 7 summarizes our adjustments for the contrast curves of stars with unconfirmed companions.

### 5.5.2. Monte Carlo Simulations of Completeness to Planets

To interpret the contrast curves as limits on planet fraction, we follow the Monte Carlo procedure developed by Nielsen et al. (2008) and Nielsen & Close (2010). Briefly, we place an ensemble of simulated planets around each target star and then determine the fraction that are detectable by comparing them to the contrast curve for that star’s NICI dataset. We begin by assigning orbital parameters to each simulated planet. The position angle of nodes represents rotation on the sky and

is generally not included in the simulations, as our contrast curves are one-dimensional (functions of separation only). The semi-major axis and mass are drawn from a regular grid (see below for details). The eccentricity, inclination angle, longitude of periastron, and mean anomaly are randomly drawn from the appropriate probability distributions. We have fit a linear function to the probability distribution for eccentricity based on known RV planets (as described in Nielsen & Close 2010), while the probability distributions of the other parameters are given by geometric considerations only. The instantaneous projected separation is then calculated for each simulated planet from its orbital parameters. In addition, the age of the star and mass of each simulated planet are used to produce an  $H$ -band flux using the Baraffe et al. (2003) models, which is converted to a flux ratio using the known distance and  $H$ -band magnitude of the star. Then, each simulated planet can be directly compared to the NICI contrast curve for that star; the detectable fraction is simply the fraction of simulated planets lying above the contrast curve.

In cases where a star was observed at multiple epochs, simulated planets are generated at the first epoch, advanced forward in their orbits to the second epoch, then compared to the contrast curve for the second epoch dataset. Similarly, the same set of simulated planets are compared separately to the ADI and ASDI contrast curves. A simulated planet that remains below all contrast curves is considered undetected, while one that is above at least one contrast curve is detected.

An additional consideration is the use of age distributions, rather than a single defined age, to describe many of the B and A stars in this paper. In Nielsen & Close (2010) each target star is assigned a single age, and the Baraffe et al. (2003) models are used to assign absolute magnitudes corresponding to that age. For stars with an external age measurement (i.e. stars belonging to a moving group) we use this same method. For the other stars with a distribution of ages from our Bayesian analysis, we define ten points logarithmically spaced along the age axis, between 5 Myr (the minimum used in our luminosity grid) and the maximum age of the star, defined as where the probability of the star having that age or larger is 1%. The fraction of detectable planets is then calculated at each of those ten values of the age and then interpolated to the age grid used in Section 3.2. The final fraction of detectable planets is the weighted average of this array of interpolated fractions weighted by the relative probabilities of each age bin derived by our Bayesian method.

We also account for SDI self-subtraction when computing the flux of the simulated planets. The effect is strongest close to the star: one narrowband methane image is demagnified to place the speckles at the same angular scale as in the other narrowband image, and so at smaller separations the on-methane and off-methane companions increasingly overlap each other and more self-subtraction occurs. If the companion is strongly methanated, it will have much more flux in the off-methane filter compared to the on-methane filter, and so the amount of self-subtraction will be minimal. However, if the companion has no methane absorption, it will have roughly equal flux between the two narrowband filters, and self-subtraction will be a strong effect.

To address this issue in the Monte Carlo simulations we modify the fluxes of the simulated planets to simulate the effect of ASDI self-subtraction. As in Nielsen & Close (2010), we calculate the flux in the off-methane ( $CH_4S$ ) filter by convolving the NICI filter transmission curve with the SpeX Prism Library of ultra-cool dwarfs and deriving a relation between ( $CH_4S - H$ ) color and spectral type. Temperatures are then derived from spectral type using the polynomial fit of Golimowski et al. (2004). Then, we use the theoretical models of Baraffe et al. (2003) to compute  $H$ -band magnitudes and temperatures as a function of age and planet mass. We then apply our synthetic photometry results to obtain a grid of  $CH_4S$  magnitudes for each combination of age and mass.

To deal with self-subtraction, we use a similar procedure to produce grids of  $CH_4S$  and  $CH_4L$  magnitudes. For small separation planets, the images of the planet in both bands overlap, and the final flux is simply the difference between the two fluxes. At large separations the two images are completely offset from each other so no self-subtraction occurs, and the final flux is just the  $CH_4S$  flux. For intermediate separations, we calculate the amount of geometric self-subtraction (the degree of overlap in the two images) as a function of radius and reduce the flux for the  $CH_4L$  image of the planet by this geometric factor before subtracting it from the  $CH_4S$  flux.

We also account for nonuniform position angle coverage of our observations at large angular separations. The NICI detector is square, with the focal plane mask and target star placed offset from the center. As a result, while we image  $360^\circ$  in position angle at small separations, at larger separations ( $\gtrsim 6.3''$ ) our coverage declines as some position angles are off the edge of the detector. We note the separations with reduced coverage in Table 8. In our Monte Carlo simulations we account for this effect by generating a uniform random variable between 0 and 1 for each simulated planet. If that random variable is greater than the fractional angular coverage at the projected separation of the simulated planet, then that planet is considered undetectable even if it is brighter than the contrast curve. This parameter is similar to the position angle of nodes (rotation of the orbit on the plane of the sky), which follows a uniform distribution. When multiple contrast curves are available for a single target star, this random variable is also preserved across all epochs so that the same set of simulated planets are compared to each contrast curve for the same star.

### 5.5.3. Planet Frequency Analysis

For each star we then compute the fraction of detectable planets with  $10^3$  simulated planets all having the same values of planet mass and orbital semi-major axis. This is then repeated for a grid of mass and semi-major axis and for each target star. As in Nielsen & Close (2010), we consider the following quantity:

$$N(a, M) = \sum_{i=1}^{N_{obs}} f_p(a, M) P_i(a, M) C_{2.0}(M_{*,i}) \quad (6)$$

where  $N(a, M)$  is the expected number of detected planets as a function of orbital semi-major axis ( $a$ ) and planet mass ( $M$ );  $N_{obs}$  is the number of stars observed;  $f_p(a, M)$  is the frequency of planets for a specific combination of mass and semi-major axis; and  $P_i(a, M)$  is the probability of detecting a planet with that mass and semi-major axis as determined from our Monte Carlo simulations. Finally to account for the different masses of the stars in the sample, we define a mass correction that weights stars of different masses by their probability of harboring giant planets. This mass correction,  $C_{2.0}(M_{*,i})$ , is given by:

$$C_{2.0}(M_*) = \frac{F_p(M_*)}{F_p(2.0M_\odot)} \quad (7)$$

where  $F_p(M_*)$  is the relative probability of hosting giant planets as a function of stellar mass. We define  $F_p(M_*)$  using RV results, specifically the power-law fit to planet frequency as a function of stellar mass from Johnson et al. (2010), where  $F_p(M_*) \propto M_*^{1.0}$ . Our approach assumes that the stellar mass dependence of close-in RV planets applies to wide-separation giant planets as well. While the current paucity of wide-separation planets makes this assumption impossible to test, we use it as a starting point for our analysis of the frequency of these planets. If wide-separation giant planets form a distinct population from close-in RV planets (as suggested by Crepp & Johnson 2011), then our adopted mass scaling might not be appropriate for long-period planets. We choose to normalize at  $2 M_\odot$ , since that is the peak of the total distribution of stellar masses in our sample from our Bayesian analysis. The total range of stellar mass in our sample is 1.5–4.6  $M_\odot$ , as given by the median of our posterior mass PDFs for each star, with 60 of our 70 stars having a median between 1.5–2.5  $M_\odot$ , and only 4 having a median greater than 3  $M_\odot$  (right panel of Figure 9). As a result, the mass correction has a modest effect on the final results.

We are seeking to define 95% confidence upper limits on the fraction of stars with planets as a function of semi-major axis and planet mass ( $f_p(a, M)$ ). We use the Poisson distribution:

$$P(k) = \frac{\mu^k e^{-\mu}}{k!} \quad (8)$$

with expectation value  $\mu$  for all integers  $k$ . In this case,  $\mu$  is the predicted number of planets in a given semi-major axis and mass bin, and  $k$  is the number of planets detected in that bin. The 95% confidence level for a null result ( $k = 0$ ) is  $\mu = 2.996$ ; that is, for an expectation value of 3 planets, the probability of a null result (i.e., detecting no planets) occurring by chance is 5%. So, solving for the fraction of stars with planets,  $f_p(a, M)$ , we obtain

$$f_p(a, M) = \frac{N(a, M)}{\sum_{i=1}^{N_{obs}} P_i(a, M) C_{2.0}(M_{*,i})} \quad (9)$$

This is the upper limit on the fraction of stars with planets, as a function of semi-major axis and planet mass. Setting  $N(a, M) = 3$  gives the 95% confidence upper limit, allowing us to map out

the upper limit that can be placed on the fraction of stars with planets at each combination of semi-major axis and planet mass.

#### 5.5.4. Binaries

An additional concern is the presence of stellar and brown dwarf binaries around some of our target stars. A target star with a 100 AU binary, for example, would not be expected to have a 100 AU planet from dynamical arguments, and so we cannot simply combine constraints on 100 AU planets from single stars with the 100 AU binary star for our statistical analysis. Holman & Wiegert (1999) suggest that a forming planet inside 20% of the binary separation should see its parent star as a single star, and so we use this factor of 5 to define an “exclusion zone” around a stellar or binary brown dwarf companion to our target stars. Between 20% and 500% of the binary semi-major axis (where a forming planet would be disrupted by the orbit of the binary), we exclude any constraints on planets from that star, i.e. we assume no information exists about planet frequency, since planets never could have formed in the first place. We caution that this approach does not account for migration in either the binary system or its potential planets (e.g. Kratter & Perets 2012). In addition, we do not change the analysis for stars with known planetary-mass companions ( $\beta$  Pic and Fomalhaut), i.e. we do not consider any dynamical effects their known planets would have on other orbital separations.

We compile a list of known binaries among our target stars in Table 9, including the binary separation (or semi-major axis when available), spectral type, and references. We also indicate the range of allowable semi-major axes, beyond the exclusion zone for that star which is excluded when deriving constraints on planet fraction. As discussed in Section 5.4.6, we treat our target star HD 31295 as a single star despite it being listed in CCDM as a binary.

#### 5.5.5. Results

In Figure 26 we show contours giving the upper limit on the fraction of  $2 M_{\odot}$  stars with planets. We also give the ranges of semi-major axis at which the upper limit on planet fraction drops below 5%, 10%, 20%, and 50% for four planet masses in Table 10. In general, the upper limits are modest, especially when compared to samples including solar type and later stars (e.g. Biller et al. 2013 and Wahhaj et al. 2013b): fewer than 20% of B and A stars can have giant planets larger than  $4 M_{Jup}$  between 59 and 460 AU, with less than 10% of stars having giant planets above  $10 M_{Jup}$  between 38 and 650 AU.

We can also determine limits on the fraction of A stars with a planet like HR 8799 b (Marois et al. 2008), by focusing on its corresponding values of mass ( $7 M_{Jup}$ ) and semi-major axis (68 AU, assuming its semi-major axis is equal to its projected separation) in Figure 26. Our survey’s non-detection of planets states that fewer than 9.8% of  $2 M_{\odot}$  stars can have a planet with the same properties

as HR 8799 b at 95% confidence. Planets like  $\beta$  Pic b (8  $M_{Jup}$ , 8 AU) are unconstrained by our results, since most of our target stars are older and more distant than  $\beta$  Pic.

The weaker constraints on planet frequency for B and A stars compared to later-type stars are expected. B and A stars are intrinsically brighter than solar-type and M stars, and so the same instrumental contrast corresponds to brighter (and more massive) detectable companions for higher-mass stars. In addition, the stars here with ages determined by our Bayesian analysis are significantly older than the young moving group stars in Biller et al. (2013) and the debris disk hosts in Wahhaj et al. (2013b), with a median age of 250 Myr and 68% confidence interval between 90 and 500 Myr (see Figure 8). In comparison, the median age for stars in the moving group sample is 12 Myr, while for the debris disk sample it is 70 Myr.

### 5.6. Comparison with Previous Studies

We compare our constraints on the fraction of high-mass stars with planets to previous predictions and survey results.

Crepp & Johnson (2011) predicted the planet yield of the NICI survey with a simplified description of the NICI contrast curve, consisting of inner and outer working angles of 0.2" and 5.5" and a contrast floor within that range that increases monotonically from 11.4 mags (flux ratio of  $2.9 \times 10^{-5}$ ) to 12.9 mags for the  $H$ -band. This assumed contrast curve is similar to our median  $CH_4$  contrast at 0.36" of 11 mags, but is far too pessimistic at larger separations: we achieve a median contrast of 16.8 mags at 4" compared to the 12.9 mags assumed by Crepp & Johnson (2011). Their calculations use simulated target stars corresponding to the age, distance, and stellar mass distributions of solar neighborhood stars. Given their preferred input model of planet populations, they predict that a NICI-like campaign of 610 stars would detect 15.4 planets around target stars with masses between 1.5 and 2.6  $M_{\odot}$ . They predict such a survey would observe 192 high-mass stars, compared to the 70 B and A stars observed by NICI, so we reduce this predicted yield by 70/192 to 5.6 planets<sup>1</sup>.

We note, however, that the null result of Nielsen & Close (2010) rules out essentially the Crepp & Johnson (2011) input model of planet populations (an extension of the RV planet population out to 120 AU) at >99% confidence (e.g. Figure 15 of Nielsen & Close 2010). The only difference is that Crepp & Johnson (2011) have a mild stellar mass dependence on their semi-major axis upper cut-off,  $a_{max} \propto (M_*/2.5M_{\odot})^{4/9}$ , while Nielsen & Close (2010) do not. Using the more plausible Crepp & Johnson (2011) planet model with an upper cut-off of 35 AU for solar-type stars (only ruled out by Nielsen & Close 2010 at the 68% confidence level), a NICI-like survey of 610 stars

---

<sup>1</sup>This is likely an underestimate. If one were to design a sub-sample of 70 stars from an initial sample of 192 stars one would choose the 70 best stars, which would account for proportionally more planet detections than the 70 worst stars.

should find only 4.1 planets around high-mass stars, or 1.5 planets given the actual number of B and A stars observed by NICI. This is consistent with our null result as a Poisson distribution rules it out at only the 78% level. Similarly, Crepp & Johnson (2011) predict that a NICI survey of 192 high-mass stars would detect only 0.1 “cold-start” planets (planets that form via the core-accretion scenario, based on the planet luminosity models of Fortney et al. 2008).

Janson et al. (2011) conducted an adaptive optics survey of 18 high-mass stars with spectral types B2-A0, more massive than the stars discussed here. Their median contrast at 1” was 12.4 mags, compared to 14.3 mags for our NICI B and A stars. They did not detect any planets around their target stars and set limits on the fraction of planets, brown dwarfs, and low-mass stars that can form by the disk instability mechanism. By applying formation model predictions of what combinations of semi-major axis and planet mass are allowed, they find an upper limit on companion fraction of 21% (95% confidence) for objects within 300 AU and smaller than  $100 M_{Jup}$ . We note that their assumed formation limits often preclude the presence of planetary-mass companions that are detectable by their contrast curve, so they are essentially comparing the theoretical prediction of brown dwarf frequency to their null result for brown dwarfs. Without assuming a formation model and using the NICI B and A star results, we find that fewer than 7% of high-mass stars can have a companion more massive than  $8 M_{Jup}$  between 85 and 300 AU, also at 95% confidence.

Vigan et al. (2012) examined the frequency of giant planets around 42 high mass stars based on the results of IDPS, which included the detections of planets around HR 8799. Their median detection limits were 12.7 mags at 1” and 15.3 mags at 5”, compared to our median NICI contrasts for B and A stars of 14.3 mags at 1” and 16.8 mags at 5”. They use a Bayesian analysis assuming a fixed mass and semi-major axis distribution, where planets are uniformly distributed between 5 and 320 AU and 3 and  $13 M_{Jup}$ , finding a planet frequency with 68% confidence between 6 and 19%. We find consistent results: at 95% confidence, fewer than 25% of B and A stars can have a giant planet more massive than  $3 M_{Jup}$  between 70 and 375 AU. And at 68% confidence we find that less than 10% of high-mass stars can have  $3 M_{Jup}$  planets in the same ranges of semi-major axis. However, we note that the analysis of Vigan et al. (2012) differs significantly from ours, as we do not specify a particular distribution of planets but instead put upper limits on the frequency of wide-separation giant planets as a function of semi-major axis and planet mass. In addition, as we illustrate in Figure 11 and discuss in Section 3, we find significantly older ages for many of their target stars than used in their analysis. With these older ages, the actual IDPS constraints on planet fraction around high-mass stars would be significantly weaker, since fewer planets would be detectable around many of their stars.

We note that our upper limits are similar to the 20% frequency of giant RV planets ( $\gtrsim 1 M_{Jup}$ ) found around high-mass ( $>1.4 M_{\odot}$ ) stars at small ( $a < 2.5$  AU) separations (Johnson et al. 2010). So while our 10% constraints on more massive ( $>10 M_{Jup}$ ), wide-separation (38–650 AU) planets around B and A stars are a factor of two more restrictive than the RV frequency for all masses, directly comparing the frequencies between RV and directly imaged planets for a similar range of masses will require larger sample sizes and/or higher contrasts.

## 6. Conclusions

We have surveyed 70 young, nearby B and A for planets as part of the Gemini NICI Planet-Finding Campaign. From this search we have discovered a brown dwarf and an M star orbiting HD 1160 and determined that the previously known brown dwarf companion HIP 79797 B is actually a tight brown dwarf binary. Deep images of  $\beta$  Pic and Fomalhaut show no new companions to either star. The non-detection of any planets in the survey implies that giant planets are not common around high mass stars. A Monte Carlo analysis shows that less than 10% of  $2 M_{\odot}$  stars host a planet more massive than  $10 M_{Jup}$  between 38 and 650 AU at 95% confidence, and fewer than 20% of B and A stars harbor a hot-start giant planet more massive than  $4 M_{Jup}$  between 59 and 460 AU. Planets like HR 8799 b are similarly uncommon, with fewer than 9.8% of  $2 M_{\odot}$  stars having such planets ( $7 M_{Jup}$ , 68 AU) at the 95% confidence level.

The 70 B and A stars in the NICI Campaign represent the largest, deepest direct imaging survey around high mass stars conducted to date. We reach similar upper limits on the fraction of massive stars with giant planets that Nielsen & Close (2010) reached for solar-type stars. We find that  $<20\%$  of  $2 M_{\odot}$  stars have a  $4 M_{Jup}$  planet between 59 and 460 AU, compared to  $<20\%$  of  $1 M_{\odot}$  stars having a  $4 M_{Jup}$  planet between 30 and 466 AU.

If wide-separation giant planets are formed by outward scattering between giant planets close to the star, then our non-detection of planets from the NICI Campaign suggests that close scattering is not common in giant planet systems around B and A stars. Such scattering is also proposed to be the origin of high eccentricities of small-separation giant planets detected by the RV method (e.g., Rasio & Ford 1996, Weidenschilling & Marzari 1996, Lin & Ida 1997).

The radial velocity observations for GK clump giant stars ( $<1.5\text{--}3 M_{\odot}$ ) that were main sequence B and A dwarfs show that the orbital distributions of giant planets around these “retired A stars” are quite different from those around solar-type stars (Johnson et al. 2010; Sato et al. 2010). One feature is that giant planets around GK clump giant stars may have smaller orbital eccentricities than intermediate separation RV planets ( $\gtrsim 1$  AU) around solar-type stars (e.g. Sato et al. 2010). Both the RV result and our null result from the NICI Campaign B and A stars suggest that systems of giant planets may be more orbitally stable around high-mass stars than around solar-type stars. Additionally, the paucity of hot Jupiters (orbital radii  $\lesssim 0.1$  AU) around high mass stars compared to solar-type stars could be due to less type II migration occurring around B and A stars (Burkert & Ida 2007; Currie 2009). The difference in hot Jupiter frequency cannot be fully accounted for by enhanced tidal decay during the RGB phase of the GK clump giant stars (Kunitomo et al. 2011). If giant planets around B and A stars are more orbitally stable as well as less affected by type II migration, this presents a challenge to planet formation theory.

While wide-separation giant planets like HR 8799 b are relatively rare, with fewer than 9.8% of high-mass stars having such a planet, we cannot place any constraints on planets like  $\beta$  Pic b, ( $8 M_{Jup}$ , 8 AU). The star  $\beta$  Pic is so much younger (12 Myr) and closer (19 pc) than any other B or A star in our sample, with the planet just at the edge of what is detectable by NICI. To detect similar

planets around the other A stars in our sample will require a planet-finding instrument coupled to an extreme adaptive optics system like GPI or SPHERE (Graham et al. 2007; Boccaletti et al. 2008). While large-separation giant planets (like HR 8799 b) are rare around high mass stars, it is possible that giant planets in similar orbital distances as Jupiter are more common. Observations of other B and A stars with future instruments will be able to answer this question definitively.

Nevertheless, our NICI sample of B and A stars is the one best suited for directly imaging planets, as it represents the youngest and closest high mass stars. The number of B and A stars in a volume-limited sample is significantly lower than for solar-type and M stars, so young high-mass stars within 100 pc will always be very limited. With the exception of the handful of nearby B and A stars whose ages can be independently determined (e.g. members of a moving group or components of a wide multiple system with a lower-mass star that can be independently age-dated), searching for “low CMD” stars is the best technique for locating young B and A stars. While we have shown that low position on the color-magnitude diagram does not indicate Pleiades age, this approach still does flag stars in the first third of their main-sequence lifetimes. So the stars discussed here are likely to be the youngest B and A stars within 100 pc, with their ages most precisely determined from our Bayesian method.

To further refine the sample, spectroscopy of nearby B and A stars can clean out the low metallicity stars (which are likely to have larger ages) from the “low CMD” stars. Evolutionary model predictions of  $\log(g)$  and  $T_{eff}$ , which can also be determined from spectroscopy, may be more accurate than the photometry we use here, but the fundamental limitation of determining accurate ages will still remain. B and A stars do not move significantly on either a color-magnitude diagram or an HR diagram in the first third of their main-sequence lifetimes. While constraints on the fraction of high mass stars with giant planets can be improved with future instruments that can achieve higher contrasts at smaller separations, the optimal target list for these future surveys is unlikely to differ significantly from the stars presented here.

We thank Jessica Lu, Adam Kraus, Rolf Kudritzki, and Lisa Kewley for helpful discussions that greatly benefited this work. We thank the anonymous referee for the constructive suggestions that have improved this work. B.A.B was supported by Hubble Fellowship grant HST-HF-01204.01-A awarded by the Space Telescope Science Institute, which is operated by AURA for NASA, under contract NAS 5-26555. This work was supported in part by NSF grants AST-0713881 and AST-0709484 awarded to M. Liu, NASA Origins grant NNX11 AC31G awarded to M. Liu, and NSF grant AAG-1109114 awarded to L. Close. The Gemini Observatory is operated by the Association of Universities for Research in Astronomy, Inc., under a cooperative agreement with the NSF on behalf of the Gemini partnership: the National Science Foundation (United States), the Science and Technology Facilities Council (United Kingdom), the National Research Council (Canada), CONICYT (Chile), the Australian Research Council (Australia), CNPq (Brazil), and CONICET (Argentina). Based on observations made with the European Southern Observatory telescopes obtained from the ESO/ST-ECF Science Archive Facility. This publication makes use of data products from the

Two Micron All Sky Survey, which is a joint project of the University of Massachusetts and the Infrared Processing and Analysis Center/California Institute of Technology, funded by the National Aeronautics and Space Administration and the National Science Foundation. This research has made use of the SIMBAD database, operated at CDS, Strasbourg, France. This research has made use of the VizieR catalogue access tool, CDS, Strasbourg, France. The Digitized Sky Survey was produced at the Space Telescope Science Institute under U.S. Government grant NAG W-2166. The images of these surveys are based on photographic data obtained using the Oschin Schmidt Telescope on Palomar Mountain and the UK Schmidt Telescope. The plates were processed into the present compressed digital form with the permission of these institutions.

*Facilities:* Gemini:South (NICI).

## REFERENCES

- Anderson, E. & Francis, C. 2012, *Astronomy Letters*, 38, 331
- Backman, D. E. & Paresce, F. 1993, in *Protostars and Planets III*, ed. E. H. Levy & J. I. Lunine, 1253–1304
- Baraffe, I., Chabrier, G., Barman, T. S., Allard, F., & Hauschildt, P. H. 2003, *A&A*, 402, 701
- Barman, T. S., Macintosh, B., Konopacky, Q. M., & Marois, C. 2011, *ApJ*, 733, 65
- Barrado y Navascues, D., Stauffer, J. R., Hartmann, L., & Balachandran, S. C. 1997, *ApJ*, 475, 313
- Barrado y Navascués, D., Stauffer, J. R., Song, I., & Caillault, J.-P. 1999, *ApJ*, 520, L123
- Bell, C. P. M., Naylor, T., Mayne, N. J., Jeffries, R. D., & Littlefair, S. P. 2012, *MNRAS*, 424, 3178
- Biazzo, K., D’Orazi, V., Desidera, S., Covino, E., Alcalá, J. M., & Zusi, M. 2012, *ArXiv e-prints*
- Biller, B. A., Liu, M. C., Wahhaj, Z., Nielsen, E. L., Close, L. M., Dupuy, T. J., Hayward, T. L., Burrows, A., Chun, M., Ftaclas, C., Clarke, F., Hartung, M., Males, J., Reid, I. N., Shkolnik, E. L., Skemer, A., Tecza, M., Thatte, N., Alencar, S. H. P., Artymowicz, P., Boss, A., de Gouveia Dal Pino, E., Gregorio-Hetem, J., Ida, S., Kuchner, M. J., Lin, D., & Toomey, D. 2010, *ApJ*, 720, L82
- Biller, B. A., Wahhaj, Z., Liu, M. C., Nielsen, E. L., Hayward, T. L., et al. 2013, *ApJ*, submitted
- Boccaletti, A., Carillet, M., Fusco, T., Mouillet, D., Langlois, M., Moutou, C., & Dohlen, K. 2008, *ArXiv e-prints*, 807
- Borucki, W. J., Koch, D. G., Basri, G., Batalha, N., Brown, T. M., Bryson, S. T., Caldwell, D., Christensen-Dalsgaard, J., Cochran, W. D., DeVore, E., Dunham, E. W., Gautier, III,

- T. N., Geary, J. C., Gilliland, R., Gould, A., Howell, S. B., Jenkins, J. M., Latham, D. W., Lissauer, J. J., Marcy, G. W., Rowe, J., Sasselov, D., Boss, A., Charbonneau, D., Ciardi, D., Doyle, L., Dupree, A. K., Ford, E. B., Fortney, J., Holman, M. J., Seager, S., Steffen, J. H., Tarter, J., Welsh, W. F., Allen, C., Buchhave, L. A., Christiansen, J. L., Clarke, B. D., Das, S., Désert, J.-M., Endl, M., Fabrycky, D., Fressin, F., Haas, M., Horch, E., Howard, A., Isaacson, H., Kjeldsen, H., Kolodziejczak, J., Kulesa, C., Li, J., Lucas, P. W., Machalek, P., McCarthy, D., MacQueen, P., Meibom, S., Miquel, T., Prsa, A., Quinn, S. N., Quintana, E. V., Ragozzine, D., Sherry, W., Shporer, A., Tenenbaum, P., Torres, G., Twicken, J. D., Van Cleve, J., Walkowicz, L., Witteborn, F. C., & Still, M. 2011, *ApJ*, 736, 19
- Bowler, B. P., Liu, M. C., Dupuy, T. J., & Cushing, M. C. 2010, *ApJ*, 723, 850
- Bryden, G., Beichman, C. A., Carpenter, J. M., Rieke, G. H., Stapelfeldt, K. R., Werner, M. W., Tanner, A. M., Lawler, S. M., Wyatt, M. C., Trilling, D. E., Su, K. Y. L., Blaylock, M., & Stansberry, J. A. 2009, *ApJ*, 705, 1226
- Burkert, A. & Ida, S. 2007, *ApJ*, 660, 845
- Casagrande, L., Schönrich, R., Asplund, M., Cassisi, S., Ramírez, I., Meléndez, J., Bensby, T., & Feltzing, S. 2011, *A&A*, 530, A138
- Chabrier, G., Baraffe, I., Allard, F., & Hauschildt, P. 2000, *ApJ*, 542, 464
- Cignoni, M., Degl’Innocenti, S., Prada Moroni, P. G., & Shore, S. N. 2006, *A&A*, 459, 783
- Crepp, J. R. & Johnson, J. A. 2011, *ApJ*, 733, 126
- Currie, T. 2009, *ApJ*, 694, L171
- Cutri, R. M., Skrutskie, M. F., van Dyk, S., Beichman, C. A., Carpenter, J. M., Chester, T., Cambresy, L., Evans, T., Fowler, J., Gizis, J., Howard, E., Huchra, J., Jarrett, T., Kopan, E. L., Kirkpatrick, J. D., Light, R. M., Marsh, K. A., McCallon, H., Schneider, S., Stiening, R., Sykes, M., Weinberg, M., Wheaton, W. A., Wheelock, S., & Zacarias, N. 2003, 2MASS All Sky Catalog of point sources.
- Dommanget, J. & Nys, O. 2002, *VizieR Online Data Catalog*, 1274, 0
- Dupuy, T. J. & Liu, M. C. 2011, *ApJ*, 733, 122
- Dupuy, T. J., Liu, M. C., & Ireland, M. J. 2009, *ApJ*, 692, 729
- Elias, J. H., Frogel, J. A., Matthews, K., & Neugebauer, G. 1982, *AJ*, 87, 1029
- Feigelson, E. D., Lawson, W. A., Stark, M., Townsley, L., & Garmire, G. P. 2006, *AJ*, 131, 1730
- Fortney, J. J., Marley, M. S., Saumon, D., & Lodders, K. 2008, *ArXiv e-prints*, 805

- Golimowski, D. A., Leggett, S. K., Marley, M. S., Fan, X., Geballe, T. R., Knapp, G. R., Vrba, F. J., Henden, A. A., Luginbuhl, C. B., Guetter, H. H., Munn, J. A., Canzian, B., Zheng, W., Tsvetanov, Z. I., Chiu, K., Glazebrook, K., Hoversten, E. A., Schneider, D. P., & Brinkmann, J. 2004, *AJ*, 127, 3516
- Graham, J. R., Macintosh, B., Doyon, R., Gavel, D., Larkin, J., Levine, M., Oppenheimer, B., Palmer, D., Saddlemyer, L., Sivaramakrishnan, A., Veran, J.-P., & Wallace, K. 2007, *ArXiv e-prints*, 704
- Holman, M. J. & Wiegert, P. A. 1999, *AJ*, 117, 621
- Huélamo, N., Nürnberger, D. E. A., Ivanov, V. D., Chauvin, G., Carraro, G., Sterzik, M. F., Melo, C. H. F., Bonnefoy, M., Hartung, M., Haubois, X., & Foellmi, C. 2010, *A&A*, 521, L54
- Janson, M., Bonavita, M., Klahr, H., Lafrenière, D., Jayawardhana, R., & Zinnecker, H. 2011, *ApJ*, 736, 89
- Jarad, M. M., Hilditch, R. W., & Skillen, I. 1989, *MNRAS*, 238, 1085
- Jayawardhana, R., Fisher, R. S., Hartmann, L., Telesco, C., Pina, R., & Fazio, G. 1998, *ApJ*, 503, L79
- Johnson, B. C., Lisse, C. M., Chen, C. H., Melosh, H. J., Wyatt, M. C., Thebault, P., Henning, W. G., Gaidos, E., Elkins-Tanton, L. T., Bridges, J. C., & Morlok, A. 2012, *ApJ*, 761, 45
- Johnson, J. A., Aller, K. M., Howard, A. W., & Crepp, J. R. 2010, *PASP*, 122, 905
- Johnson, J. A., Butler, R. P., Marcy, G. W., Fischer, D. A., Vogt, S. S., Wright, J. T., & Peek, K. M. G. 2007, *ApJ*, 670, 833
- Jura, M., Ghez, A. M., White, R. J., McCarthy, D. W., Smith, R. C., & Martin, P. G. 1995, *ApJ*, 445, 451
- Kalas, P., Graham, J. R., Chiang, E., Fitzgerald, M. P., Clampin, M., Kite, E. S., Stapelfeldt, K., Marois, C., & Krist, J. 2008, *Science*, 322, 1345
- Kastner, J. H., Zuckerman, B., & Bessell, M. 2008, *A&A*, 491, 829
- Koerner, D. W., Ressler, M. E., Werner, M. W., & Backman, D. E. 1998, *ApJ*, 503, L83
- Kouwenhoven, M. B. N., Brown, A. G. A., Zinnecker, H., Kaper, L., & Portegies Zwart, S. F. 2005, *A&A*, 430, 137
- Kratter, K. M. & Perets, H. B. 2012, *ApJ*, 753, 91
- Kunitomo, M., Ikoma, M., Sato, B., Katsuta, Y., & Ida, S. 2011, *ApJ*, 737, 66

- Lagrange, A.-M., Bonnefoy, M., Chauvin, G., Apai, D., Ehrenreich, D., Boccaletti, A., Gratadour, D., Rouan, D., Mouillet, D., Lacour, S., & Kasper, M. 2010, *Science*, 329, 57
- Lawler, S. M. & Gladman, B. 2012, *ApJ*, 752, 53
- Lin, D. N. C. & Ida, S. 1997, *ApJ*, 477, 781
- Liu, M. C., Dupuy, T. J., & Ireland, M. J. 2008, *ApJ*, 689, 436
- Liu, M. C., Wahhaj, Z., Biller, B. A., Nielsen, E. L., Chun, M., Close, L. M., Ftaclas, C., Hartung, M., Hayward, T. L., Clarke, F., Reid, I. N., Shkolnik, E. L., Tecza, M., Thatte, N., Alencar, S., Artymowicz, P., Boss, A., Burrows, A., de Gouveia Dal Pino, E., Gregorio-Hetem, J., Ida, S., Kuchner, M. J., Lin, D., & Toomey, D. 2010, in *Society of Photo-Optical Instrumentation Engineers (SPIE) Conference Series*, Vol. 7736, *Society of Photo-Optical Instrumentation Engineers (SPIE) Conference Series*
- Lowrance, P. J., Schneider, G., Kirkpatrick, J. D., Becklin, E. E., Weinberger, A. J., Zuckerman, B., Plait, P., Malmuth, E. M., Heap, S. R., Schultz, A., Smith, B. A., Terrile, R. J., & Hines, D. C. 2000, *ApJ*, 541, 390
- Mamajek, E. E. 2009, in *IAU Symposium*, Vol. 258, *IAU Symposium*, ed. E. E. Mamajek, D. R. Soderblom, & R. F. G. Wyse, 375–382
- Mamajek, E. E. 2012, *ApJ*, 754, L20
- Marcy, G. W., Butler, R. P., Vogt, S. S., Fischer, D. A., Wright, J. T., Johnson, J. A., Tinney, C. G., Jones, H. R. A., Carter, B. D., Bailey, J., O’Toole, S. J., & Upadhyay, S. 2008, *Physica Scripta Volume T*, 130, 014001
- Marois, C., Macintosh, B., Barman, T., Zuckerman, B., Song, I., Patience, J., Lafrenière, D., & Doyon, R. 2008, *Science*, 322, 1348
- Marois, C., Zuckerman, B., Konopacky, Q. M., Macintosh, B., & Barman, T. 2010, *Nature*, 468, 1080
- Merín, B., Montesinos, B., Eiroa, C., Solano, E., Mora, A., D’Alessio, P., Calvet, N., Oudmaijer, R. D., de Winter, D., Davies, J. K., Harris, A. W., Collier Cameron, A., Deeg, H. J., Ferlet, R., Garzón, F., Grady, C. A., Horne, K., Miranda, L. F., Palacios, J., Penny, A., Quirrenbach, A., Rauer, H., Schneider, J., & Wesselius, P. R. 2004, *A&A*, 419, 301
- Moerchen, M. M., Telesco, C. M., & Packham, C. 2010, *ApJ*, 723, 1418
- Moerchen, M. M., Telesco, C. M., Packham, C., & Kehoe, T. J. J. 2007, *ApJ*, 655, L109
- Moór, A., Abraham, P., Derekas, A., Kiss, C., Kiss, L. L., Apai, D., Grady, C., & Henning, T. 2006, *ApJ*, 644, 525

- Mouillet, D., Lagrange, A.-M., Beuzit, J.-L., & Renaud, N. 1997, *A&A*, 324, 1083
- Nakajima, T. & Morino, J.-I. 2012, *AJ*, 143, 2
- Neuhäuser, R., Ginski, C., Schmidt, T. O. B., & Mugrauer, M. 2011, *MNRAS*, 416, 1430
- Nielsen, E. L. & Close, L. M. 2010, *ApJ*, 717, 878
- Nielsen, E. L., Close, L. M., Biller, B. A., Masciadri, E., & Lenzen, R. 2008, *ApJ*, 674, 466
- Nielsen, E. L., Liu, M. C., Wahhaj, Z., Biller, B. A., Hayward, T. L., Boss, A., Bowler, B., Kraus, A., Shkolnik, E. L., Tecza, M., Chun, M., Clarke, F., Close, L. M., Ftaclas, C., Hartung, M., Males, J. R., Reid, I. N., Skemer, A. J., Alencar, S. H. P., Burrows, A., de Gouveia Dal Pino, E., Gregorio-Hetem, J., Kuchner, M., Thatte, N., & Toomey, D. W. 2012, *ApJ*, 750, 53
- Nieva, M.-F. & Przybilla, N. 2012, *A&A*, 539, A143
- Rasio, F. A. & Ford, E. B. 1996, *Science*, 274, 954
- Rhee, J. H., Song, I., Zuckerman, B., & McElwain, M. 2007, *ApJ*, 660, 1556
- Riviere-Marichalar, P., Barrado, D., Augereau, J.-C., Thi, W. F., Roberge, A., Eiroa, C., Montesinos, B., Meeus, G., Howard, C., Sandell, G., Duchêne, G., Dent, W. R. F., Lebreton, J., Mendigutía, I., Huélamo, N., Ménard, F., & Pinte, C. 2012, *A&A*, 546, L8
- Salpeter, E. E. 1955, *ApJ*, 121, 161
- Sato, B., Omiya, M., Liu, Y., Harakawa, H., Izumiura, H., Kambe, E., Toyota, E., Murata, D., Lee, B.-C., Masuda, S., Takeda, Y., Yoshida, M., Itoh, Y., Ando, H., Kokubo, E., Ida, S., Zhao, G., & Han, I. 2010, *PASJ*, 62, 1063
- Siess, L., Dufour, E., & Forestini, M. 2000, *A&A*, 358, 593
- Skemer, A. J., Hinz, P. M., Esposito, S., Burrows, A., Leisenring, J., Skrutskie, M., Desidera, S., Mesa, D., Arcidiacono, C., Mannucci, F., Rodigas, T. J., Close, L., McCarthy, D., Kulesa, C., Agapito, G., Apai, D., Argomedo, J., Bailey, V., Boutsia, K., Briguglio, R., Brusa, G., Busoni, L., Claudi, R., Eisner, J., Fini, L., Follette, K. B., Garnavich, P., Gratton, R., Guerra, J. C., Hill, J. M., Hoffmann, W. F., Jones, T., Krejny, M., Males, J., Masciadri, E., Meyer, M. R., Miller, D. L., Morzinski, K., Nelson, M., Pinna, E., Puglisi, A., Quanz, S. P., Quiros-Pacheco, F., Riccardi, A., Stefanini, P., Vaitheeswaran, V., Wilson, J. C., & Xompero, M. 2012, *ApJ*, 753, 14
- Smith, R., Churcher, L. J., Wyatt, M. C., Moerchen, M. M., & Telesco, C. M. 2009, *A&A*, 493, 299
- Soderblom, D. R. 2010, *ARA&A*, 48, 581

- Song, I., Caillault, J.-P., Barrado y Navascués, D., & Stauffer, J. R. 2001, *ApJ*, 546, 352
- Stauffer, J. R., Hartmann, L. W., Fazio, G. G., Allen, L. E., Patten, B. M., Lowrance, P. J., Hurt, R. L., Rebull, L. M., Cutri, R. M., Ramirez, S. V., Young, E. T., Rieke, G. H., Gorlova, N. I., Muzerolle, J. C., Slesnick, C. L., & Skrutskie, M. F. 2007, *ApJS*, 172, 663
- Stauffer, J. R., Schultz, G., & Kirkpatrick, J. D. 1998, *ApJ*, 499, L199
- Su, K. Y. L., Rieke, G. H., Stansberry, J. A., Bryden, G., Stapelfeldt, K. R., Trilling, D. E., Muzerolle, J., Beichman, C. A., Moro-Martín, A., Hines, D. C., & Werner, M. W. 2006, *ApJ*, 653, 675
- Su, K. Y. L., Rieke, G. H., Stapelfeldt, K. R., Smith, P. S., Bryden, G., Chen, C. H., & Trilling, D. E. 2008, *ApJ*, 679, L125
- Takeda, G., Ford, E. B., Sills, A., Rasio, F. A., Fischer, D. A., & Valenti, J. A. 2007, *ApJS*, 168, 297
- Thalmann, C., Janson, M., Buenzli, E., Brandt, T. D., Wisniewski, J. P., Moro-Martín, A., Usuda, T., Schneider, G., Carson, J., McElwain, M. W., Grady, C. A., Goto, M., Abe, L., Brandner, W., Dominik, C., Egner, S., Feldt, M., Fukue, T., Golota, T., Guyon, O., Hashimoto, J., Hayano, Y., Hayashi, M., Hayashi, S., Henning, T., Hodapp, K. W., Ishii, M., Iye, M., Kandori, R., Knapp, G. R., Kudo, T., Kusakabe, N., Kuzuhara, M., Matsuo, T., Miyama, S., Morino, J.-I., Nishimura, T., Pyo, T.-S., Serabyn, E., Suto, H., Suzuki, R., Takahashi, Y. H., Takami, M., Takato, N., Terada, H., Tomono, D., Turner, E. L., Watanabe, M., Yamada, T., Takami, H., & Tamura, M. 2011, *ApJ*, 743, L6
- van Leeuwen, F. 2007, *A&A*, 474, 653
- Vigan, A., Patience, J., Marois, C., Bonavita, M., De Rosa, R. J., Macintosh, B., Song, I., Doyon, R., Zuckerman, B., Lafrenière, D., & Barman, T. 2012, *A&A*, 544, A9
- Wahhaj, Z., Koerner, D. W., Backman, D. E., Werner, M. W., Serabyn, E., Ressler, M. E., & Lis, D. C. 2005, *ApJ*, 618, 385
- Wahhaj, Z., Liu, M. C., Biller, B. A., Clarke, F., Nielsen, E. L., Close, L. M., Hayward, T. L., Mamajek, E. E., Cushing, M., Dupuy, T., Tecza, M., Thatte, N., Chun, M., Ftaclas, C., Hartung, M., Reid, I. N., Shkolnik, E. L., Alencar, S. H. P., Artymowicz, P., Boss, A., de Gouveia Dal Pino, E., Gregorio-Hetem, J., Ida, S., Kuchner, M., Lin, D. N. C., & Toomey, D. W. 2011, *ApJ*, 729, 139
- Wahhaj, Z., Liu, M. C., Biller, B. A., Nielsen, E. L., Hayward, T. L., et al. 2013a, *ApJ*, submitted
- . 2013b, *ApJ*, submitted
- Weidenschilling, S. J. & Marzari, F. 1996, *Nature*, 384, 619

- Weinberger, A. J., Becklin, E. E., Schneider, G., Smith, B. A., Lowrance, P. J., Silverstone, M. D., Zuckerman, B., & Terrile, R. J. 1999, *ApJ*, 525, L53
- Weinberger, A. J., Rich, R. M., Becklin, E. E., Zuckerman, B., & Matthews, K. 2000, *ApJ*, 544, 937
- Wyatt, M. C., Kennedy, G., Sibthorpe, B., Moro-Martín, A., Lestrade, J.-F., Ivison, R. J., Matthews, B., Udry, S., Greaves, J. S., Kalas, P., Lawler, S., Su, K. Y. L., Rieke, G. H., Booth, M., Bryden, G., Horner, J., Kavelaars, J. J., & Wilner, D. 2012, *MNRAS*, 424, 1206
- Zuckerman, B., Rhee, J. H., Song, I., & Bessell, M. S. 2011, *ApJ*, 732, 61
- Zuckerman, B. & Song, I. 2004, *ARA&A*, 42, 685
- . 2012, ArXiv e-prints
- Zuckerman, B., Song, I., Bessell, M. S., & Webb, R. A. 2001, *ApJ*, 562, L87

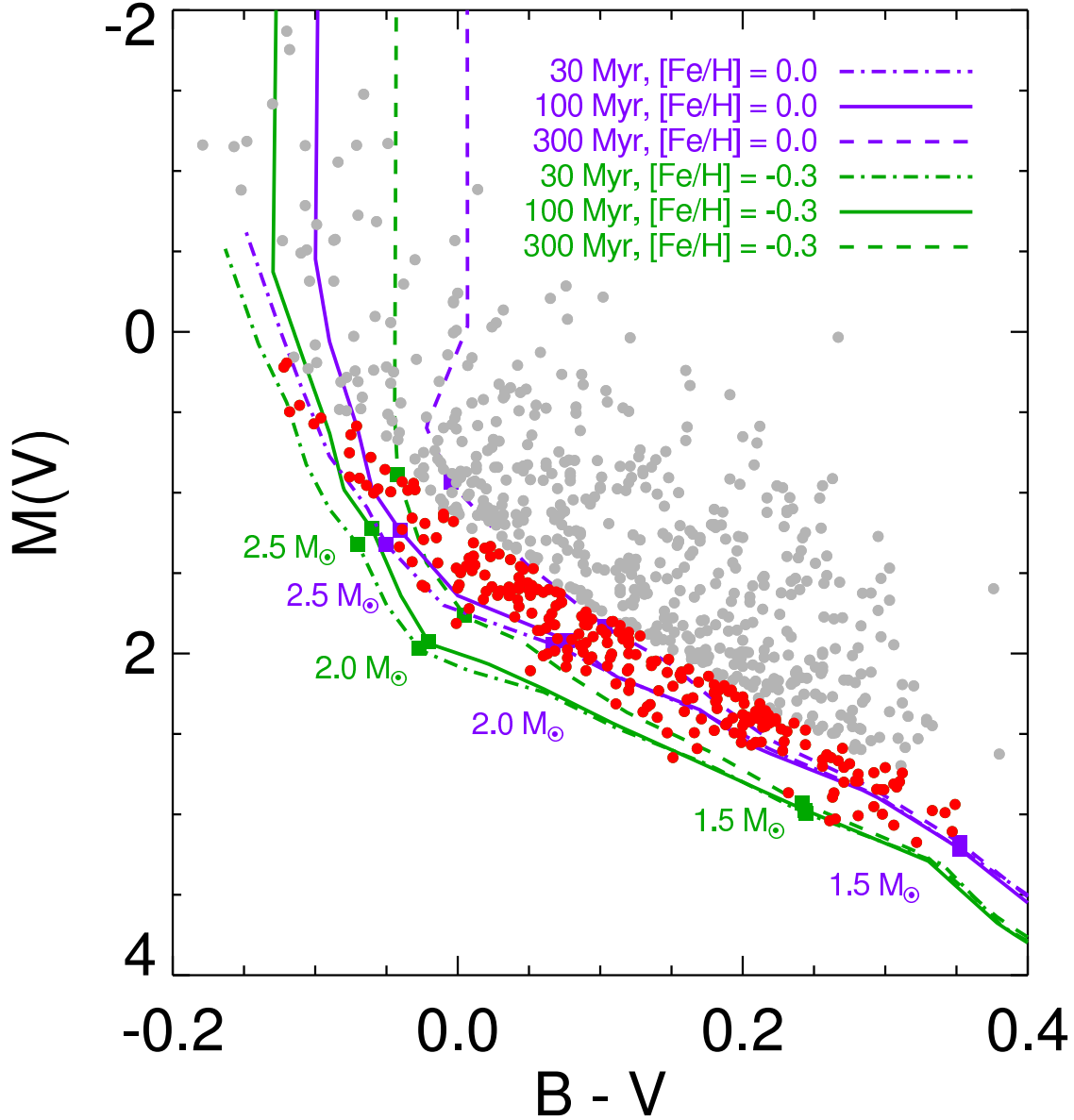


Fig. 1.— Color-magnitude diagram for a volume-limited ( $<100$  pc) sample of Hipparcos B and A stars, with isochrones from Siess et al. (2000) overlaid. Squares mark the locations on the isochrones of  $2.5$ ,  $2.0$ , and  $1.5 M_{\odot}$ . We select candidate young stars (red points) as those that lie below the fit to the young cluster A stars from Lowrance et al. (2000). These stars appear young when compared to the solar metallicity isochrones; however, the half-solar abundance isochrones ( $[\text{Fe}/\text{H}] = -0.3$ ) with older ages ( $\geq 100$  Myr) can fit these “low CMD” stars equally well.

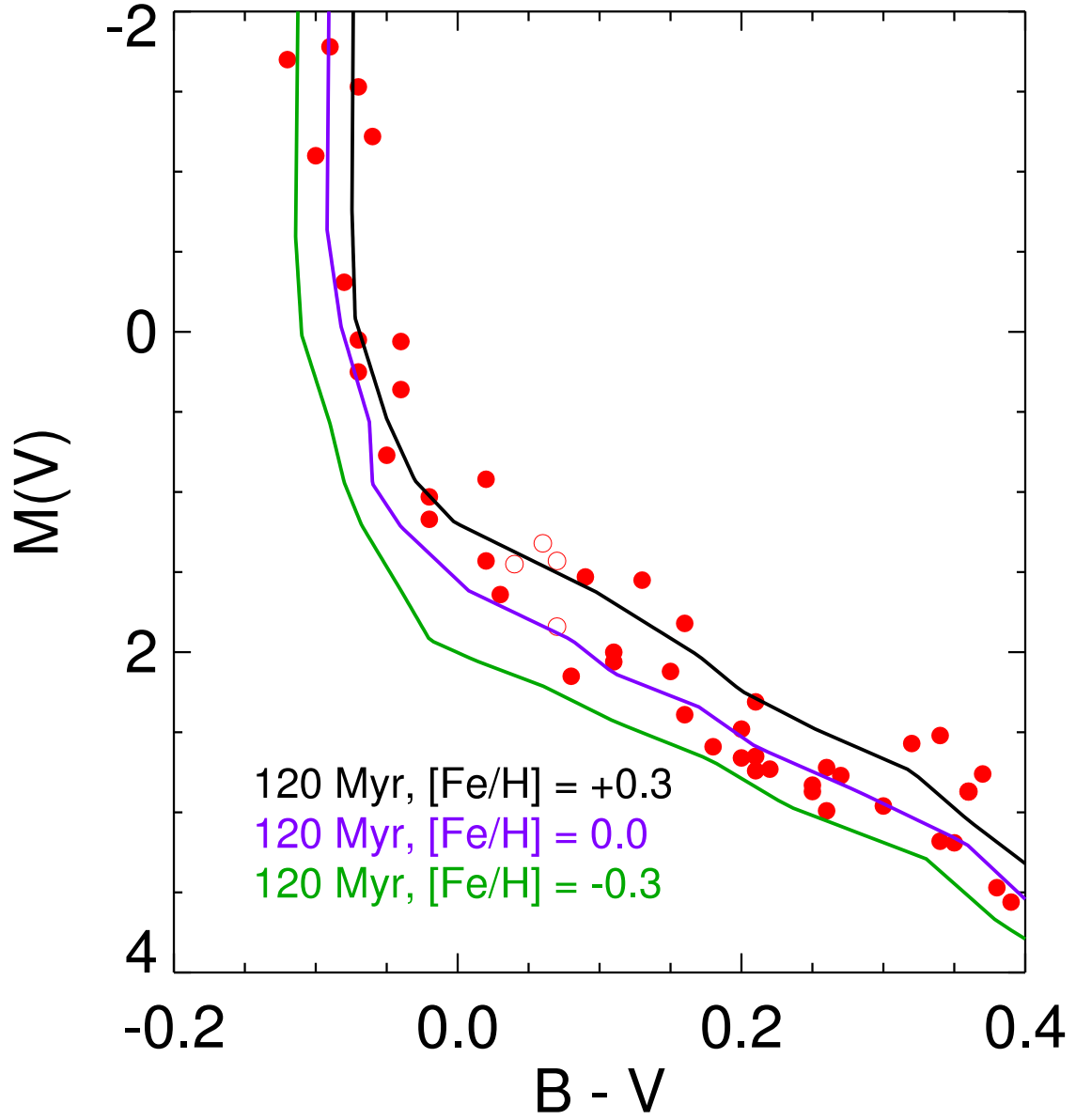


Fig. 2.— High-mass Pleiades stars (Stauffer et al. 2007), with known binaries plotted as open circles, compared to 120 Myr tracks of three metallicities from Siess et al. (2000). The solar metallicity isochrone is consistent with the Pleiades single-star sequence.

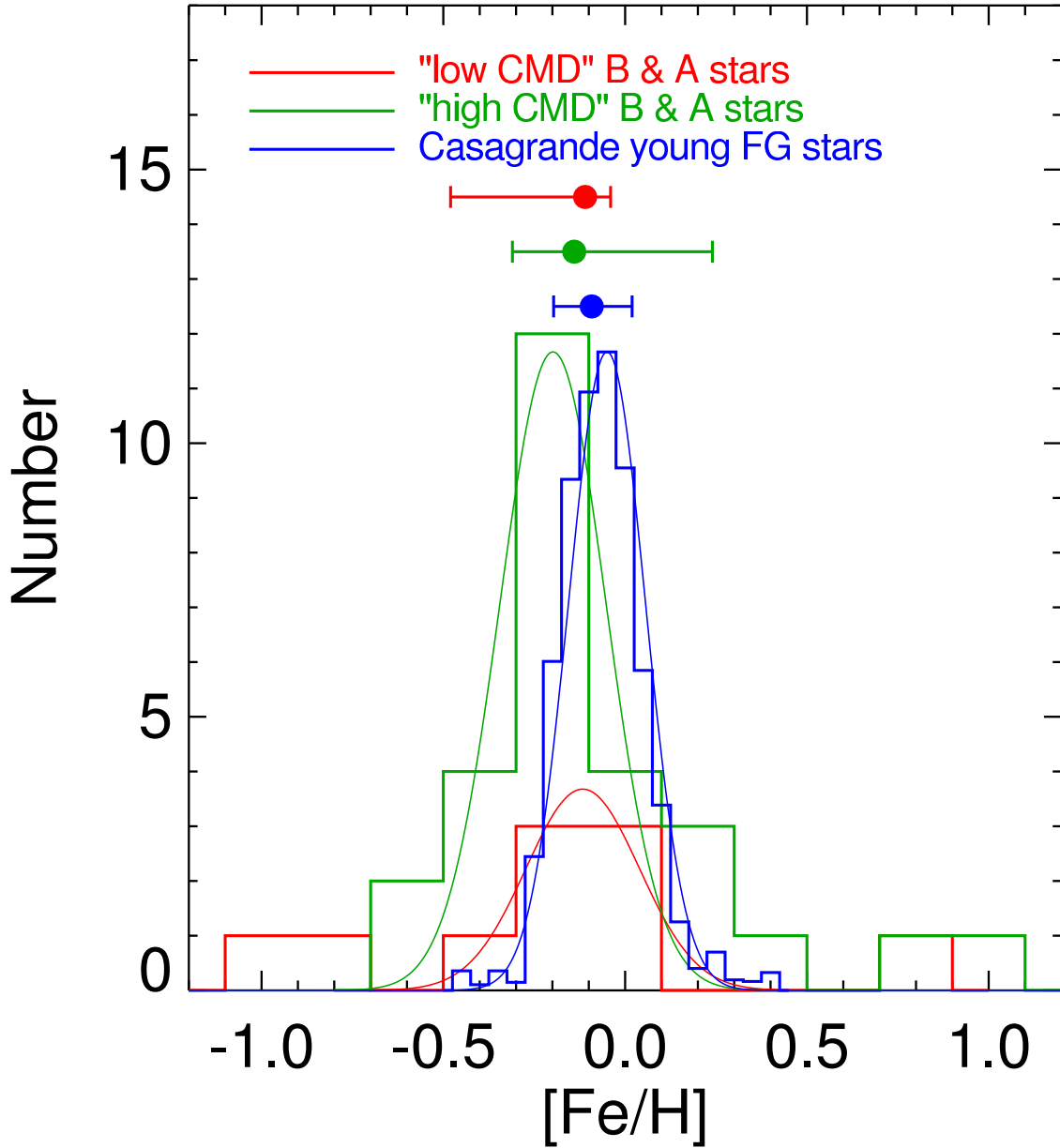


Fig. 3.— Histogram of metallicities for Hipparcos B and A stars from literature measurements. Both “low CMD” (red histogram) and “high CMD” (green histogram) stars agree well with each other and also to the Casagrande et al. (2011) measurement of young (<1 Gyr) solar neighborhood F and G stars (blue histogram). The Casagrande et al. (2011) histogram has been extracted from their Figure 16 and normalized to match the peak of our fit for the “high CMD” stars. Filled circles with error bars indicate the median and 68% confidence intervals for each histogram.

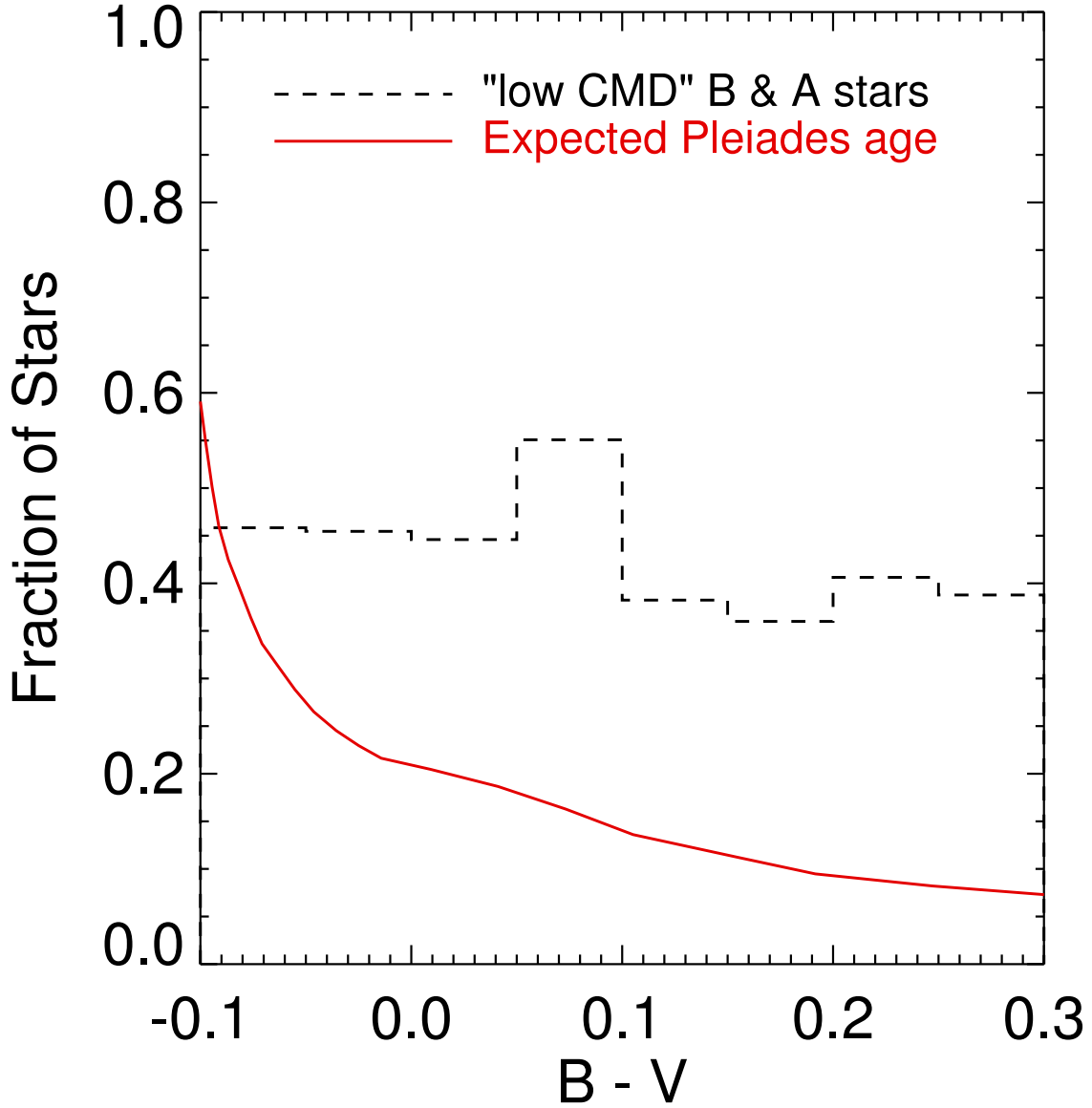


Fig. 4.— The fraction of stars lying low on the color-magnitude diagram (“low CMD”) from our Hipparcos volume-limited sample as a function of  $B - V$  color (black histogram), compared to the expected number of stars the same age as the Pleiades or younger ( $\leq 125$  Myr, red curve), given the mean main-sequence lifetime of solar metallicity stars as a function of zero-age main-sequence color (Siess et al. 2000) and assuming a constant star formation rate. Even ignoring the presence of low-metallicity stars, assigning Pleiades age to all “low CMD” stars overpredicts the fraction of young A stars in a sample, especially at later spectral types.

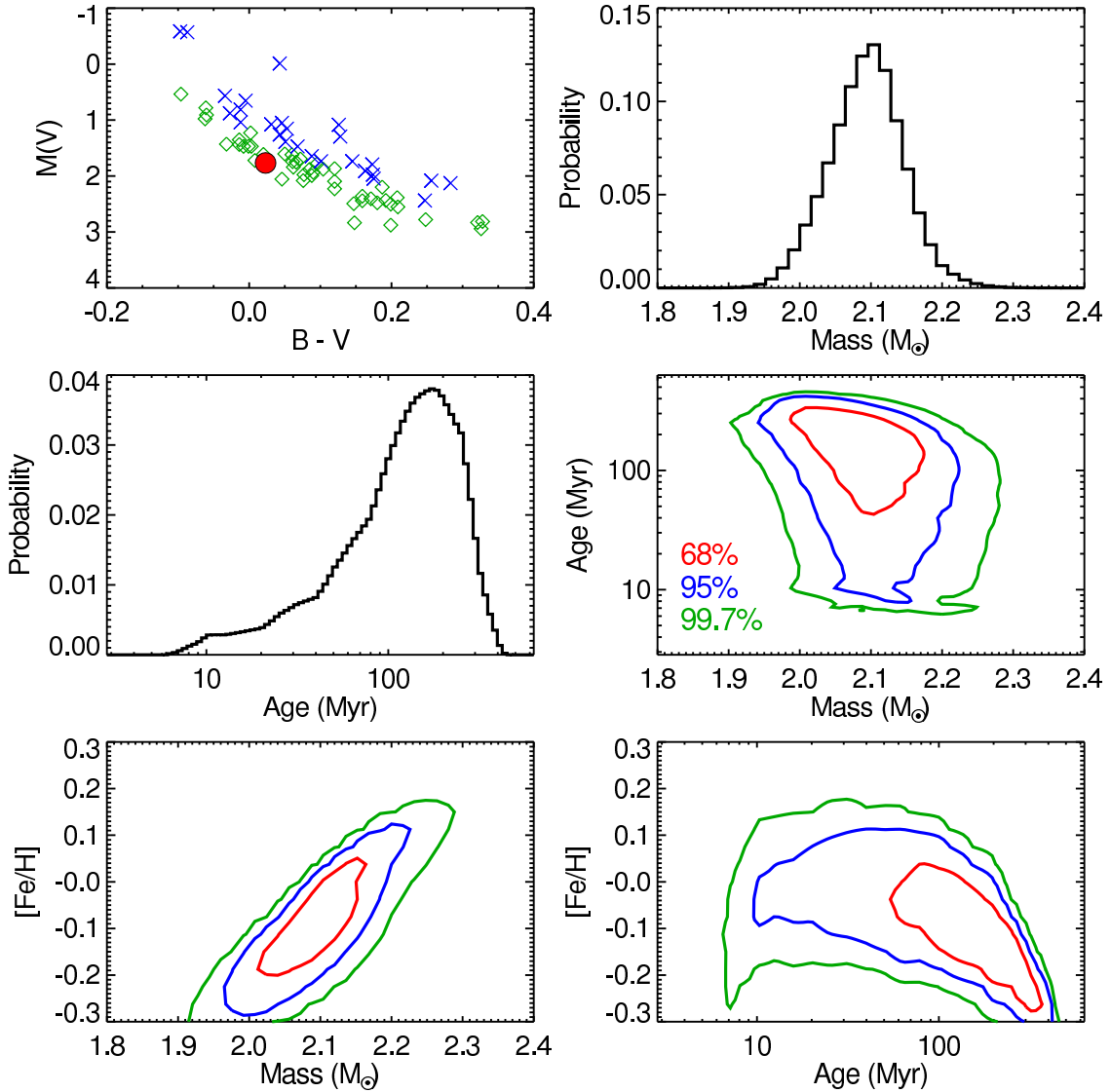


Fig. 5.— An example of our Bayesian method for determining ages, applied to the A0 star HD 24966. Top left: the position of HD 24966 (filled red circle) on the color-magnitude diagram compared to the other NICI Campaign B and A stars; the star lies among the “low CMD” (green diamonds) stars. Blue crosses denote the “high CMD” NICI B and A target stars. Top right and middle left panels: the posterior PDFs for mass and age from our Bayesian analysis, showing a well-defined mass and a relatively wide age distribution. The median age is 128 Myr with 68% confidence limit from 51–227 Myr. Middle right, bottom left, and bottom right panels: 2D contour plots indicating the covariance of the three stellar parameters. In general, older ages correspond to lower metallicities for this star.

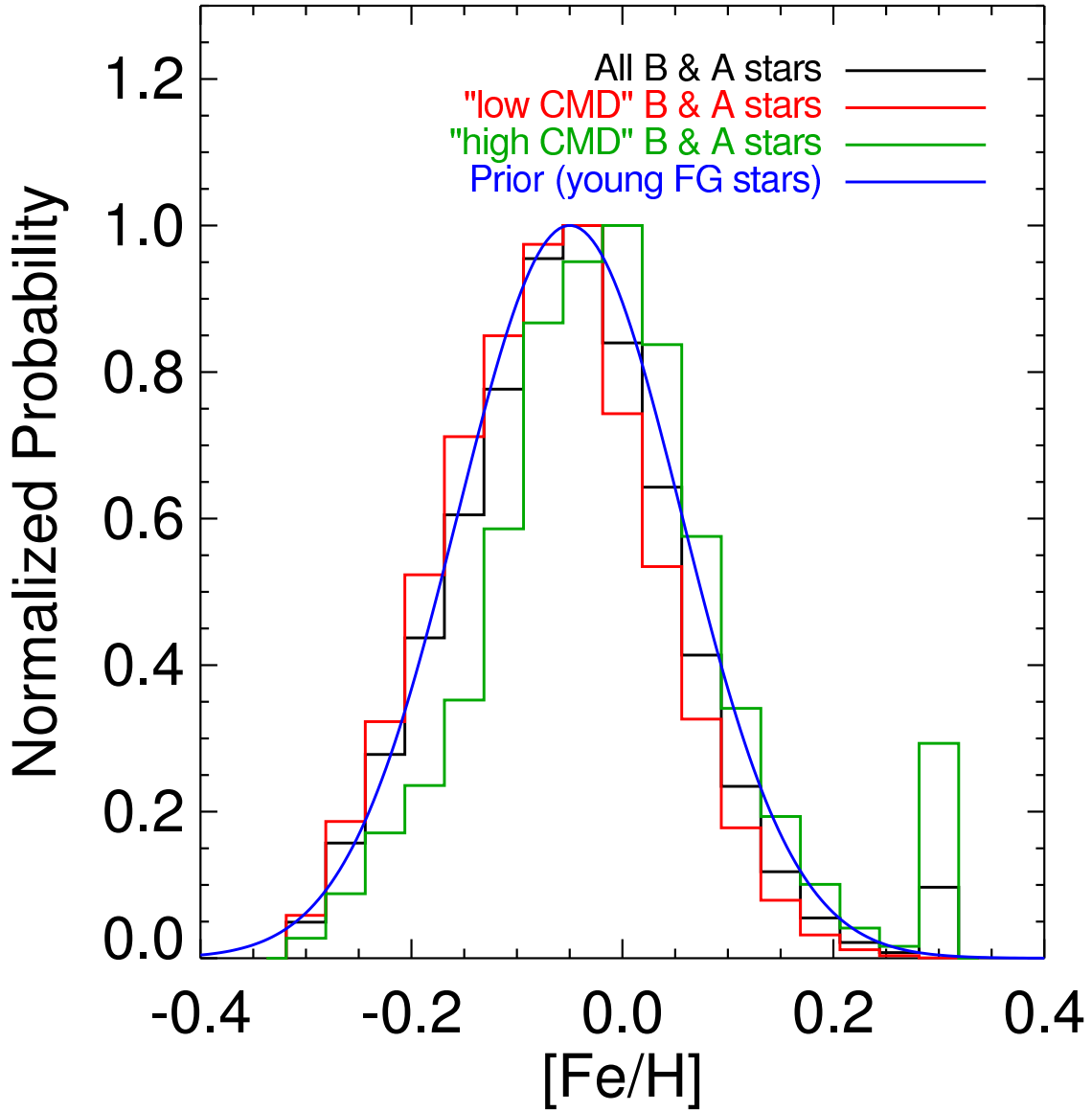


Fig. 6.— Combined metallicity posterior PDFs for all B and A stars in our NICI sample (black histogram) compared to our adopted metallicity prior, the Casagrande et al. (2011) measurements for F and G stars younger than 1 Gyr (blue curve). In general, our Bayesian method finds lower metallicities (consistent with the prior) for “low CMD” B and A stars (red histogram) and slightly higher metallicities for “high CMD” stars (green histogram).

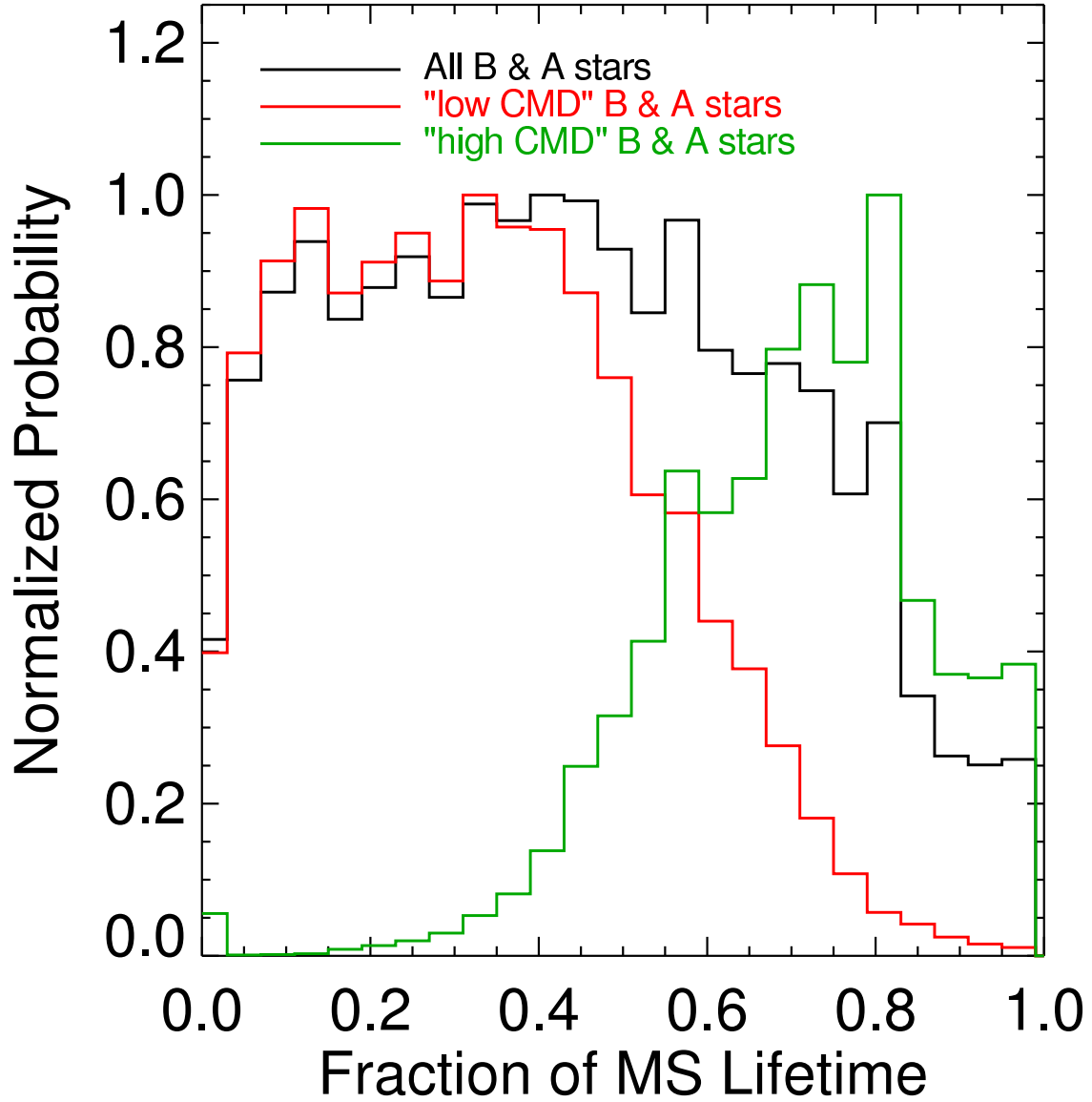


Fig. 7.— Combined age posterior PDFs for our NICI sample of B and A stars normalized to the inferred main-sequence lifetime (black histogram). As expected, the “low CMD” stars (red histogram) are systematically closer to the beginning of the main sequence compared to “high CMD” stars (green histogram), even when metallicity is taken into account.

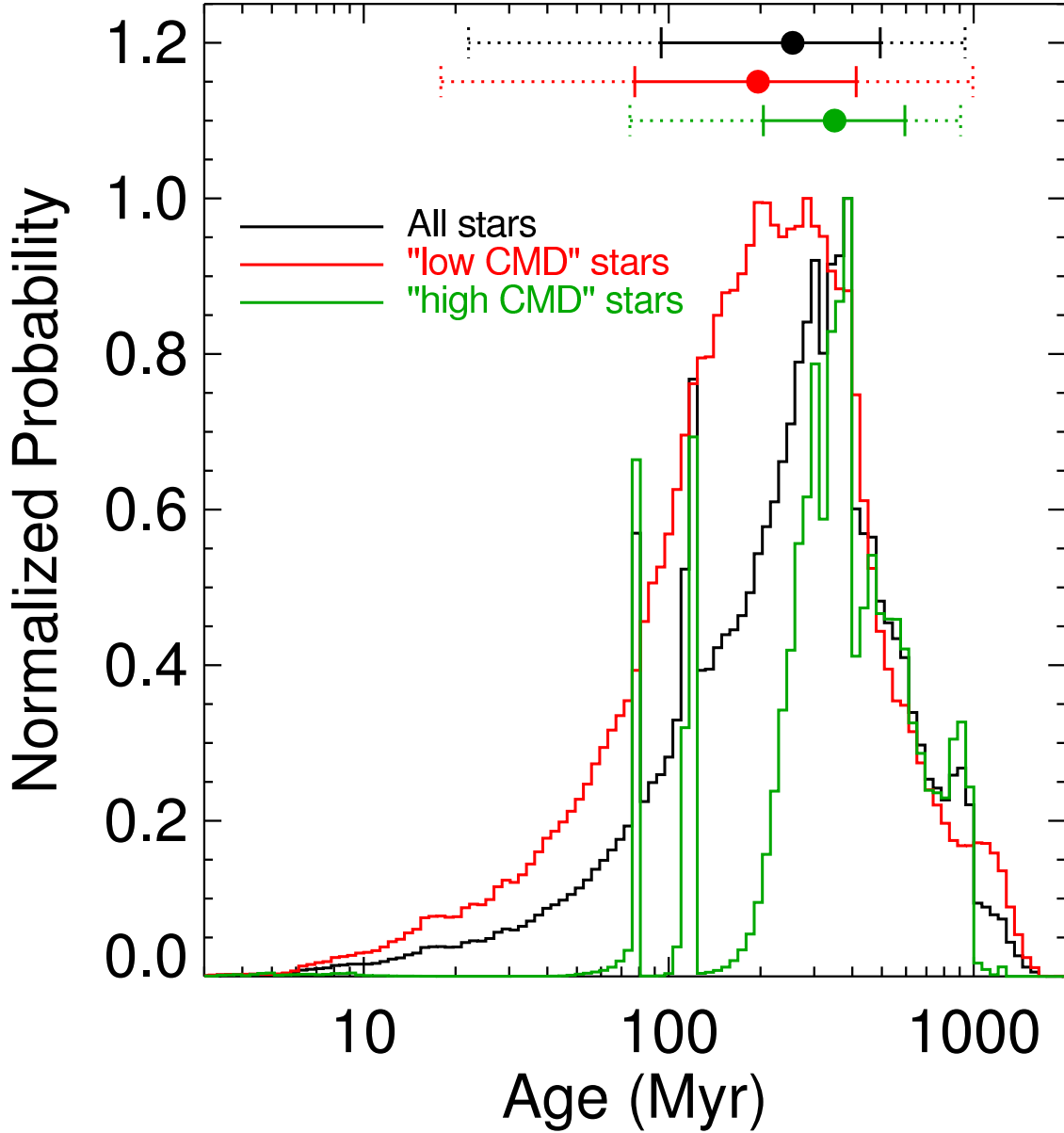


Fig. 8.— As in Figure 7, the combined age PDFs for our targets but now with absolute ages. At the top of the plot we note the location of the median (filled circle), 68% confidence level (inner brackets) and 95% confidence level (outer brackets) for each combined PDF. The overall sample is peaked at 300 Myr, falling quickly to  $\sim 1$  Gyr, with a young age tail extending to  $\sim 10$  Myr. Spikes in the distribution for “high CMD” stars at 78, 115, and 118 Myr are due to the stars HIP 74785, HIP 49669, and HIP 36188, which have spectral types B8, B7, and B8 respectively. The posterior age PDFs of these stars are essentially delta functions at the oldest allowable ages in the Siess et al. (2000) isochrones at the  $B - V$  of these stars, since their  $V$  magnitudes are significantly brighter than the isochrone values at the end of the main sequence.

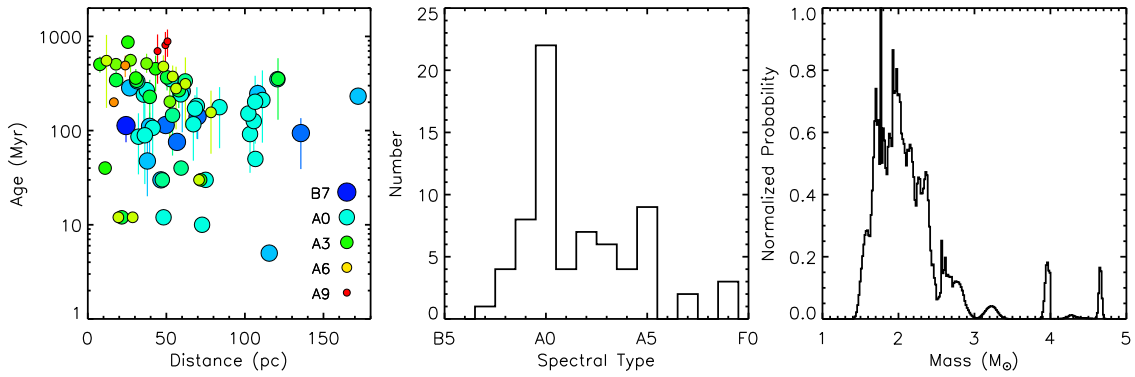


Fig. 9.— Properties of the 70 B and A stars observed by the Gemini NICI Planet-Finding Campaign. (*left*) Age and distance of our target stars, with symbol size and color corresponding to spectral type. Stars in a moving group are presented at a single age, while stars where we derive the age from our Bayesian method are plotted at the median age, with error bars indicating the 68% confidence interval. (*middle*) A histogram showing the spectral types of our target stars. (*right*) The mass distribution of our sample, produced by combining the mass posterior PDFs for each of our target stars from our Bayesian analysis. The median of the mass distribution is  $2 M_{\odot}$ , 60 of our 70 stars have a median mass between  $1.5\text{--}2.5 M_{\odot}$ , and 66 have a median mass less than  $3 M_{\odot}$ .

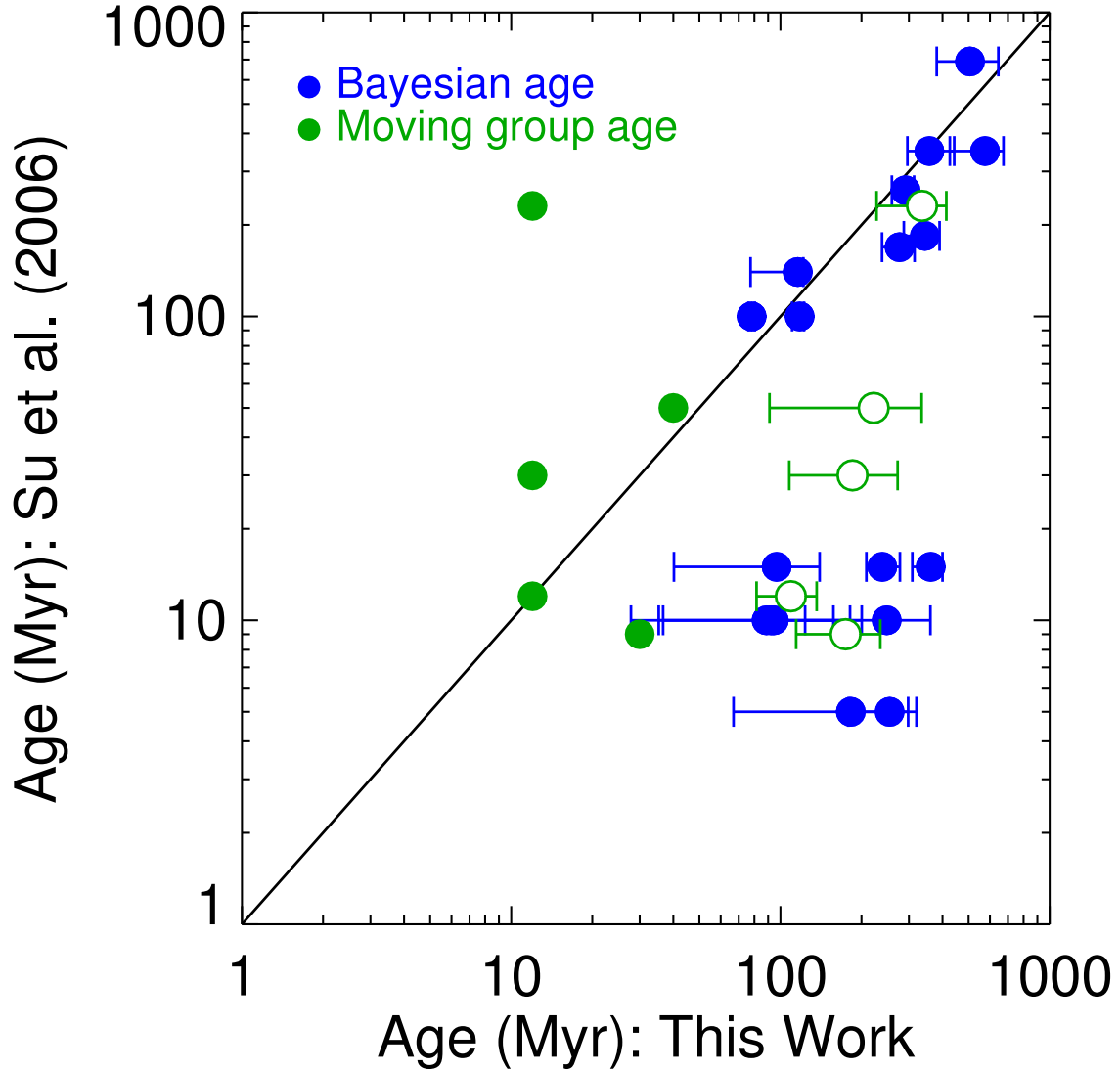


Fig. 10.— Comparison of the ages derived using our Bayesian analysis to ages from Su et al. (2006) based on CMD analysis. For stars that do not belong to known moving groups we give the Bayesian age as the median and 68% confidence interval (filled blue circle and error bars). Stars with an independent age measurement from membership in a moving group (as detailed in Table 1) are plotted twice, once as an empty green circle with error bars indicating the results of the Bayesian analysis and again as a filled green circle indicating the age of the moving group, which we adopt as the final age for that star. There is good agreement between our work and Su et al. (2006) for stars that Su et al. (2006) flag as older than 100 Myr, but below that age our Bayesian analysis finds systematically older ages as expected. For the moving group stars, since the Bayesian analysis of photometry can only place a star in the first third of its main-sequence lifetime, additional information is needed to age-date young stars with greater accuracy.

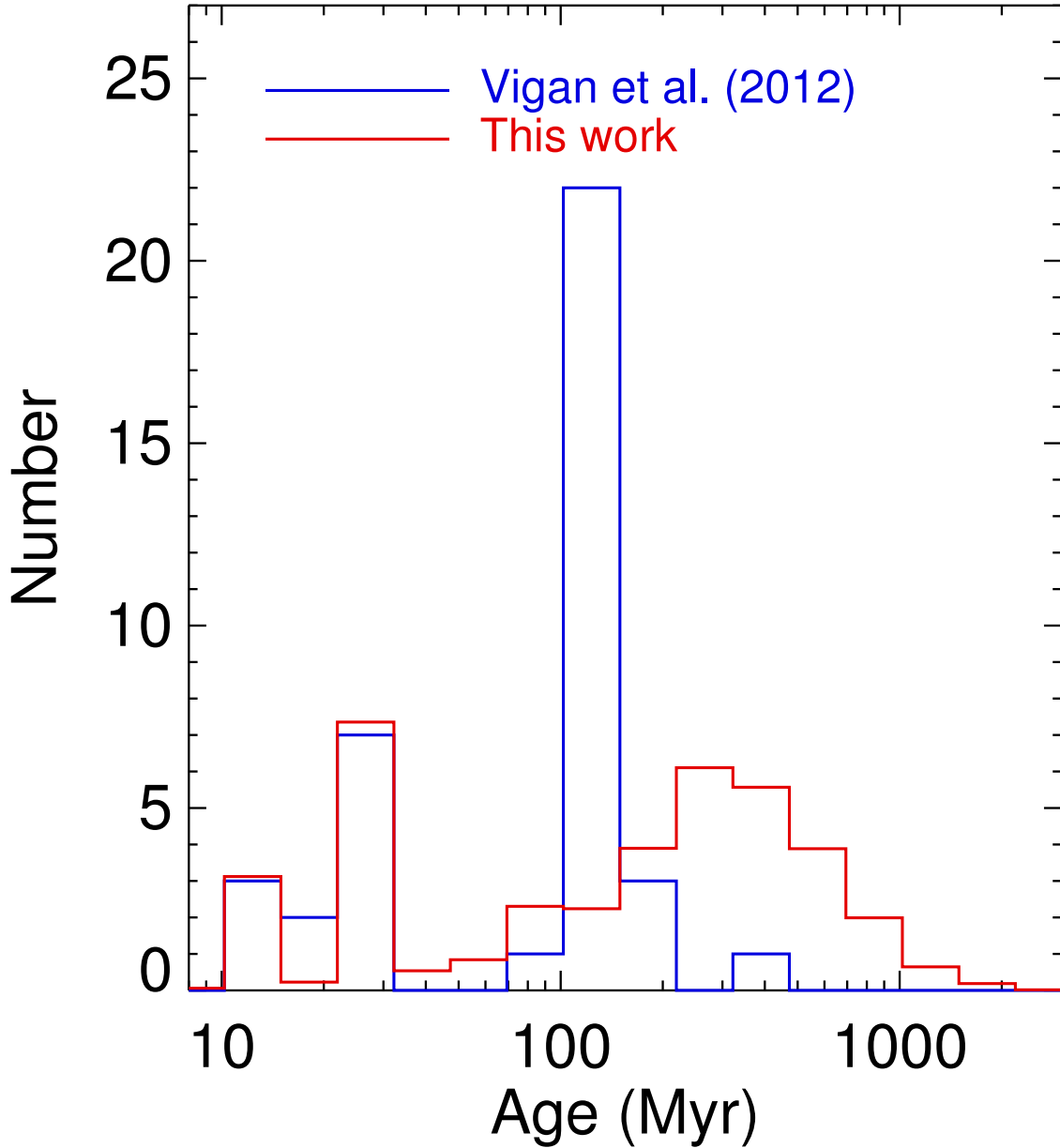


Fig. 11.— Ages for stars in the Vigan et al. (2012) sample, using their ages (blue) and ages from our Bayesian analysis (red). Ages for stars in moving groups (at 12, 30 and 70 Myr) are the same in both histograms, while for the remaining stars the posterior PDFs from our Bayesian analysis are used to populate each age bin. Vigan et al. (2012) have a significant spike at 125 Myr, where 17 of their 39 stars are assumed to have the age of the Pleiades. Our Bayesian analysis suggests much older ages for these stars, with a peak at 300 Myr and a tail extending beyond 1 Gyr.

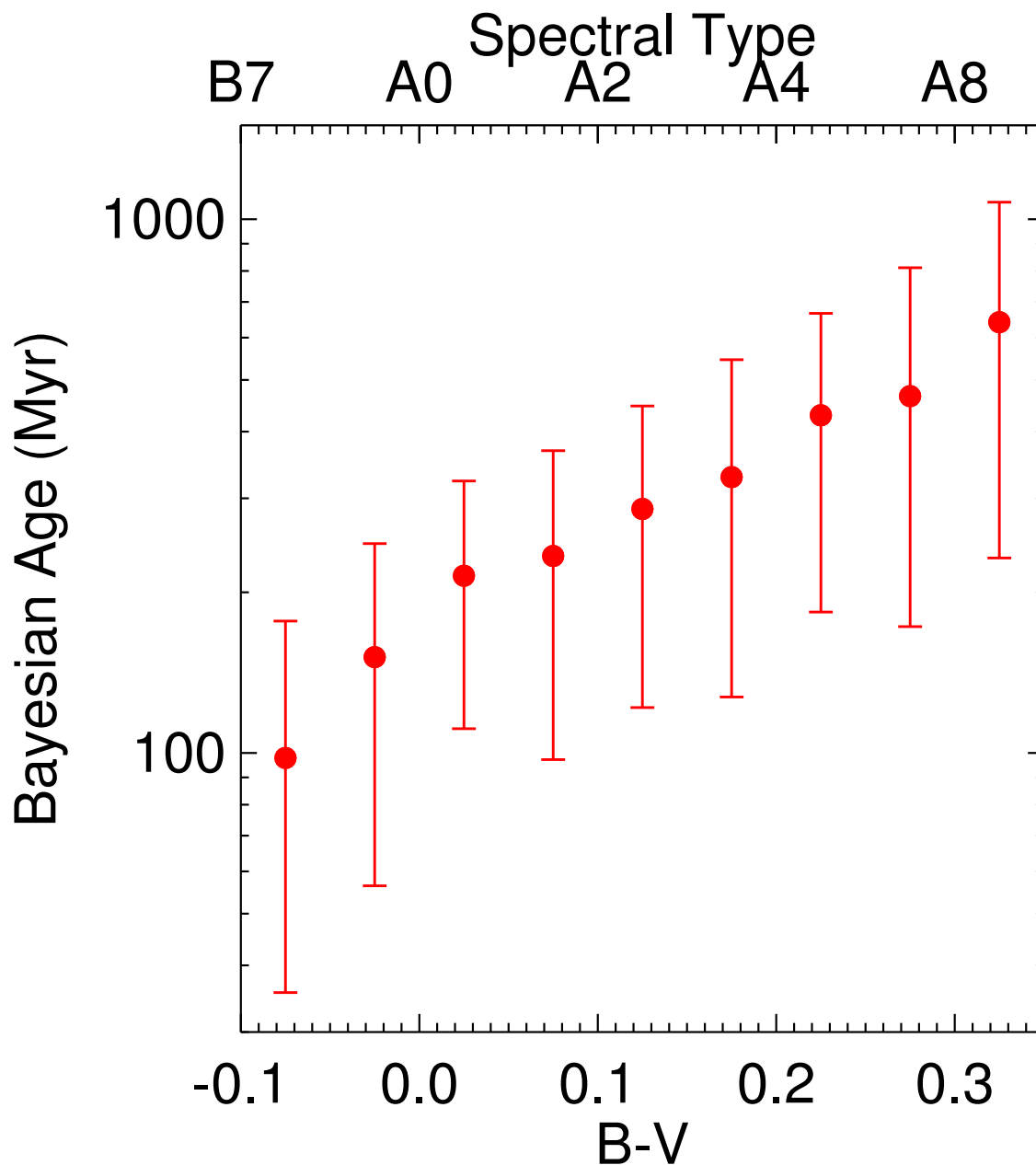


Fig. 12.— Bayesian ages for “low CMD” stars in our volume-limited sample. The stars are divided into bins by  $B - V$  color, and the age posterior PDFs are combined within each bin. Approximate spectral type as a function of  $B - V$  color is given on the top axis. The filled circle and error bars then give the median and 68% confidence interval for that bin, with most bins containing about 25 stars. Assigning Pleiades ages (125 Myr) to these stars is reasonable only at the bluest colors; later-type A stars that are faint on the color-magnitude diagram are likely to be significantly older.

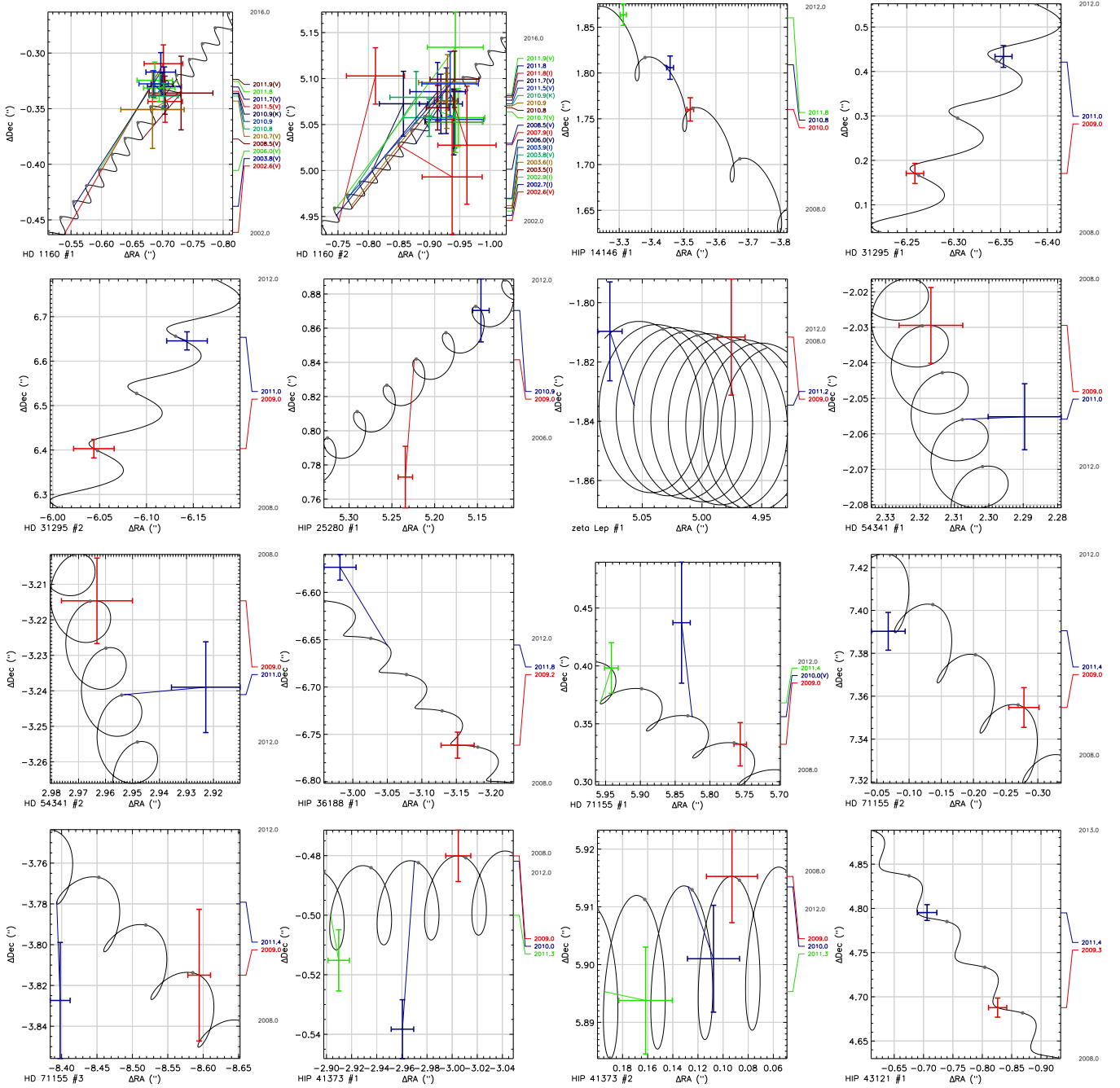


Fig. 13.— On-sky motion of candidate companions listed in Table 3. For each candidate, the background track (black curve) is calculated from the proper motion and parallax of the star and position of the candidate at the initial reference epoch. Astrometry at the reference epoch and additional epochs are shown as points with error bars, and a colored line connects the position at additional epochs to the expected position on the background track. The labels at the right of each plot give the epochs of each astrometric data point, at the vertical position corresponding to the location on the background track for that epoch. When the epoch is given alone, the observation was conducted with the NICI instrument. Otherwise observational data are taken from VLT NACO (V), Keck NIRC2 (K), HST NICMOS (H), VLT ISAAC (I), ESO 3.6m COME-ON-PLUS/ADONIS (E), and Gemini-North NIRI (G).

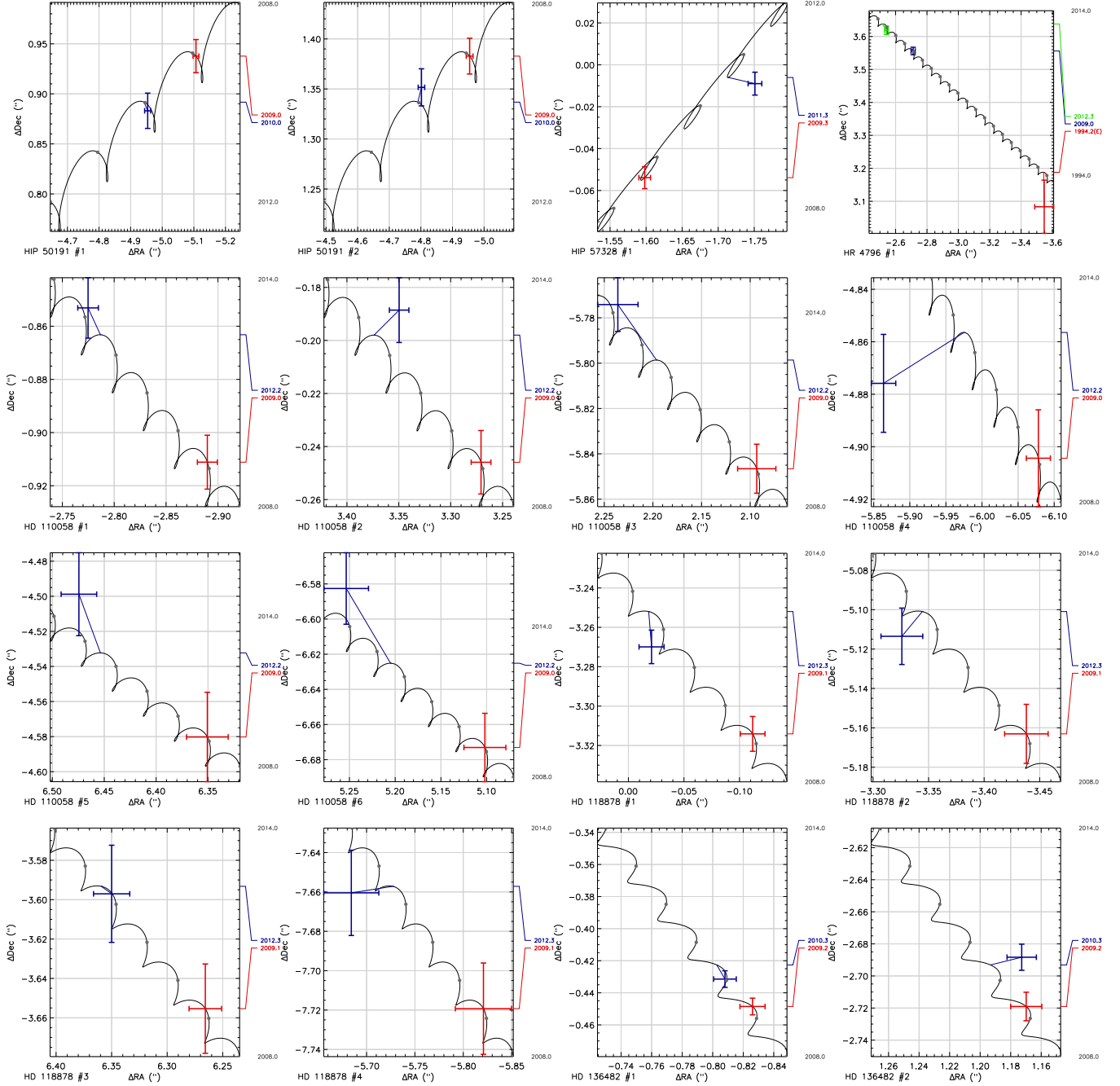


Fig. 14.— Candidate companion on-sky motion, continued from Figure 13.

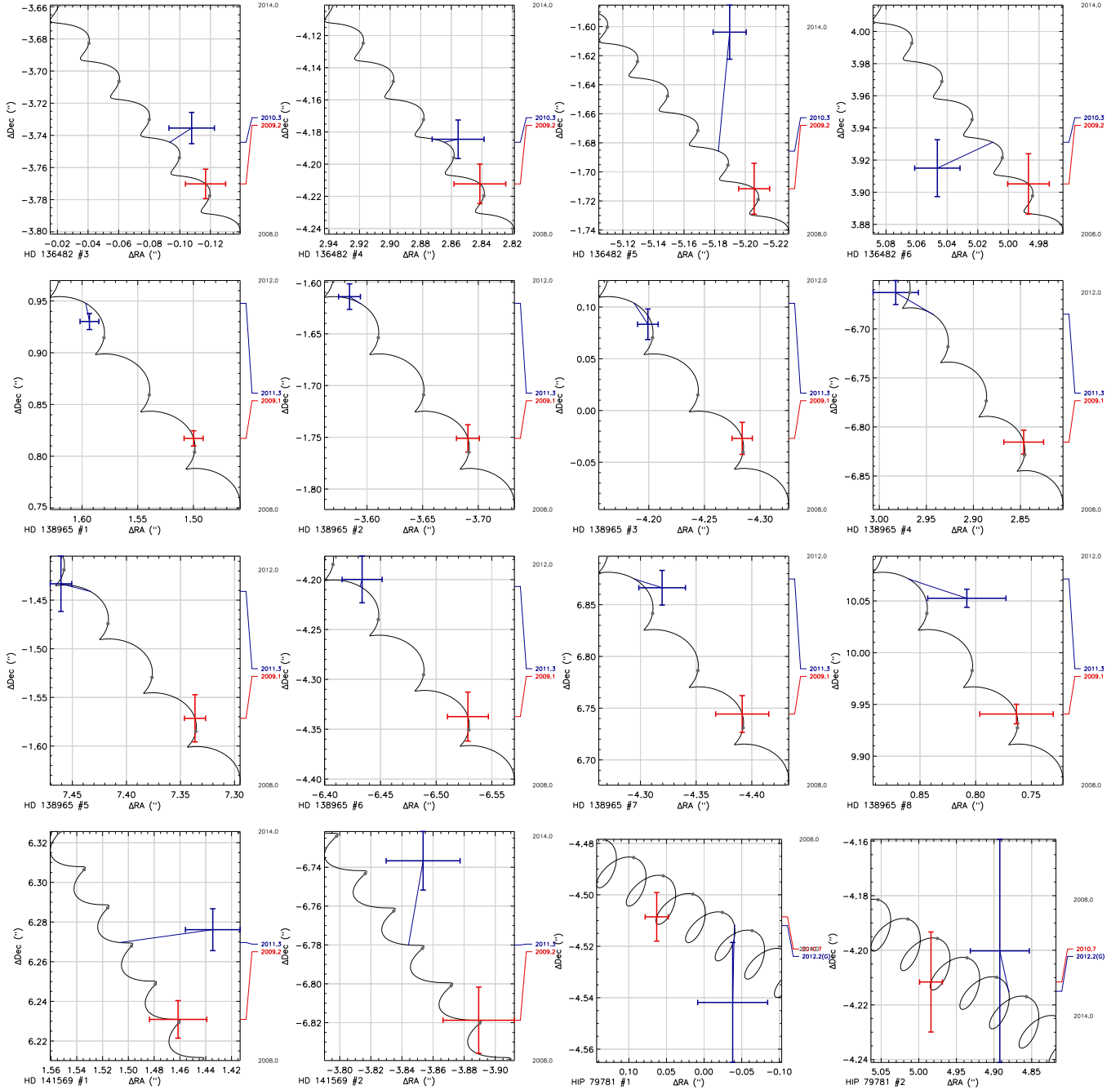


Fig. 15.— Candidate companion on-sky motion, continued from Figures 13 and 14.

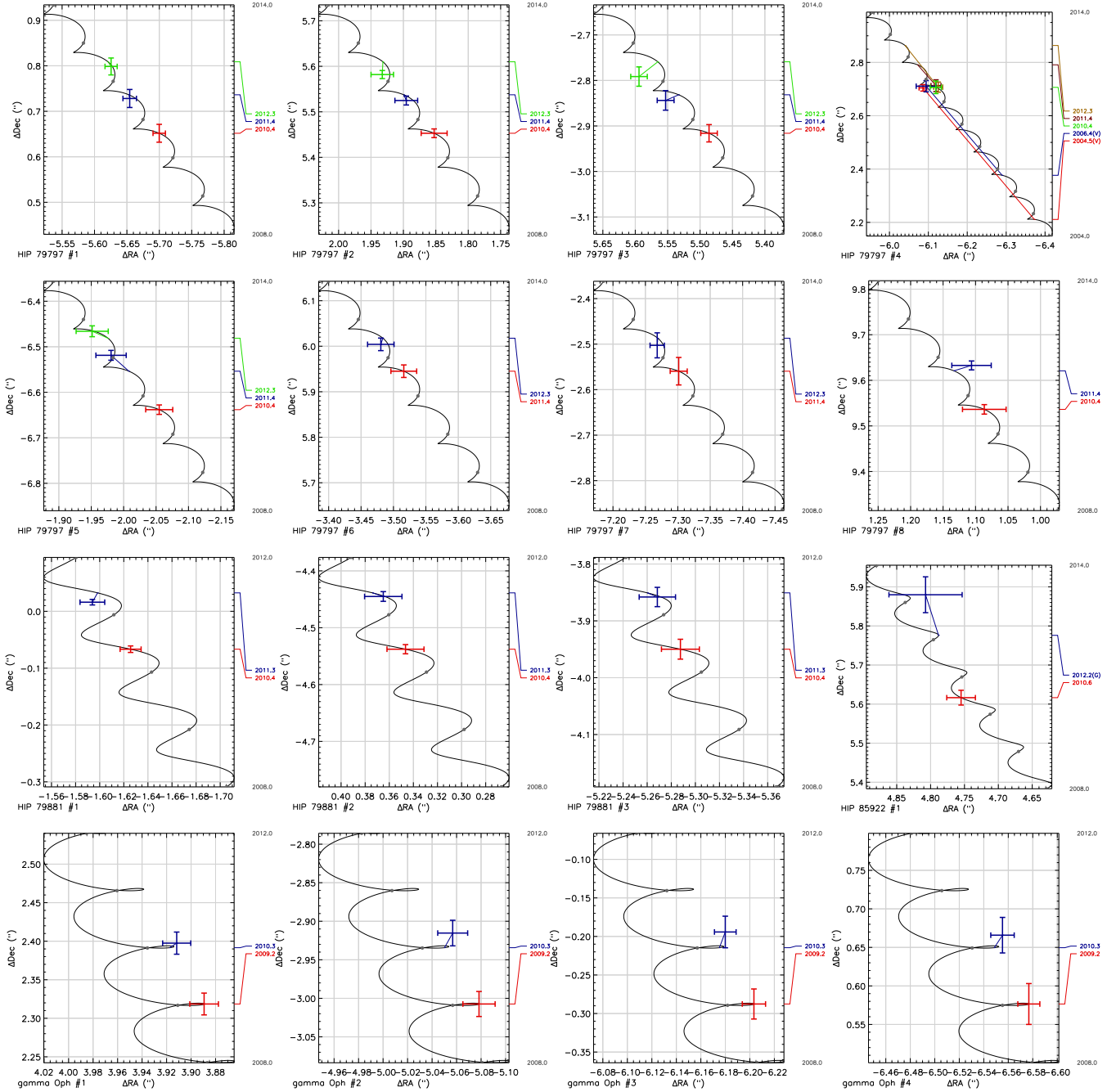


Fig. 16.— Candidate companion on-sky motion, continued from Figures 13–15.

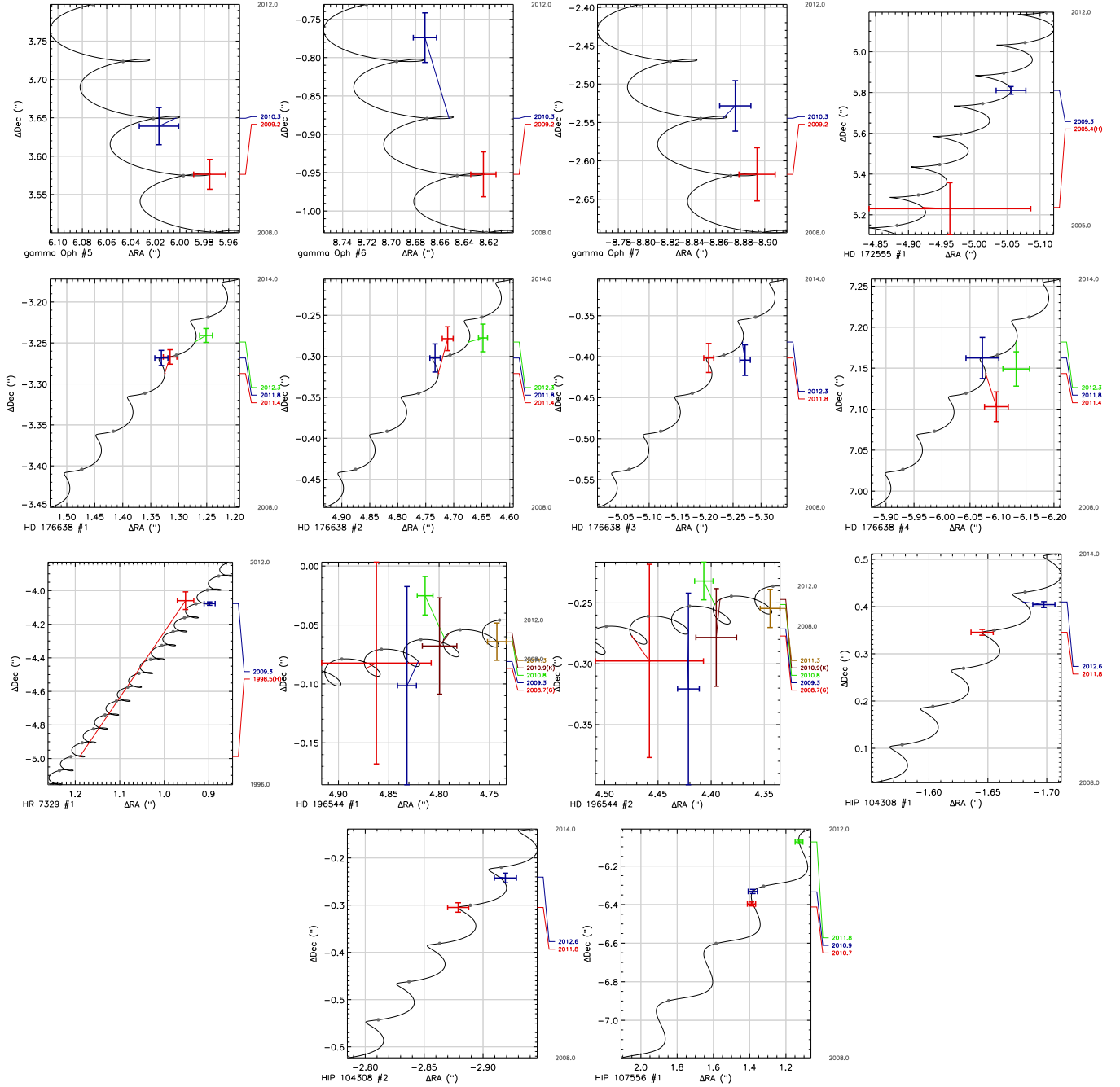


Fig. 17.— Candidate companion on-sky motion, continued from Figures 13–16.

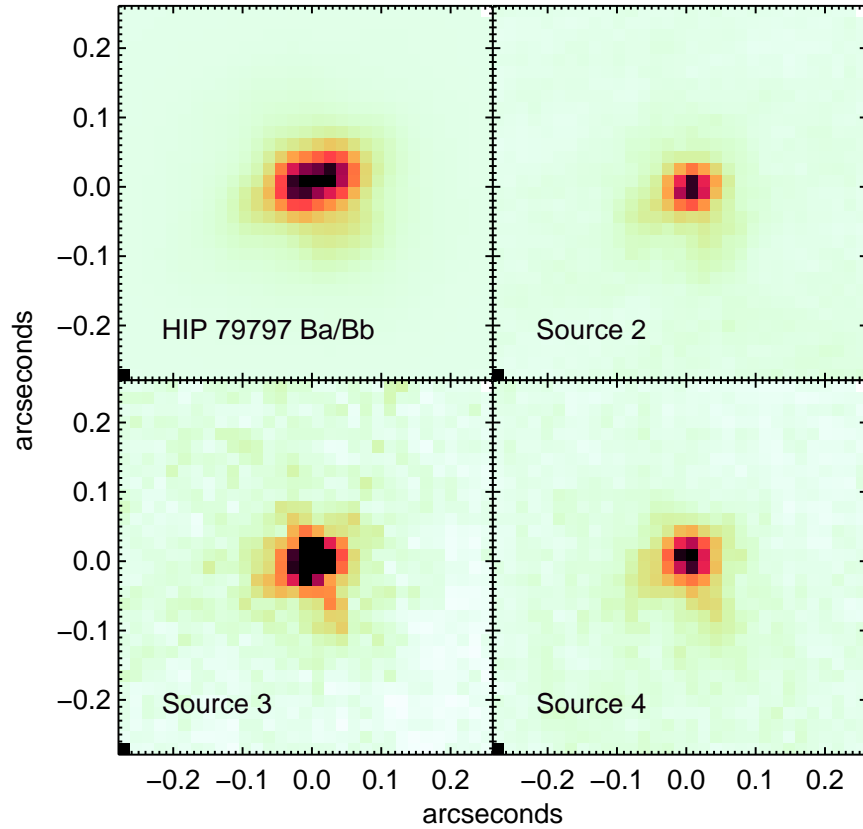


Fig. 18.— (upper left panel) The binary HIP 79797 Ba/Bb in the  $H$ -band as imaged by NICI on UT 2012-04-06. Ba is down and to the left, Bb is up and to the right. The binary is clearly resolved, and the two components have near equal flux. The other three panels show three background objects in the same image. All the background objects appear circular, while only HIP 79797 Ba/Bb is extended. The separation of the components is  $60 \pm 6$  mas. The images are oriented with north up and east to the left.

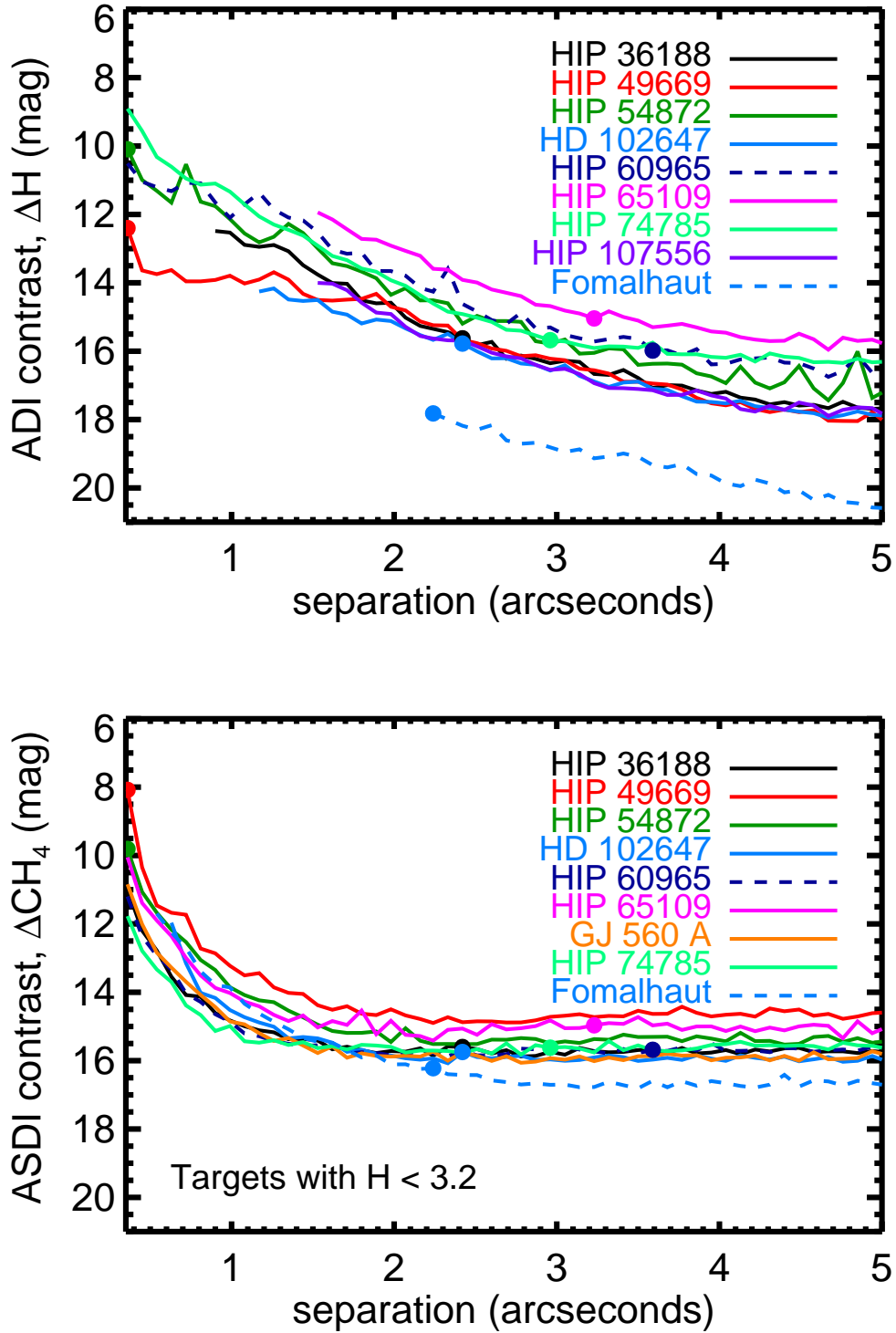


Fig. 19.— 95% completeness contrast plots for the brightest 10 stars, with  $H < 3.2$  mag, given for ADI (top) and ASDI (bottom). Some stars have observations only in one mode. For stars with both ADI and ASDI data we mark with a filled circle the angular separation where the ADI curve reaches larger contrasts than the ASDI curve. A contrast of 15 magnitudes represents a flux ratio of  $10^6$ .

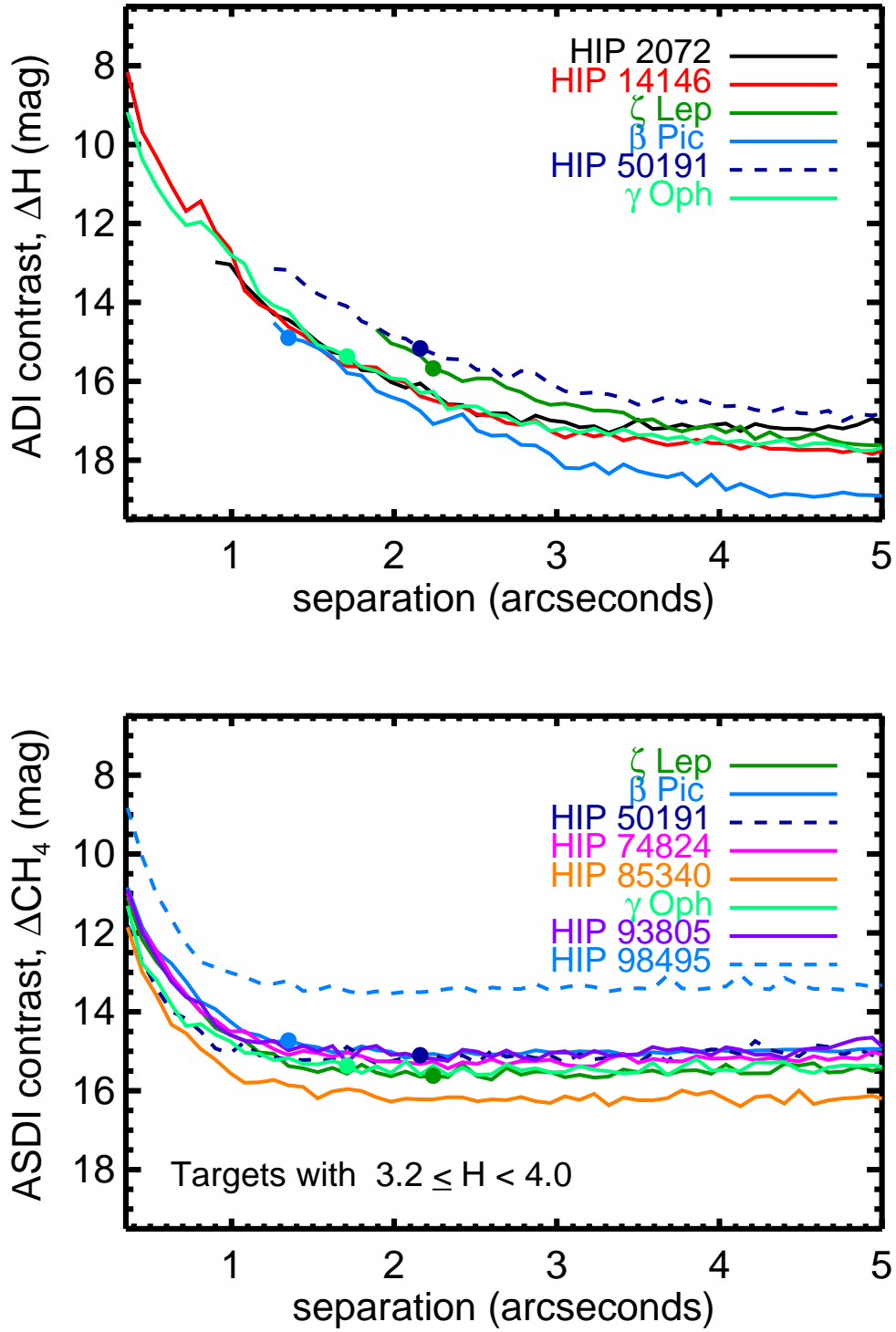


Fig. 20.— Contrast plots for stars with  $3.2 \leq H < 4.0$  mag. See Figure 19 caption for details.

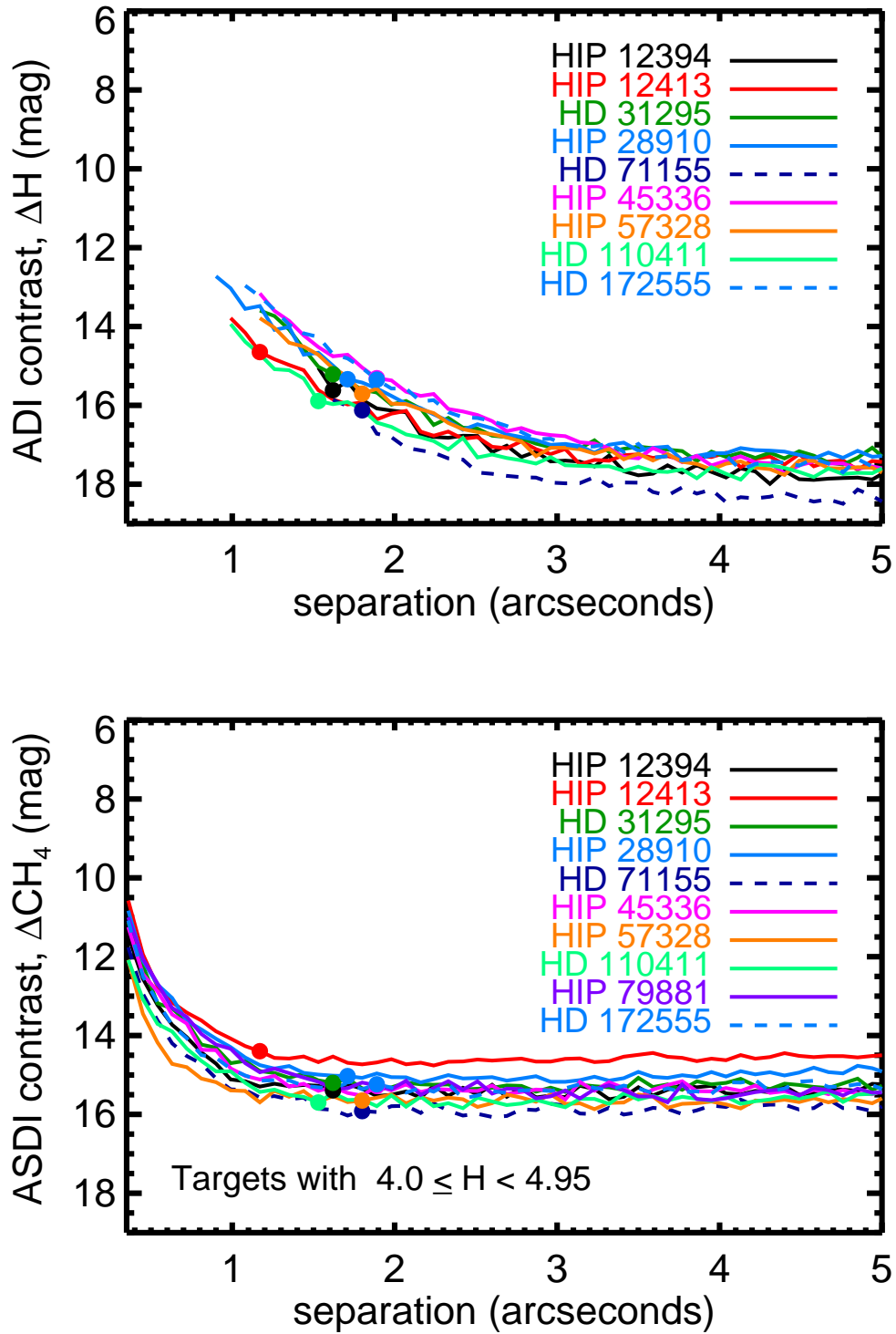


Fig. 21.— Contrast plots for stars with  $4.0 \leq H < 4.95$  mag. See Figure 19 caption for details.

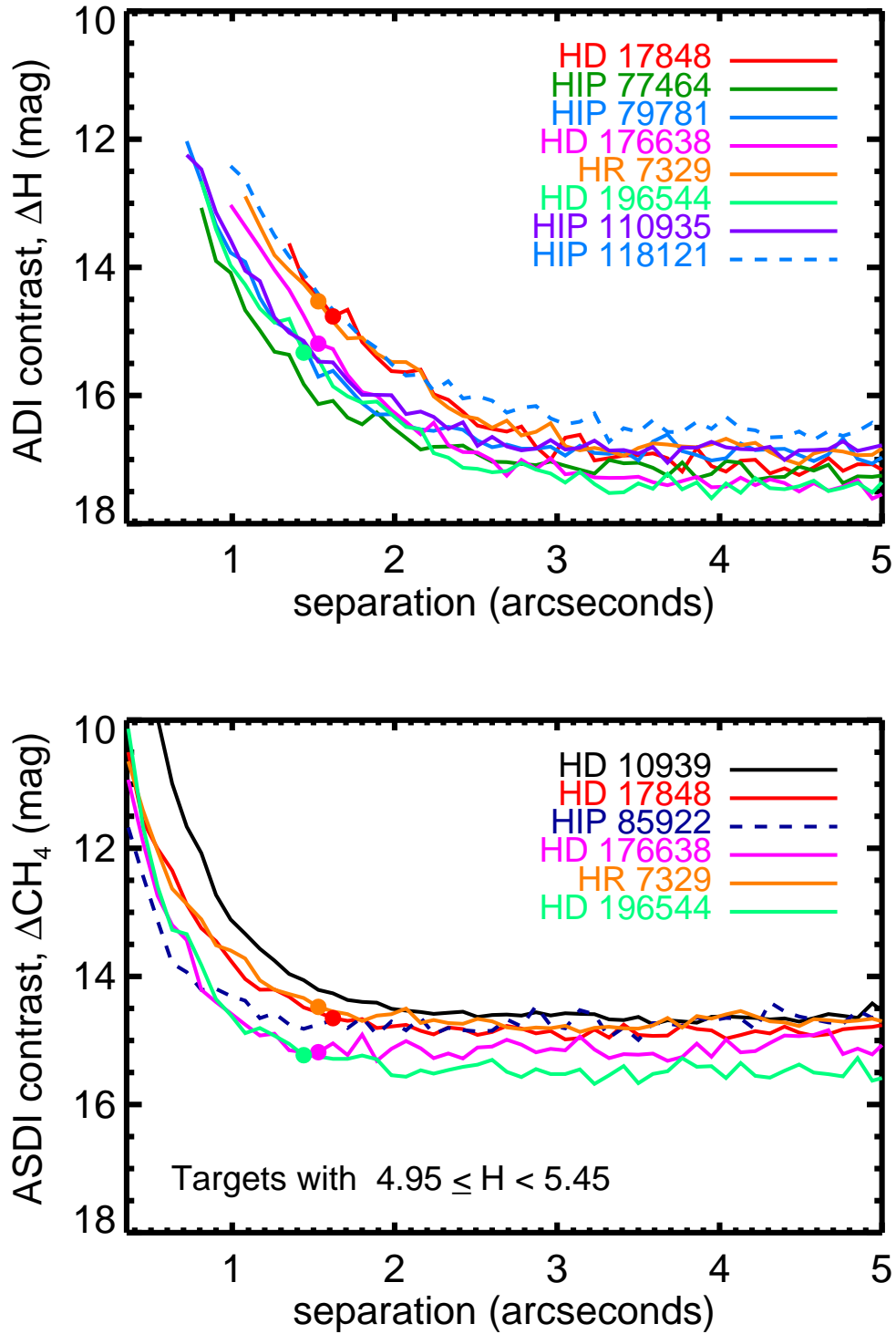


Fig. 22.— Contrast plots for stars with  $4.95 \leq H < 5.45$  mag. See Figure 19 caption for details.

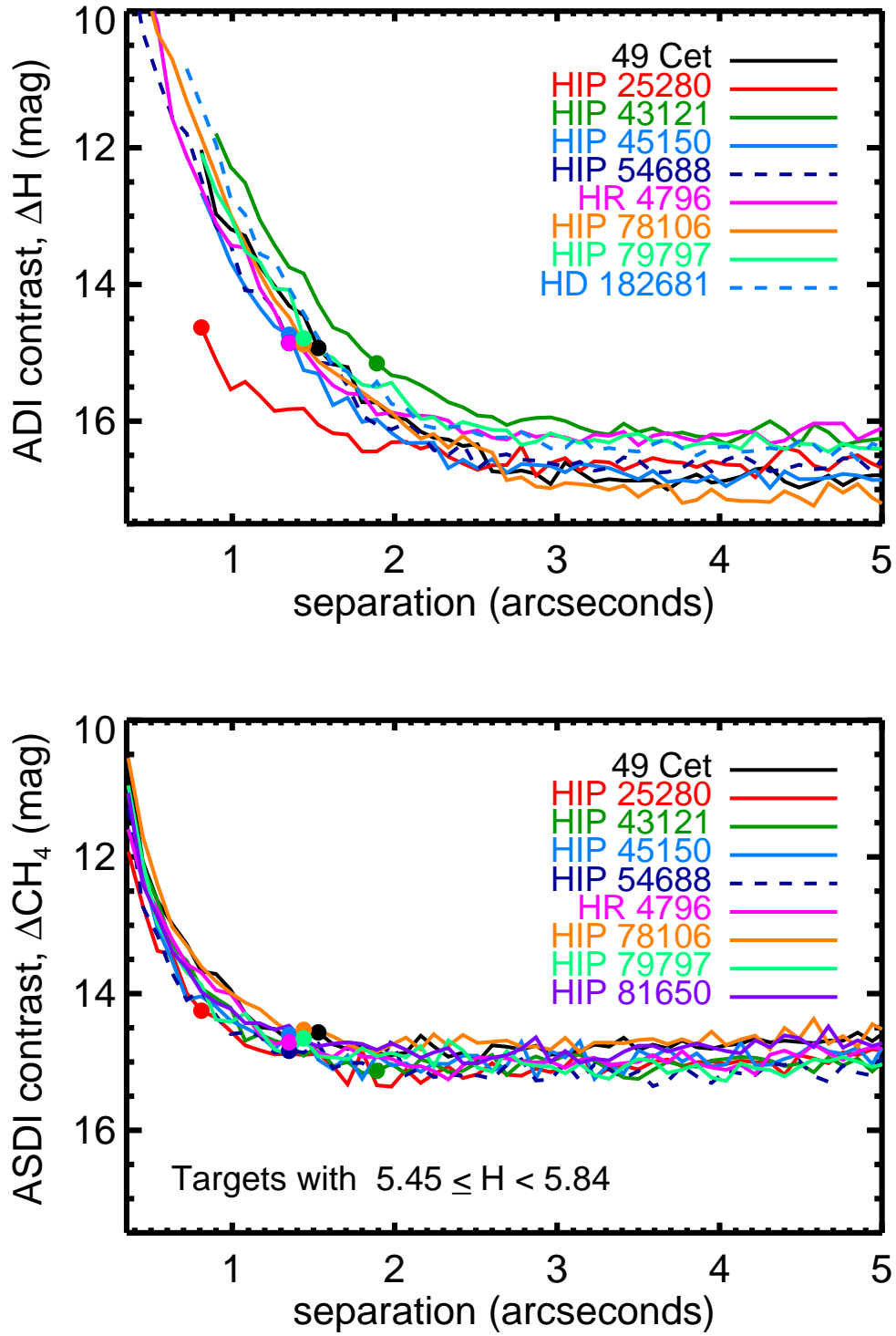


Fig. 23.— Contrast plots for stars with  $5.45 \leq H < 5.84$  mag. See Figure 19 caption for details.

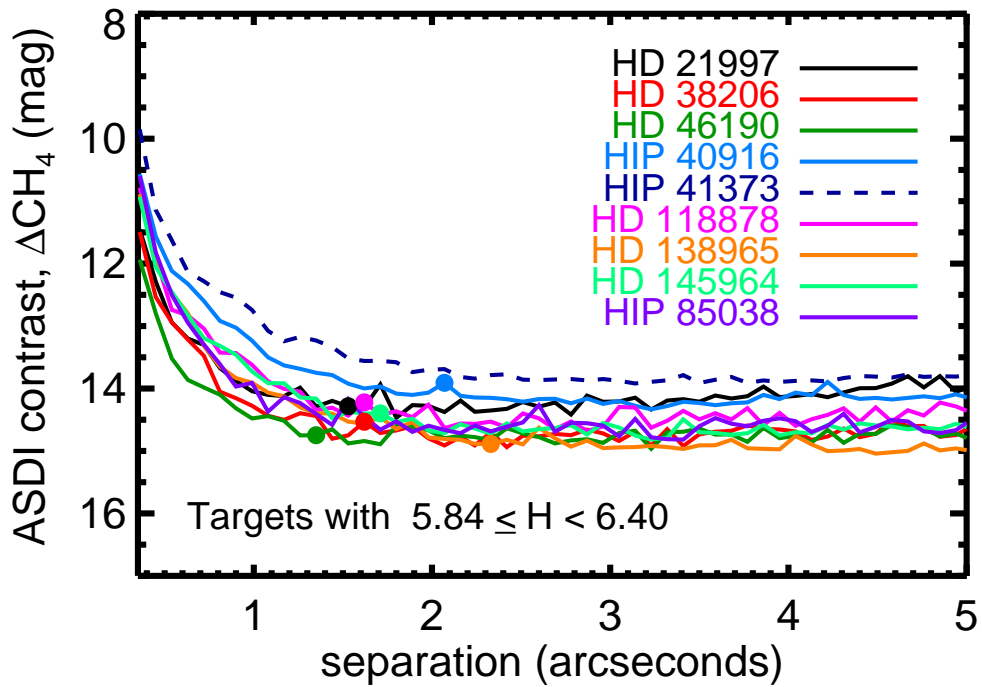
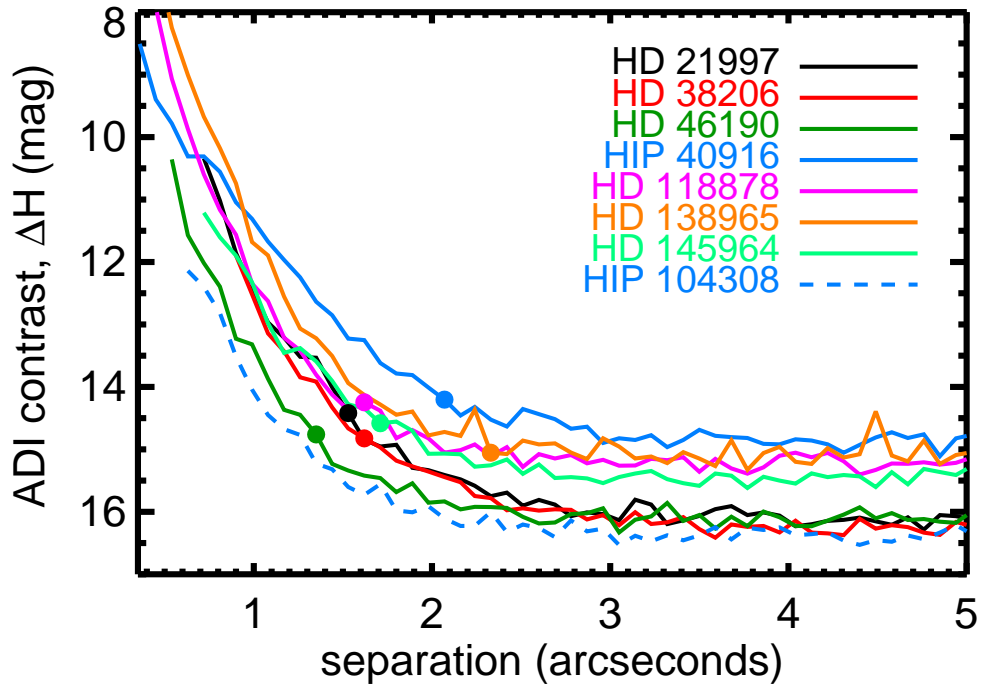


Fig. 24.— Contrast plots for stars with  $5.84 \leq H < 6.40$  mag. See Figure 19 caption for details.

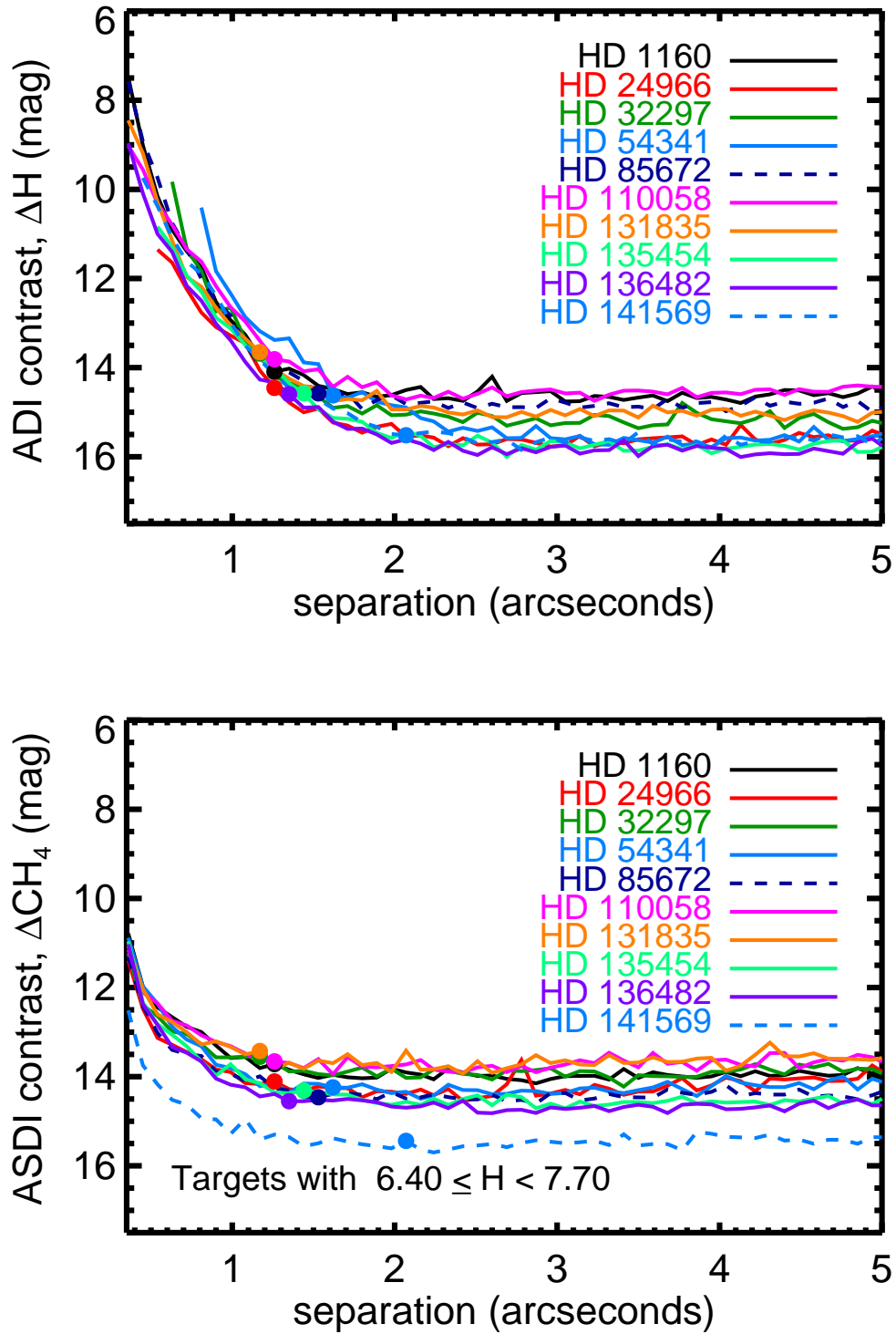


Fig. 25.— Contrast plots for stars with  $6.40 \leq H < 7.70$  mag. See Figure 19 caption for details.

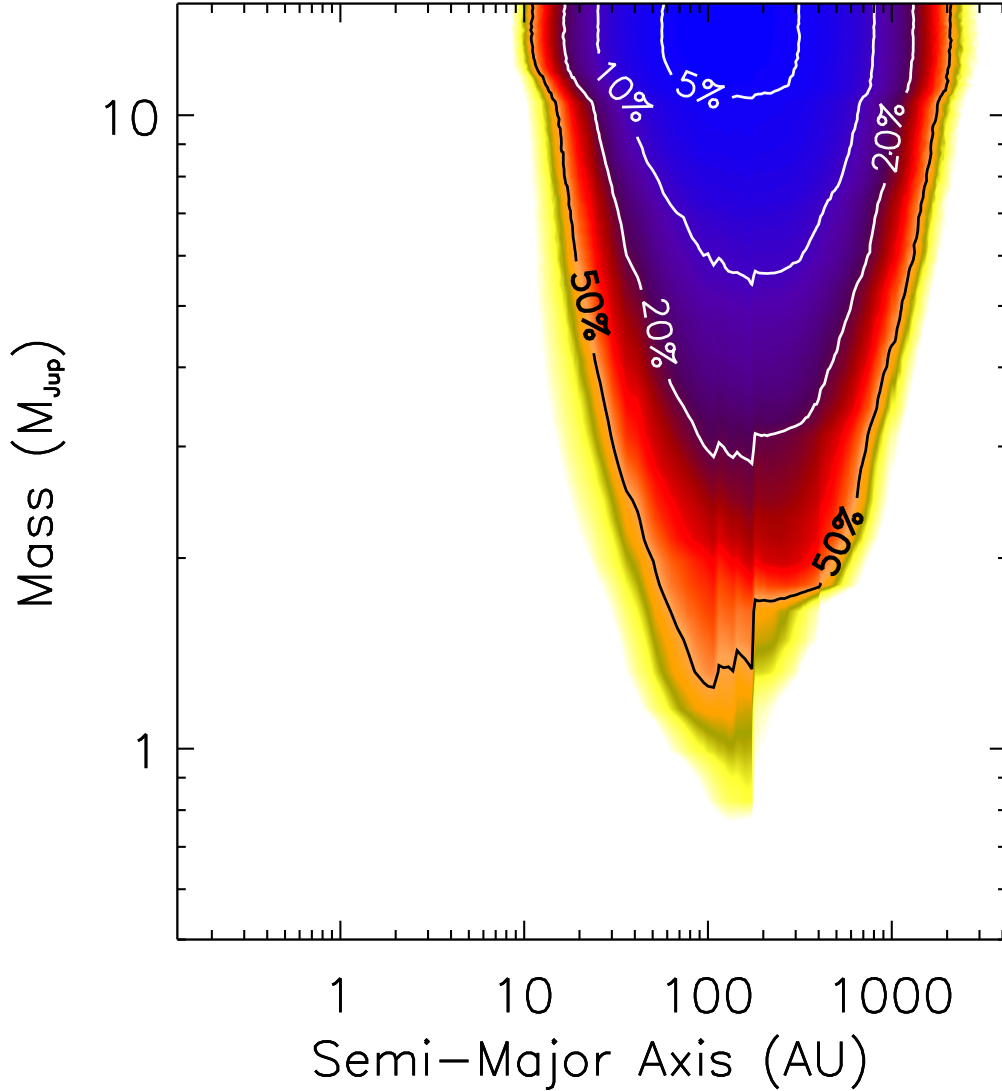


Fig. 26.— The 95% confidence upper limit on planet frequency from our Monte Carlo analysis of our 70 B and A star sample. We used the Johnson et al. (2010) relation between stellar mass and RV planet frequency to scale the range of stellar host masses to a common mass of  $2 M_{\odot}$ , the median for our sample. For the 5% frequency contour, for example, fewer than 1 in 20 high-mass stars can have giant planets with masses and semi-major axes inside the contour. The sawtooth pattern between 100 and 200 AU occurs as the constraints from the very young target stars HR 4796, HD 141569, and GJ 560 A are excluded at 110, 140, and 180 AU due to the presence of stellar binaries around those stars. The effect is most pronounced at contours for high upper limits on planet fraction, where the removal of a single star with large completeness to planets most impacts the statistics.

Table 1. Properties of Target Stars

Name	HD	HIP	RA	Dec	SpT	Dist (pc)	$\sigma_{Dist}$ (pc)	$B - V$ (mag)	$V$ (mag)	$H$ (mag)	$K_S$ (mag)	Age			Ref	
												Median (Myr)	68% (Myr)	95% (Myr)		Adopted (Myr)
HD 1160	1160	1272	00:15:57.302	+04:15:04.01	A0	103	5	0.05	7.13	7.01	7.04	92	36–178	14–267	...	...
HIP 2072	2262	2072	00:26:12.202	-43:40:47.39	A7	23.81	0.09	0.17	3.93	3.59	3.59	498	375–637	243–761	...	...
49 Cet	9672	7345	01:34:37.779	-15:40:34.90	A1	59.4	1.0	0.07	5.62	5.53	5.46	255	150–361	49–446	40	Z12
HD 10939	10939	8241	01:46:06.263	-53:31:19.33	A1	62.0	0.7	0.03	5.04	5.03	4.96	346	305–379	266–398	...	...
HIP 12394	16978	12394	02:39:35.357	-68:16:01.00	B9	46.55	0.20	-0.06	4.12	4.43	4.25	132	93–172	45–214	30	B13
HIP 12413	16754	12413	02:39:48.002	-42:53:30.08	A2	39	3	0.06	4.74	4.62	4.46	236	104–356	21–451	...	...
HD 17848	17848	13141	02:49:01.487	-62:48:23.48	A2	50.5	0.5	0.10	5.25	5.16	4.97	372	269–467	159–580	...	...
HIP 14146	18978	14146	03:02:23.499	-23:37:28.09	A4	27.17	0.13	0.16	4.08	3.54	3.57	567	419–670	261–757	...	...
HD 21997	21997	16449	03:31:53.647	-25:36:50.94	A3	72	3	0.12	6.38	6.11	6.10	225	91–377	21–532	30	Z12
HD 24966	24966	18437	03:56:29.376	-38:57:43.81	A0	106	4	0.02	6.89	6.87	6.86	128	51–227	13–322	...	...
HD 31295	31295	22845	04:54:53.729	+10:09:03.00	A0	35.7	0.3	0.09	4.64	4.52	4.42	241	119–355	21–461	...	...
HD 32297	32297	23451	05:02:27.436	+07:27:39.67	A0	111	11	0.20	8.13	7.62	7.59	224	78–455	25–706	...	...
HIP 25280	35505	25280	05:24:28.490	-16:58:32.81	A0	68.2	1.6	0.00	5.64	5.68	5.65	173	106–241	24–337	...	...
HD 38206	38206	26966	05:43:21.671	-18:33:26.92	A0	75	2	-0.01	5.73	5.84	5.78	172	112–232	36–316	30	Z11
$\zeta$ Lep	38678	27288	05:46:57.341	-14:49:19.02	A2	21.61	0.07	0.10	3.55	3.31	3.29	330	224–410	81–583	12	N12
$\beta$ Pic	39060	27321	05:47:17.088	-51:03:59.44	A5	19.44	0.05	0.17	3.85	3.54	3.53	109	82–134	17–284	12	B13
HIP 28910	41695	28910	06:06:09.324	-14:56:06.92	A0	52.9	1.5	0.05	4.67	4.59	4.52	361	320–387	278–403	...	...
HD 46190	46190	30760	06:27:48.617	-62:08:59.73	A0	83.8	1.9	0.09	6.61	6.39	6.36	178	65–293	17–419	...	...
HD 54341	54341	34276	07:06:20.933	-43:36:38.70	A0	102	4	-0.01	6.52	6.48	6.48	154	88–221	18–310	...	...
HIP 36188	58715	36188	07:27:09.042	+08:17:21.54	B8	49.6	0.5	-0.10	2.89	3.11	3.10	118	110–122	65–126	...	...
HIP 40916	70703	40916	08:21:00.460	-52:13:40.69	A0	67.2	1.2	0.15	6.63	6.31	6.28	119	49–215	20–335	...	...
HD 71155	71155	41307	08:25:39.632	-03:54:23.12	A0	37.5	0.3	-0.01	3.91	4.09	4.08	276	237–313	192–369	...	...
HIP 41373	71722	41373	08:26:25.205	-52:48:26.99	A0	69.4	1.2	0.06	6.05	5.91	5.89	183	81–293	16–387	...	...
HIP 43121	74873	43121	08:46:56.019	+12:06:35.82	A1	53.9	1.3	0.12	5.89	5.64	5.55	147	55–282	17–415	...	...
HIP 45150	79066	45150	09:11:55.634	+05:28:07.05	A9	50.7	1.1	0.33	6.34	5.63	5.56	889	612–1203	319–1418	...	...
HIP 45336	79469	45336	09:14:21.868	+02:18:51.38	B9	39	2	-0.06	3.89	4.04	3.94	113	55–159	13–201	...	...
HD 85672	85672	48541	09:53:59.150	+27:41:43.64	A0	106	7	0.16	7.59	7.20	7.19	205	74–389	22–578	...	...
HIP 49669	87901	49669	10:08:22.311	+11:58:01.95	B7	24.3	0.2	-0.09	1.36	1.66	1.64	115	75–121	1–125	...	...
HIP 50191	88955	50191	10:14:44.156	-42:07:18.99	A2	31.07	0.14	0.05	3.85	3.71	3.78	345	270–417	210–479	...	...
HIP 54688	97244	54688	11:11:43.757	+14:24:00.56	A5	56.2	1.1	0.21	6.30	5.83	5.76	279	102–479	26–726	...	...
HIP 54872	97603	54872	11:14:06.501	+20:31:25.39	A4	17.91	0.08	0.13	2.56	2.19	2.14	519	453–573	378–609	...	...
HIP 57328	102124	57328	11:45:17.040	+08:15:29.22	A4	37.4	0.3	0.17	4.84	4.54	4.41	523	416–662	263–792	...	...
HD 102647	102647	57632	11:49:03.578	+14:34:19.41	A3	11.00	0.06	0.09	2.14	1.92	1.88	215	88–330	16–458	40	Z11
HIP 60965	108767	60965	12:29:51.855	-16:30:55.55	B9	26.63	0.11	-0.01	2.94	3.00	3.00	290	258–312	210–385	...	...
HR 4796	109573	61498	12:36:01.034	-39:52:10.19	A0	72.7	1.7	0.00	5.78	5.79	5.77	184	117–254	30–350	10	Z04
HD 110058	110058	61782	12:39:46.197	-49:11:55.54	A0	107	9	0.15	7.99	7.59	7.58	136	53–274	20–444	50	K05
HD 110411	110411	61960	12:41:53.057	+10:14:08.25	A0	36.3	0.3	0.08	4.88	4.76	4.68	90	27–198	14–285	...	...
HIP 65109	115892	65109	13:20:35.817	-36:42:44.25	A2	18.02	0.06	0.07	2.75	2.74	2.76	352	293–438	212–503	...	...
HD 118878	118878	66722	13:40:37.651	-44:19:48.84	A0	121	7	0.05	6.57	6.35	6.34	360	309–396	249–502	...	...
GJ 560 A	128898	71908	14:42:30.420	-64:58:30.49	A7	16.57	0.04	0.26	3.18	2.47	2.42	827	702–925	586–991	200	B13
HD 131835	131835	73145	14:56:54.468	-35:41:43.66	A2	121	14	0.19	7.88	7.56	7.52	368	136–604	30–791	...	...
HD 135454	135454	74752	15:16:37.151	-42:22:12.58	B9	172	14	-0.03	6.76	6.82	6.83	238	208–275	171–306	...	...
HIP 74785	135742	74785	15:17:00.414	-09:22:58.49	B8	56.8	0.5	-0.07	2.61	2.89	2.90	78	76–80	74–82	...	...
HIP 74824	135379	74824	15:17:30.850	-58:48:04.34	A3	30.55	0.18	0.09	4.07	3.81	3.88	367	272–458	164–562	...	...
HD 136482	136482	75210	15:22:11.255	-37:38:08.25	B8	136	10	-0.06	6.65	6.83	6.76	97	40–139	10–175	...	...
HD 138965	138965	76736	15:40:11.556	-70:13:40.38	A5	78	2	0.08	6.45	6.34	6.27	157	57–270	16–378	...	...
HIP 77464	141378	77464	15:48:56.797	-03:49:06.64	A5	54.0	0.8	0.12	5.53	5.27	5.26	381	264–499	129–623	...	...
HD 141569	141569	77542	15:49:57.748	-03:55:16.35	B9	115	8	0.09	7.11	6.86	6.82	318	163–440	34–560	5	W00
HIP 78106	142630	78106	15:56:54.113	-33:57:51.35	B9	61	18	0.07	5.59	5.49	5.42	285	108–405	22–501	...	...

Table 1—Continued

Name	HD	HIP	RA	Dec	SpT	Dist (pc)	$\sigma_{Dist}$ (pc)	$B - V$ (mag)	$V$ (mag)	$H$ (mag)	$K_S$ (mag)	Age			Ref	
												Median (Myr)	68% (Myr)	95% (Myr)		Adopted (Myr)
HD 145964	145964	79599	16:14:28.884	-21:06:27.49	B9	108	7	0.00	6.41	6.39	6.35	254	179–318	92–379	...	...
HIP 79781	146514	79781	16:16:55.302	-03:57:12.05	A9	44.4	0.9	0.33	6.18	5.41	5.34	692	306–1064	56–1317	...	...
HIP 79797	145689	79797	16:17:05.411	-67:56:28.62	A4	52.2	1.1	0.16	5.95	5.68	5.66	203	71–372	21–525	...	...
HIP 79881	146624	79881	16:18:17.900	-28:36:50.48	A0	41.3	0.4	0.01	4.80	4.94	4.74	107	44–206	12–314	...	...
HIP 81650	149989	81650	16:40:44.400	-51:28:41.74	A9	49.4	1.0	0.32	6.30	5.52	5.48	809	503–1133	157–1351	...	...
HIP 85038	156751	85038	17:22:47.891	-58:28:23.67	A5	62	3	0.25	6.75	6.30	6.24	315	108–605	29–888	...	...
HIP 85340	157792	85340	17:26:22.217	-24:10:31.11	A3	25.50	0.16	0.28	4.16	3.34	3.34	894	802–964	670–1017	...	...
HIP 85922	159170	85922	17:33:29.845	-05:44:41.29	A5	48.1	0.8	0.19	5.61	5.25	5.14	483	331–641	167–784	...	...
$\gamma$ Oph	161868	87108	17:47:53.561	+02:42:26.20	A0	31.5	0.2	0.04	3.75	3.66	3.62	342	285–388	237–487	...	...
HD 172555	172555	92024	18:45:26.901	-64:52:16.53	A5	28.55	0.15	0.20	4.78	4.25	4.30	276	83–462	24–724	12	B13
HD 176638	176638	93542	19:03:06.877	-42:05:42.39	A0	59.2	1.0	-0.03	4.74	4.96	4.75	248	205–288	162–329	...	...
HIP 93805	177756	93805	19:06:14.939	-04:52:57.20	B9	37.9	0.9	-0.10	3.43	3.48	3.56	48	20–76	6–98	...	...
HR 7329	181296	95261	19:22:51.206	-54:25:26.15	A0	48.2	0.5	0.02	5.03	5.15	5.01	182	101–268	21–370	12	B13
HD 182681	182681	95619	19:26:56.483	-29:44:35.62	B8	69.9	1.8	-0.01	5.66	5.66	5.68	144	80–208	17–292	...	...
HIP 98495	188228	98495	20:00:35.556	-72:54:37.82	A0	32.22	0.18	-0.03	3.97	3.76	3.80	86	34–152	10–239	...	...
HD 196544	196544	101800	20:37:49.119	+11:22:39.63	A2	57.9	1.1	0.05	5.42	5.37	5.30	272	173–365	69–444	...	...
HIP 104308	200798	104308	21:07:51.221	-54:12:59.46	A5	71	2	0.25	6.69	6.12	6.07	659	464–852	210–1044	30	B13
HIP 107556	207098	107556	21:47:02.444	-16:07:38.23	A5	11.87	0.03	0.18	2.85	2.06	2.01	542	168–1047	33–1457	...	...
HIP 110935	212728	110935	22:28:37.671	-67:29:20.61	A3	43.1	0.7	0.21	5.56	5.14	5.05	457	260–635	77–830	...	...
Fomalhaut	216956	113368	22:57:39.046	-29:37:20.05	A3	7.70	0.03	0.15	1.17	0.94	0.94	515	418–623	297–719	...	...
HIP 118121	224392	118121	23:57:35.078	-64:17:53.63	A1	47.4	1.1	0.06	5.00	4.95	4.82	296	197–388	87–470	30	B13

Note. — For most stars we use the results of our Bayesian age-dating. For stars with an independent age measurement in the literature, we use that value, given in the “Adopted” column. We only use literature ages for cases where there is solid evidence that the star belongs to a well-known moving group. The source of these external ages is given by B13: Biller et al. (2013), K05: Kouwenhoven et al. (2005), N12: Nakajima & Morino (2012), W00: Weinberger et al. (2000), Z04: Zuckerman & Song (2004), Z11: Zuckerman et al. (2011), and Z12: Zuckerman & Song (2012).

Table 2. NICI Observation of Young B and A Stars

Target	UT Date	Obs Mode	$N_{images}$	Exp. Time (s)	Rotation (deg)
HD 1160	2010-10-31	ADI	20	1208	6.4
HD 1160	2010-10-31	ASDI	45	2701	18.1
HIP 2072	2011-11-03	ADI	40	2508	46.2
49 Cet	2009-12-02	ASDI	45	2736	40.6
49 Cet	2009-12-02	ADI	20	1208	16.4
HD 10939	2010-12-26	ASDI	44	2708	3.5
HIP 12394	2008-12-15	ASDI	42	2633	21.3
HIP 12394	2008-12-15	ADI	20	1200	7.9
HIP 12413	2010-12-25	ASDI	45	2770	43.7
HIP 12413	2010-12-25	ADI	20	1208	10.2
HD 17848	2008-12-16	ADI	20	1200	9.7
HD 17848	2008-12-16	ASDI	45	2650	22.3
HIP 14146	2010-01-10	ADI	20	1185	4.0
HIP 14146	2010-10-31	ADI	20	1185	14.2
HIP 14146	2011-10-21	ADI	20	1185	2.4
HD 21997	2009-01-16	ASDI	45	2530	55.6
HD 21997	2009-01-16	ADI	20	1208	3.6
HD 21997	2010-01-09	ADI	20	1208	0.8
HD 21997	2010-10-31	ASDI	50	3021	89.2
HD 21997	2010-12-25	ASDI	27	1631	43.5
HD 24966	2009-01-15	ADI	20	1208	17.1
HD 24966	2009-01-15	ASDI	48	2699	72.3
HD 31295	2009-01-14	ASDI	45	2616	16.4
HD 31295	2009-01-14	ADI	20	1208	8.0
HD 31295	2010-12-25	ADI	20	1208	7.3
HD 32297	2008-12-17	ADI	20	1200	4.5
HD 32297	2008-12-17	ASDI	45	2701	14.1
HIP 25280	2009-01-18	ASDI	45	2513	44.1
HIP 25280	2009-01-18	ADI	20	1208	11.8
HD 38206	2008-12-18	ADI	20	1200	5.2
HD 38206	2008-12-18	ASDI	50	2964	41.2
$\zeta$ Lep	2008-12-15	ADI	20	1200	29.4
$\zeta$ Lep	2008-12-15	ASDI	40	2432	34.3
$\beta$ Pic	2008-11-22	ASDI	90	5472	2.3
HIP 28910	2009-01-17	ADI	21	1244	12.3
HIP 28910	2009-01-17	ASDI	43	2647	43.7
HD 46190	2009-02-12	ADI	20	1208	6.9
HD 46190	2009-02-12	ASDI	42	2537	17.3
HD 46190	2012-03-30	ADI	20	1208	7.1
HD 54341	2008-12-15	ADI	20	1200	17.0
HD 54341	2008-12-15	ASDI	44	2641	48.0
HIP 36188	2009-03-08	ADI	20	1185	5.9
HIP 36188	2009-03-08	ASDI	43	2614	19.4
HIP 36188	2010-05-10	ASDI	50	3040	13.1
HIP 40916	2009-01-18	ADI	20	1208	13.5
HIP 40916	2009-01-18	ASDI	45	3009	28.4

Table 2—Continued

Target	UT Date	Obs Mode	$N_{images}$	Exp. Time (s)	Rotation (deg)
HD 71155	2008-12-16	ADI	20	1200	15.5
HD 71155	2008-12-16	ASDI	46	2691	20.2
HD 71155	2011-05-14	ADI	20	1200	3.5
HIP 41373	2009-01-18	ASDI	45	3129	33.0
HIP 43121	2009-04-08	ASDI	45	2736	17.1
HIP 43121	2009-04-09	ADI	20	1208	7.3
HIP 43121	2011-05-14	ADI	25	1510	7.9
HIP 45150	2009-03-11	ADI	20	1208	7.7
HIP 45150	2009-03-11	ASDI	45	2736	19.6
HIP 45336	2009-03-07	ASDI	44	2574	19.5
HIP 45336	2009-03-07	ADI	20	1208	9.1
HD 85672	2009-01-13	ADI	20	1208	5.7
HD 85672	2009-01-13	ASDI	45	2701	13.7
HIP 49669	2009-03-12	ADI	21	1244	7.6
HIP 49669	2009-03-12	ASDI	49	2859	23.4
HIP 50191	2008-12-16	ASDI	45	2565	38.1
HIP 50191	2010-01-05	ADI	42	829	25.2
HIP 54688	2010-04-11	ADI	20	1208	6.3
HIP 54688	2010-04-11	ASDI	50	3021	17.9
HIP 54872	2009-04-09	ADI	20	1185	6.3
HIP 54872	2009-04-09	ASDI	45	2736	17.1
HIP 57328	2009-04-10	ADI	20	1208	5.4
HIP 57328	2009-04-10	ASDI	45	2616	15.7
HIP 57328	2010-04-07	ADI	20	1185	7.8
HIP 57328	2011-05-03	ASDI	73	4438	10.1
HD 102647	2009-01-18	ASDI	37	2109	15.1
HD 102647	2009-01-18	ADI	20	1185	6.9
HIP 60965	2009-03-07	ADI	20	1185	23.1
HIP 60965	2009-03-07	ASDI	45	2736	31.0
HR 4796	2009-01-14	ASDI	45	2821	25.2
HR 4796	2009-01-14	ADI	20	1208	21.8
HR 4796	2009-02-12	ADI	45	2718	34.8
HR 4796	2012-04-06	ADI	64	3793	82.4
HD 110058	2009-01-17	ADI	20	1208	14.8
HD 110058	2009-01-17	ASDI	45	2701	26.1
HD 110058	2012-03-28	ADI	20	1208	15.0
HD 110411	2009-02-07	ASDI	45	2513	16.8
HD 110411	2009-02-07	ADI	20	1208	7.5
HIP 65109	2009-03-12	ADI	20	1185	24.7
HIP 65109	2009-03-12	ASDI	42	2042	16.9
HD 118878	2009-02-08	ASDI	45	2701	31.3
HD 118878	2012-04-07	ADI	20	1208	4.6
GJ 560 A	2009-03-11	ASDI	45	2565	19.9
HD 131835	2009-02-12	ASDI	52	3122	35.0
HD 131835	2009-04-10	ADI	45	2718	9.1
HD 135454	2009-03-12	ASDI	45	2411	15.7

Table 2—Continued

Target	UT Date	Obs Mode	$N_{images}$	Exp. Time (s)	Rotation (deg)
HD 135454	2009-03-12	ADI	20	1208	12.2
HIP 74785	2010-04-09	ASDI	44	2675	34.1
HIP 74785	2010-04-09	ADI	20	1185	8.7
HIP 74824	2009-03-09	ASDI	45	2770	20.8
HD 136482	2009-03-11	ASDI	45	2445	11.6
HD 136482	2009-03-11	ADI	20	1208	9.9
HD 136482	2010-04-08	ASDI	45	2445	27.2
HD 138965	2009-02-12	ASDI	68	4702	31.5
HD 138965	2011-04-26	ADI	10	604	2.8
HIP 77464	2010-07-27	ADI	20	1208	7.4
HD 141569	2009-03-07	ADI	20	1208	10.6
HD 141569	2009-03-07	ASDI	65	3902	25.1
HD 141569	2010-04-08	ASDI	45	2701	23.6
HD 141569	2011-05-03	ASDI	114	6844	58.7
HIP 78106	2009-04-11	ASDI	45	2736	35.9
HIP 78106	2009-04-11	ADI	20	1208	4.7
HD 145964	2009-03-12	ASDI	45	3249	23.1
HD 145964	2009-03-12	ADI	20	1208	25.1
HIP 79781	2010-08-30	ADI	25	1510	5.4
HIP 79797	2010-04-10	ASDI	53	3222	10.4
HIP 79797	2011-05-12	ADI	20	1208	8.7
HIP 79881	2010-05-11	ASDI	45	2565	146.5
HIP 79881	2011-05-03	ASDI	41	2492	4.4
HIP 81650	2010-05-10	ASDI	45	2736	21.3
HIP 85038	2010-05-11	ASDI	45	2701	16.9
HIP 85340	2009-04-13	ASDI	50	3040	16.1
HIP 85922	2010-07-27	ASDI	43	2401	23.3
$\gamma$ Oph	2009-04-08	ASDI	45	2736	20.0
$\gamma$ Oph	2009-04-08	ADI	20	1185	5.9
$\gamma$ Oph	2010-04-08	ADI	20	1185	6.4
HD 172555	2009-04-09	ADI	20	1208	6.8
HD 172555	2009-04-09	ASDI	47	2786	22.0
HD 176638	2011-05-12	ASDI	45	2667	32.4
HD 176638	2011-10-17	ADI	16	966	4.6
HD 176638	2012-04-06	ADI	20	1208	3.9
HIP 93805	2010-04-10	ASDI	32	1957	18.8
HR 7329	2009-04-11	ADI	20	1208	8.1
HR 7329	2009-04-11	ASDI	45	2565	22.4
HD 182681	2010-08-29	ADI	20	1208	3.3
HIP 98495	2010-05-11	ASDI	23	1398	12.0
HD 196544	2009-04-26	ADI	20	1208	5.0
HD 196544	2009-04-27	ASDI	65	3952	5.2
HD 196544	2010-10-31	ASDI	20	1216	5.4
HD 196544	2011-04-25	ADI	30	1812	9.9
HIP 104308	2011-10-30	ADI	40	2416	17.6
HIP 107556	2010-08-30	ADI	20	1185	14.3

Table 2—Continued

Target	UT Date	Obs Mode	$N_{images}$	Exp. Time (s)	Rotation (deg)
HIP 107556	2010-11-12	ADI	30	1778	12.3
HIP 107556	2011-10-03	ASDI	22	1304	4.3
HIP 110935	2011-11-07	ADI	40	2371	16.6
Fomalhaut	2008-11-17	ASDI	77	5149	6.3
Fomalhaut	2009-12-04	ASDI	99	5868	7.0
Fomalhaut	2009-12-04	ADI	99	5868	6.9
Fomalhaut	2011-10-17	ASDI	80	4864	22.0
HIP 118121	2010-08-29	ADI	20	1208	8.5

Table 3. Properties of Candidate Companions

Name	#	Sep (")	PA (deg)	$\Delta H$ (mag)	$\Delta\tau$ (years)	Epochs	$\chi^2_{\nu}$ (BG)	$\chi^2_{\nu}$ (CPM)	dof	Comp?
HD 1160	1	0.780	244.3	9.6	9.28	12	11.22	0.47	22	CPM <sup>1</sup>
HD 1160	2	5.150	349.8	7.5	9.28	19	2.47	0.49	36	CPM <sup>1</sup>
HIP 14146	1	3.936	296.6	17.3	1.78	3	0.31	57.65	4	BG
HD 31295	1	6.261	271.6	13.3	1.95	2	0.09	69.71	2	BG
HD 31295	2	8.805	316.7	14.5	1.95	2	0.02	187.48	2	BG
HIP 25280	1	5.219	80.4	14.9	1.84	2	1.82	25.00	2	BG
ζ Lep	1	5.295	110.0	18.0	2.24	2	0.44	28.80	2	BG
HD 54341	1	3.080	131.2	12.7	2.03	2	0.40	3.05	2	BG
HD 54341	2	4.372	137.3	11.8	2.03	2	0.91	2.56	2	BG
HIP 36188	1	7.460	205.0	16.1	2.66	2	15.38	182.97	2	BG
HD 71155	1	5.766	86.7	14.9	2.41	3	0.84	65.12	4	BG
HD 71155	2	7.360	357.8	16.8	2.41	2	0.02	19.78	2	BG
HD 71155	3	9.403	246.1	14.2	2.41	2	1.12	95.44	2	BG
HIP 41373	1	3.043	260.9	12.0	2.28	3	2.00	21.35	4	BG
HIP 41373	2	5.916	0.9	11.7	2.28	3	0.39	2.39	4	BG
HIP 43121	1	4.760	350.0	14.9	2.10	2	0.11	39.74	2	BG
HIP 50191	1	5.192	280.4	9.9	1.05	2	0.20	79.56	2	BG
HIP 50191	2	5.144	285.6	13.3	1.05	2	0.43	74.46	2	BG
HIP 57328	1	1.599	268.1	15.4	2.06	2	1.98	88.06	2	BG
HR 4796	1	4.472	322.7	8.6	18.07	3	0.73	57.48	4	BG
HD 110058	1	3.030	252.5	12.9	3.19	2	0.37	50.83	2	BG
HD 110058	2	3.280	94.3	13.2	3.19	2	0.94	24.62	2	BG
HD 110058	3	6.210	160.3	8.7	3.19	2	0.64	14.51	2	BG
HD 110058	4	7.810	231.1	8.2	3.19	2	9.77	108.96	2	BG
HD 110058	5	7.830	125.8	12.2	3.19	2	0.31	15.33	2	BG
HD 110058	6	8.400	142.6	11.3	3.19	2	0.56	10.39	2	BG
HD 118878	1	3.316	181.9	10.7	3.16	2	0.52	21.90	2	BG
HD 118878	2	6.203	213.7	14.2	3.16	2	0.12	35.13	2	BG
HD 118878	3	7.254	120.3	11.1	3.16	2	0.07	9.30	2	BG
HD 118878	4	9.668	217.0	12.5	3.16	2	0.94	52.59	2	BG
HD 136482	1	0.940	241.5	11.4	1.08	2	0.42	2.78	2	BG
HD 136482	2	2.960	156.7	11.3	1.08	2	0.58	2.78	2	BG
HD 136482	3	3.772	181.8	14.1	1.08	2	0.28	3.88	2	BG
HD 136482	4	5.081	146.0	13.5	1.08	2	0.09	1.29	2	BG
HD 136482	5	5.480	251.8	8.9	1.08	2	2.79	13.70	2	BG
HD 136482	6	6.334	51.9	12.3	1.08	2	0.85	9.09	2	BG
HD 138965	1	1.708	61.4	10.6	2.20	2	0.79	75.76	2	BG
HD 138965	2	4.085	244.6	12.2	2.20	2	0.19	81.31	2	BG
HD 138965	3	4.284	269.6	14.6	2.20	2	0.43	35.78	2	BG
HD 138965	4	7.386	157.3	11.4	2.20	2	0.37	35.91	2	BG
HD 138965	5	7.503	102.1	12.8	2.20	2	1.06	36.51	2	BG
HD 138965	6	7.838	236.4	11.4	2.20	2	0.02	75.49	2	BG
HD 138965	7	8.048	326.9	11.3	2.20	2	0.16	17.66	2	BG
HD 138965	8	9.970	4.4	13.6	2.20	2	1.13	41.08	2	BG
HD 141569	1	6.400	13.2	14.6	2.16	2	1.50	5.12	2	BG

Table 3—Continued

Name	#	Sep (")	PA (deg)	$\Delta H$ (mag)	$\Delta\tau$ (years)	Epochs	$\chi^2_{\nu}$ (BG)	$\chi^2_{\nu}$ (CPM)	dof	Comp?
HD 141569	2	7.850	209.7	12.8	2.16	2	1.80	24.48	2	BG
HIP 79781	1	4.509	179.2	11.9	1.50	2	0.46	3.78	2	BG
HIP 79781	2	6.525	130.2	8.9	1.50	2	0.03	5.59	2	BG
HIP 79797	1	5.737	276.5	14.4	1.91	3	0.04	16.31	4	BG
HIP 79797	2	5.759	18.8	13.4	1.91	3	0.64	44.62	4	BG
HIP 79797	3	6.213	118.0	11.6	1.91	3	1.64	12.56	4	BG
HIP 79797	4	6.691	293.9	7.4	7.77	5	54.54	0.81	8	CPM <sup>2</sup>
HIP 79797	5	6.949	197.2	14.9	1.91	3	1.65	88.02	4	BG
HIP 79797	6	6.907	329.4	13.6	0.90	2	0.28	4.92	2	BG
HIP 79797	7	7.737	250.7	12.5	0.90	2	0.07	8.35	2	BG
HIP 79797	8	9.598	6.5	10.7	1.01	2	0.22	29.66	2	BG
HIP 79881	1	1.627	267.7	12.5	0.98	2	0.96	56.83	2	BG
HIP 79881	2	4.551	175.6	10.0	0.98	2	0.09	26.23	2	BG
HIP 79881	3	6.600	233.2	12.6	0.98	2	0.20	16.98	2	BG
HIP 85922	1	7.359	40.3	13.2	1.59	2	4.44	50.95	2	BG
$\gamma$ Oph	1	4.528	59.2	14.6	1.07	2	0.04	14.21	2	BG
$\gamma$ Oph	2	5.902	239.4	16.0	1.07	2	0.13	15.85	2	BG
$\gamma$ Oph	3	6.210	267.3	12.6	1.07	2	0.15	6.82	2	BG
$\gamma$ Oph	4	6.602	275.0	15.0	1.07	2	0.16	4.42	2	BG
$\gamma$ Oph	5	6.964	59.1	13.6	1.07	2	0.11	14.71	2	BG
$\gamma$ Oph	6	8.677	96.3	12.3	1.07	2	1.71	11.78	2	BG
$\gamma$ Oph	7	9.271	253.6	15.5	1.07	2	0.09	7.01	2	BG
HD 172555	1	7.702	319.0	14.5	3.92	2	0.04	11.29	2	BG
HD 176638	1	3.529	157.8	14.1	0.90	3	0.64	8.34	4	BG
HD 176638	2	4.743	93.7	12.6	0.90	3	1.18	12.96	4	BG
HD 176638	3	5.222	265.6	14.5	0.47	2	0.24	13.04	2	BG
HD 176638	4	9.390	319.7	10.6	0.90	3	0.92	3.33	4	BG
HR 7329	1	4.175	167.6	6.6	10.78	2	133.91	3.79	2	CPM <sup>3</sup>
HD 196544	1	4.743	90.8	13.1	2.63	5	0.34	12.06	8	BG
HD 196544	2	4.352	93.4	14.5	2.63	5	0.19	9.60	8	BG
HIP 104308	1	1.681	281.9	12.4	0.75	2	0.69	27.31	2	BG
HIP 104308	2	2.895	264.0	15.5	0.75	2	0.05	14.08	2	BG
HIP 107556	1	6.179	169.5	17.7	1.09	3	0.15	368.24	4	BG

<sup>1</sup>Nielsen et al. (2012)

<sup>2</sup>Originally identified by Huélamo et al. (2010)

<sup>3</sup>Originally identified by Lowrance et al. (2000)

Note. — Summary of the candidate companions detected around each target star. For each candidate we list the separation and position angle at the reference epoch, the contrast between candidate and host star, the time baseline for our astrometric data, the number of epochs, the reduced chi-square statistic for the candidate to be background (BG) or common proper motion (CPM), the number of degrees of freedom for the astrometric fit, and the final determination of each candidate: background or common proper motion. Astrometry for individual epochs is in Table 4.

Table 4. Astrometry of Candidate Companions

Name	#	Epoch	Measured Position				Background Position				Inst.	Comp?
			Sep (")	$\sigma_{Sep}$	PA (deg)	$\sigma_{PA}$	Sep (")	$\sigma_{Sep}$	PA (deg)	$\sigma_{PA}$		
HD 1160	1	2010.83	0.780	0.025	244.3	0.2	...	...	...	...	N	CPM
		2002.57	0.767	0.030	246.2	1.0	0.711	0.025	229.528	0.629	V	CPM
		2003.84	0.766	0.030	245.6	1.0	0.706	0.025	231.709	0.546	V	CPM
		2005.98	0.760	0.030	244.7	1.0	0.721	0.025	235.770	0.392	V	CPM
		2008.50	0.804	0.060	245.3	2.0	0.766	0.026	240.510	0.238	V	CPM
		2010.71	0.769	0.060	242.8	2.0	0.785	0.026	244.094	0.183	V	CPM
		2010.89	0.760	0.025	244.5	0.2	0.778	0.026	244.367	0.184	N	CPM
		2010.90	0.773	0.020	244.9	0.5	0.778	0.026	244.390	0.184	K	CPM
		2011.52	0.784	0.030	244.0	1.0	0.804	0.026	245.416	0.181	V	CPM
		2011.67	0.777	0.030	244.9	1.0	0.800	0.026	245.615	0.183	V	CPM
		2011.80	0.770	0.030	244.5	0.2	0.794	0.026	245.814	0.186	N	CPM
2011.85	0.781	0.030	244.4	1.0	0.792	0.026	245.893	0.188	V	CPM		
HD 1160	2	2010.83	5.150	0.025	349.8	0.2	...	...	...	...	N	CPM
		2002.57	5.167	0.030	351.0	0.5	5.002	0.025	351.358	0.218	V	CPM
		2002.74	5.167	0.035	349.8	0.5	5.007	0.025	351.415	0.217	I	CPM
		2002.87	5.220	0.035	349.6	0.5	5.011	0.025	351.464	0.217	I	CPM
		2003.53	5.185	0.035	349.5	0.5	5.019	0.025	351.142	0.216	I	CPM
		2003.64	5.180	0.035	349.7	0.5	5.021	0.025	351.159	0.215	I	CPM
		2003.84	5.155	0.030	350.2	0.5	5.028	0.025	351.241	0.214	V	CPM
		2003.86	5.179	0.035	349.6	0.5	5.028	0.025	351.248	0.214	I	CPM
		2005.98	5.145	0.030	350.4	0.5	5.066	0.025	350.832	0.211	V	CPM
		2007.90	5.080	0.070	349.4	0.5	5.099	0.025	350.415	0.208	I	CPM
		2008.50	5.155	0.030	349.7	0.5	5.106	0.025	350.095	0.209	V	CPM
		2010.71	5.146	0.030	349.4	0.5	5.146	0.025	349.729	0.208	V	CPM
		2010.89	5.160	0.030	349.6	0.2	5.152	0.025	349.796	0.207	N	CPM
		2010.90	5.137	0.020	349.9	0.5	5.152	0.025	349.798	0.207	K	CPM
		2011.52	5.142	0.030	349.4	0.5	5.159	0.025	349.480	0.208	V	CPM
		2011.67	5.140	0.030	349.5	0.5	5.163	0.025	349.508	0.208	V	CPM
2011.76	5.119	0.070	349.2	0.5	5.166	0.025	349.547	0.208	I	CPM		
2011.80	5.160	0.030	349.6	0.2	5.167	0.025	349.566	0.207	N	CPM		
2011.85	5.140	0.030	349.4	0.5	5.168	0.025	349.584	0.207	V	CPM		
HIP 14146	1	2010.02	3.936	0.009	296.6	0.2	...	...	...	...	N	BG
		2010.83	3.901	0.009	297.6	0.2	3.886	0.008	297.744	0.175	N	BG
		2011.80	3.801	0.009	299.4	0.2	3.790	0.008	299.396	0.180	N	BG
HD 31295	1	2009.04	6.261	0.009	271.6	0.2	...	...	...	...	N	BG
		2010.98	6.368	0.009	273.9	0.2	6.362	0.009	273.794	0.200	N	BG
HD 31295	2	2009.04	8.805	0.009	316.7	0.2	...	...	...	...	N	BG
		2010.98	9.050	0.009	317.2	0.2	9.049	0.008	317.329	0.216	N	BG
HIP 25280	1	2010.89	5.219	0.009	80.4	0.2	...	...	...	...	N	BG
		2009.05	5.336	0.009	81.7	0.2	5.291	0.009	80.852	0.198	N	BG
ζ Lep	1	2008.95	5.295	0.009	110.0	0.2	...	...	...	...	N	BG
		2011.20	5.390	0.009	109.6	0.2	5.379	0.009	109.940	0.198	N	BG
HD 54341	1	2008.95	3.080	0.009	131.2	0.2	...	...	...	...	N	BG

Table 4—Continued

Name	#	Epoch	Measured Position				Background Position				Inst.	Comp?
			Sep (")	$\sigma_{Sep}$	PA (deg)	$\sigma_{PA}$	Sep (")	$\sigma_{Sep}$	PA (deg)	$\sigma_{PA}$		
HD 54341	2	2010.98	3.077	0.009	131.9	0.2	3.090	0.009	131.710	0.220	N	BG
		2008.95	4.372	0.009	137.3	0.2	...	...	...	...	N	BG
		2010.98	4.363	0.009	137.9	0.2	4.385	0.010	137.663	0.210	N	BG
HIP 36188	1	2009.18	7.460	0.009	205.0	0.2	...	...	...	...	N	BG
		2011.84	7.218	0.009	204.4	0.2	7.321	0.009	204.616	0.202	N	BG
HD 71155	1	2008.96	5.766	0.009	86.7	0.2	...	...	...	...	N	BG
		2009.97	5.857	0.013	85.7	0.5	5.836	0.009	86.502	0.225	V	BG
HD 71155	2	2011.37	5.955	0.009	86.2	0.2	5.969	0.009	86.464	0.221	N	BG
		2008.96	7.360	0.009	357.8	0.2	...	...	...	...	N	BG
		2011.37	7.391	0.009	359.5	0.2	7.391	0.009	359.401	0.203	N	BG
HD 71155	3	2008.96	9.403	0.009	246.1	0.2	...	...	...	...	N	BG
		2011.37	9.229	0.009	245.5	0.2	9.205	0.009	245.760	0.208	N	BG
HIP 41373	1	2009.05	3.074	0.009	260.9	0.2	...	...	...	...	N	BG
		2010.02	3.012	0.009	259.7	0.2	3.040	0.010	260.785	0.207	N	BG
		2011.33	2.955	0.009	260.0	0.2	2.977	0.010	260.236	0.212	N	BG
HIP 41373	2	2009.05	5.927	0.009	0.7	0.2	...	...	...	...	N	BG
		2010.02	5.910	0.009	1.0	0.2	5.926	0.009	1.032	0.195	N	BG
		2011.33	5.896	0.009	1.6	0.2	5.909	0.009	1.681	0.195	N	BG
HIP 43121	1	2009.27	4.760	0.009	350.0	0.2	...	...	...	...	N	BG
		2011.37	4.847	0.009	351.6	0.2	4.844	0.008	351.809	0.201	N	BG
HIP 50191	1	2008.96	5.192	0.009	280.4	0.2	...	...	...	...	N	BG
		2010.01	5.032	0.009	280.1	0.2	5.022	0.009	280.226	0.219	N	BG
HIP 50191	2	2008.96	5.144	0.009	285.6	0.2	...	...	...	...	N	BG
		2010.01	4.988	0.009	285.7	0.2	4.973	0.009	285.592	0.197	N	BG
HIP 57328	1	2009.27	1.599	0.009	268.1	0.2	...	...	...	...	N	BG
		2011.33	1.751	0.009	269.7	0.2	1.714	0.009	269.799	0.195	N	BG
		2009.04	4.472	0.009	322.7	0.2	...	...	...	...	N	BG
HR 4796	1	1994.20	4.700	0.050	311.0	1.0	4.767	0.010	311.974	0.193	E <sup>1</sup>	BG
		2012.27	4.422	0.009	324.9	0.2	4.423	0.009	325.341	0.212	N	BG
		2009.04	3.028	0.009	252.7	0.2	...	...	...	...	N	BG
HD 110058	1	2012.24	2.908	0.009	252.6	0.2	2.915	0.008	253.046	0.236	N	BG
		2009.04	3.259	0.009	94.1	0.2	...	...	...	...	N	BG
HD 110058	2	2012.24	3.336	0.009	92.9	0.2	3.359	0.010	93.167	0.206	N	BG
		2009.04	6.181	0.009	160.3	0.2	...	...	...	...	N	BG
HD 110058	3	2012.24	6.192	0.009	158.8	0.2	6.172	0.009	159.250	0.213	N	BG
		2009.04	7.792	0.009	231.2	0.2	...	...	...	...	N	BG
HD 110058	4	2012.24	7.626	0.009	230.3	0.2	7.682	0.009	230.972	0.211	N	BG
		2009.04	7.796	0.009	125.8	0.2	...	...	...	...	N	BG
HD 110058	5	2012.24	7.884	0.009	124.8	0.2	7.852	0.011	125.090	0.213	N	BG
		2009.04	8.366	0.009	142.6	0.2	...	...	...	...	N	BG
HD 110058	6	2012.24	8.422	0.009	141.4	0.2	8.391	0.009	141.831	0.206	N	BG
		2009.10	3.316	0.009	181.9	0.2	...	...	...	...	N	BG
HD 118878	1	2009.10	3.316	0.009	181.9	0.2	...	...	...	...	N	BG
		2012.27	3.270	0.009	180.4	0.2	3.252	0.010	180.322	0.217	N	BG

Table 4—Continued

Name	#	Epoch	Measured Position				Background Position				Inst.	Comp?
			Sep (")	$\sigma_{Sep}$	PA (deg)	$\sigma_{PA}$	Sep (")	$\sigma_{Sep}$	PA (deg)	$\sigma_{PA}$		
HD 118878	2	2009.10	6.203	0.009	213.7	0.2	...	...	...	...	N	BG
		2012.27	6.100	0.009	213.0	0.2	6.100	0.008	213.251	0.189	N	BG
HD 118878	3	2009.10	7.254	0.009	120.3	0.2	...	...	...	...	N	BG
		2012.27	7.298	0.009	119.5	0.2	7.304	0.009	119.468	0.201	N	BG
HD 118878	4	2009.10	9.668	0.009	217.0	0.2	...	...	...	...	N	BG
		2012.27	9.539	0.009	216.6	0.2	9.562	0.010	216.795	0.218	N	BG
HD 136482	1	2009.19	0.921	0.009	240.6	0.2	...	...	...	...	N	BG
		2010.27	0.916	0.009	241.9	0.2	0.888	0.009	241.350	0.191	N	BG
HD 136482	2	2009.19	2.954	0.009	156.7	0.2	...	...	...	...	N	BG
		2010.27	2.920	0.009	156.4	0.2	2.940	0.009	156.102	0.193	N	BG
HD 136482	3	2009.19	3.772	0.009	181.8	0.2	...	...	...	...	N	BG
		2010.27	3.737	0.009	181.7	0.2	3.745	0.009	181.429	0.175	N	BG
HD 136482	4	2009.19	5.081	0.009	146.0	0.2	...	...	...	...	N	BG
		2010.27	5.066	0.009	145.7	0.2	5.073	0.010	145.616	0.197	N	BG
HD 136482	5	2009.19	5.477	0.009	251.9	0.2	...	...	...	...	N	BG
		2010.27	5.414	0.009	252.8	0.2	5.447	0.009	252.061	0.183	N	BG
HD 136482	6	2009.19	6.334	0.009	51.9	0.2	...	...	...	...	N	BG
		2010.27	6.387	0.009	52.2	0.2	6.368	0.009	51.883	0.196	N	BG
HD 138965	1	2009.12	1.708	0.009	61.4	0.2	...	...	...	...	N	BG
		2011.32	1.845	0.009	59.7	0.2	1.857	0.009	59.310	0.188	N	BG
HD 138965	2	2009.12	4.085	0.009	244.6	0.2	...	...	...	...	N	BG
		2011.32	3.931	0.009	245.8	0.2	3.942	0.010	245.727	0.203	N	BG
HD 138965	3	2009.12	4.284	0.009	269.6	0.2	...	...	...	...	N	BG
		2011.32	4.200	0.009	271.1	0.2	4.188	0.008	271.417	0.221	N	BG
HD 138965	4	2009.12	7.386	0.009	157.3	0.2	...	...	...	...	N	BG
		2011.32	7.300	0.009	155.9	0.2	7.304	0.009	156.236	0.210	N	BG
HD 138965	5	2009.12	7.503	0.009	102.1	0.2	...	...	...	...	N	BG
		2011.32	7.597	0.009	100.9	0.2	7.572	0.009	100.971	0.212	N	BG
HD 138965	6	2009.12	7.838	0.009	236.4	0.2	...	...	...	...	N	BG
		2011.32	7.683	0.009	236.9	0.2	7.685	0.010	236.811	0.218	N	BG
HD 138965	7	2009.12	8.048	0.009	326.9	0.2	...	...	...	...	N	BG
		2011.32	8.112	0.009	327.8	0.2	8.106	0.008	328.008	0.209	N	BG
HD 138965	8	2009.12	9.970	0.009	4.4	0.2	...	...	...	...	N	BG
		2011.32	10.085	0.009	4.6	0.2	10.108	0.009	4.882	0.192	N	BG
HD 141569	1	2009.18	6.400	0.009	13.2	0.2	...	...	...	...	N	BG
		2011.33	6.438	0.009	12.9	0.2	6.448	0.009	13.512	0.189	N	BG
HD 141569	2	2009.18	7.850	0.009	209.7	0.2	...	...	...	...	N	BG
		2011.33	7.761	0.009	209.8	0.2	7.794	0.009	209.553	0.204	N	BG
HIP 79781	1	2010.66	4.473	0.009	179.4	0.2	...	...	...	...	N	BG
		2012.16	4.542	0.022	180.5	0.5	4.476	0.009	180.671	0.198	G	BG
HIP 79781	2	2010.66	6.492	0.009	130.2	0.2	...	...	...	...	N	BG
		2012.16	6.448	0.022	130.6	0.5	6.416	0.010	130.842	0.189	G	BG
HIP 79797	1	2010.35	5.737	0.009	276.5	0.2	...	...	...	...	N	BG

Table 4—Continued

Name	#	Epoch	Measured Position				Background Position				Inst.	Comp?
			Sep (")	$\sigma_{Sep}$	PA (deg)	$\sigma_{PA}$	Sep (")	$\sigma_{Sep}$	PA (deg)	$\sigma_{PA}$		
HIP 79797	2	2011.36	5.701	0.009	277.3	0.2	5.701	0.010	277.420	0.179	N	BG
		2012.26	5.682	0.009	278.1	0.2	5.679	0.010	278.188	0.179	N	BG
	2010.35	5.759	0.009	18.8	0.2	...	...	...	...	N	BG	
	2011.36	5.841	0.009	18.9	0.2	5.854	0.010	18.933	0.174	N	BG	
HIP 79797	3	2012.26	5.907	0.009	19.1	0.2	5.933	0.009	19.000	0.172	N	BG
		2010.35	6.213	0.009	118.0	0.2	...	...	...	...	N	BG
		2011.36	6.239	0.009	117.1	0.2	6.215	0.009	117.102	0.180	N	BG
HIP 79797	4	2012.26	6.252	0.009	116.5	0.2	6.212	0.009	116.371	0.180	N	BG
		2010.35	6.691	0.009	293.9	0.2	...	...	...	...	N	CPM
		2004.49	6.660	0.010	294.0	0.1	6.745	0.009	289.134	0.172	V <sup>2</sup>	CPM
		2006.44	6.670	0.030	294.0	0.2	6.724	0.009	290.699	0.172	V <sup>2</sup>	CPM
HIP 79797	5	2011.36	6.694	0.009	293.9	0.2	6.683	0.009	294.685	0.173	N	CPM
		2012.26	6.697	0.009	293.8	0.2	6.684	0.009	295.365	0.173	N	CPM
		2010.35	6.949	0.009	197.2	0.2	...	...	...	...	N	BG
		2011.36	6.813	0.009	196.9	0.2	6.854	0.010	197.035	0.197	N	BG
HIP 79797	6	2012.26	6.754	0.009	196.8	0.2	6.776	0.010	196.954	0.199	N	BG
		2011.36	6.907	0.009	329.4	0.2	...	...	...	...	N	BG
HIP 79797	7	2012.26	6.940	0.009	329.9	0.2	6.953	0.009	329.933	0.202	N	BG
		2011.36	7.737	0.009	250.7	0.2	...	...	...	...	N	BG
HIP 79797	8	2012.26	7.687	0.009	251.0	0.2	7.683	0.008	251.112	0.199	N	BG
		2010.35	9.598	0.009	6.5	0.2	...	...	...	...	N	BG
HIP 79881	1	2011.36	9.696	0.009	6.6	0.2	9.687	0.008	6.719	0.193	N	BG
		2010.36	1.627	0.009	267.7	0.2	...	...	...	...	N	BG
HIP 79881	2	2011.33	1.594	0.009	270.6	0.2	1.599	0.010	271.163	0.215	N	BG
		2010.36	4.551	0.009	175.6	0.2	...	...	...	...	N	BG
HIP 79881	3	2011.33	4.460	0.009	175.3	0.2	4.454	0.010	175.184	0.204	N	BG
		2010.36	6.600	0.009	233.2	0.2	...	...	...	...	N	BG
HIP 85922	1	2011.33	6.530	0.009	233.8	0.2	6.519	0.008	233.793	0.181	N	BG
		2010.57	7.359	0.009	40.3	0.2	...	...	...	...	N	BG
$\gamma$ Oph	1	2012.16	7.595	0.022	39.3	0.5	7.503	0.008	39.659	0.208	G	BG
		2009.19	4.500	0.009	59.5	0.2	...	...	...	...	N	BG
$\gamma$ Oph	2	2010.27	4.571	0.009	58.5	0.2	4.562	0.009	58.935	0.193	N	BG
		2009.19	5.886	0.009	239.4	0.2	...	...	...	...	N	BG
$\gamma$ Oph	3	2010.27	5.825	0.009	240.0	0.2	5.825	0.008	239.843	0.164	N	BG
		2009.19	6.203	0.009	267.3	0.2	...	...	...	...	N	BG
$\gamma$ Oph	4	2010.27	6.163	0.009	268.3	0.2	6.172	0.009	268.010	0.211	N	BG
		2009.19	6.581	0.009	275.0	0.2	...	...	...	...	N	BG
$\gamma$ Oph	5	2010.27	6.591	0.009	275.9	0.2	6.560	0.008	275.667	0.225	N	BG
		2009.19	6.962	0.009	59.8	0.2	...	...	...	...	N	BG
$\gamma$ Oph	6	2010.27	7.010	0.009	58.8	0.2	7.023	0.009	59.398	0.210	N	BG
		2009.19	8.689	0.009	96.2	0.2	...	...	...	...	N	BG
$\gamma$ Oph	7	2010.27	8.711	0.009	95.2	0.2	8.710	0.008	95.672	0.209	N	BG
		2009.19	9.240	0.009	253.4	0.2	...	...	...	...	N	BG

Table 4—Continued

Name	#	Epoch	Measured Position				Background Position				Inst.	Comp?
			Sep (")	$\sigma_{Sep}$	PA (deg)	$\sigma_{PA}$	Sep (")	$\sigma_{Sep}$	PA (deg)	$\sigma_{PA}$		
HD 172555	1	2010.27	9.222	0.009	254.2	0.2	9.192	0.010	253.783	0.177	N	BG
		2009.27	7.702	0.009	319.0	0.2	...	...	...	...	N	BG
		2005.35	7.210	0.120	316.5	1.0	7.186	0.009	316.771	0.212	H	BG
HD 176638	1	2011.79	3.500	0.009	157.8	0.2	...	...	...	...	N	BG
		2011.36	3.517	0.009	158.0	0.2	3.515	0.009	158.048	0.194	N	BG
		2012.26	3.474	0.009	158.9	0.2	3.460	0.009	158.640	0.197	N	BG
HD 176638	2	2011.36	4.723	0.009	93.4	0.2	...	...	...	...	N	BG
		2011.79	4.732	0.009	93.3	0.2	4.728	0.010	93.145	0.198	N	BG
		2012.26	4.669	0.009	93.4	0.2	4.667	0.010	92.947	0.200	N	BG
HD 176638	3	2011.79	5.233	0.009	265.6	0.2	...	...	...	...	N	BG
		2011.79	5.236	0.009	265.2	0.2	5.233	0.010	265.571	0.204	N	BG
		2012.26	5.287	0.009	265.6	0.2	5.291	0.010	265.831	0.202	N	BG
HD 176638	4	2011.79	9.416	0.009	319.6	0.2	...	...	...	...	N	BG
		2011.36	9.359	0.009	319.4	0.2	9.405	0.009	319.540	0.174	N	BG
		2012.26	9.414	0.009	319.5	0.2	9.470	0.009	319.443	0.173	N	BG
HR 7329	1	2009.27	4.175	0.009	167.6	0.2	...	...	...	...	N	CPM
		1998.49	4.170	0.050	166.8	0.2	5.128	0.009	166.582	0.139	H <sup>3</sup>	CPM
HD 196544	1	2011.31	4.743	0.009	90.8	0.2	...	...	...	...	N	BG
		2008.69	4.863	0.050	91.0	1.0	4.873	0.010	91.021	0.208	G	BG
		2009.32	4.833	0.009	91.2	1.0	4.821	0.010	90.962	0.210	N	BG
		2010.83	4.814	0.009	90.3	0.2	4.795	0.010	90.728	0.211	N	BG
		2010.91	4.800	0.020	90.8	0.5	4.790	0.010	90.680	0.212	K	BG
HD 196544	2	2011.31	4.352	0.009	93.4	0.2	...	...	...	...	N	BG
		2008.69	4.468	0.050	93.8	1.0	4.483	0.008	93.545	0.199	G	BG
		2009.32	4.433	0.009	94.1	1.0	4.431	0.008	93.511	0.201	N	BG
		2010.83	4.413	0.009	93.0	0.2	4.404	0.008	93.272	0.202	N	BG
		2010.91	4.404	0.020	93.6	0.5	4.399	0.008	93.222	0.202	K	BG
HIP 104308	1	2011.82	1.681	0.009	281.9	0.2	...	...	...	...	N	BG
		2012.57	1.745	0.009	283.4	0.2	1.729	0.008	283.708	0.234	N	BG
HIP 104308	2	2011.82	2.895	0.009	264.0	0.2	...	...	...	...	N	BG
		2012.57	2.929	0.009	265.3	0.2	2.924	0.011	265.279	0.192	N	BG
HIP 107556	1	2011.75	6.179	0.009	169.5	0.2	...	...	...	...	N	BG
		2010.66	6.546	0.009	167.7	0.2	6.558	0.009	167.903	0.183	N	BG
		2010.86	6.481	0.009	167.7	0.2	6.483	0.009	167.685	0.185	N	BG

<sup>1</sup>Astrometry from Mouillet et al. (1997)

<sup>2</sup>Astrometry from Huélamo et al. (2010)

<sup>3</sup>Astrometry from Lowrance et al. (2000)

Note. — Astrometry for each candidate companion detected around our target stars from NICI and archival observations. At each epoch we give the measured separation, position angle, and uncertainties as well as the predicted separation and position angle for a background object based on the proper motion and parallax of the primary and the candidate position at the reference epoch, which is the first epoch listed for each candidate. Astrometry is taken from Gemini-South NICI (N), VLT NACO (V), Keck NIRC2 (K), HST NICMOS (H), VLT ISAAC (I), ESO 3.6m COME-ON-PLUS/ADONIS (E), and Gemini-North NIRI (G).

Table 5. Relative Astrometry of HIP 79797 Bb with respect to Ba

UT Epoch	Sep (mas)	PA ( $^{\circ}$ )
2010.2712	$60 \pm 20$	$331 \pm 13$
2010.3534	$60 \pm 6$	$339 \pm 3$
2011.3589	$63 \pm 15$	$340 \pm 10$
2012.2623	$63 \pm 7$	$342 \pm 3$
2012.6667	$77 \pm 14$	$338 \pm 9$

Table 6. Properties of the HIP 79797 System

	HIP 79797 A	HIP 79797 Ba	HIP 79797 Bb
Age (Myr)	$200^{+170}_{-130}$		
Distance (pc)	$52.2 \pm 1.1^1$		
Spectral Type	A4	M9 <sup>2</sup>	M9 <sup>2</sup>
$\Delta J$ (Bab – A, mag)		$8.55 \pm 0.14$	
$\Delta H$ (Bab – A, mag)		$7.37 \pm 0.17$	
$\Delta K_S$ (Bab – A, mag)		$7.31 \pm 0.19$	
$\Delta J$ (Bb – Ba, mag)		$0.33 \pm 0.07$	
$\Delta H$ (Bb – Ba, mag)		$0.12 \pm 0.06$	
$\Delta K_S$ (Bb – Ba, mag)		$0.20 \pm 0.06$	
$J$ (mag)	$5.77 \pm 0.03^3$	$14.92 \pm 0.19$	$15.26 \pm 0.19$
$H$ (mag)	$5.68 \pm 0.05^3$	$13.74 \pm 0.15$	$13.87 \pm 0.15$
$K_s$ (mag)	$5.66 \pm 0.02^3$	$13.62 \pm 0.17$	$13.81 \pm 0.17$
$M_J$ (mag)	$2.18 \pm 0.06$	$11.3 \pm 0.2$	$11.7 \pm 0.2$
$M_H$ (mag)	$2.10 \pm 0.07$	$10.16 \pm 0.16$	$10.28 \pm 0.16$
$M_{K_s}$ (mag)	$2.07 \pm 0.05$	$10.03 \pm 0.17$	$10.23 \pm 0.17$
Mass	$1.76 \pm 0.4 M_\odot$	$58^{+21}_{-20} M_{Jup}$	$55^{+20}_{-19} M_{Jup}$
Mass ratio (Bb/Ba)		$0.93 \pm 0.03$	
Separation (from A, arcseconds) <sup>4</sup>		$6.691 \pm 0.009$	
Position angle (from A, degrees) <sup>4</sup>		$293.9 \pm 0.2$	

<sup>1</sup>van Leeuwen (2007)

<sup>2</sup>Huélamo et al. (2010), and assuming the integrated light spectrum is similar to the spectra of the individual objects, which is consistent with the near-unity flux ratios.

<sup>3</sup>Cutri et al. (2003)

<sup>4</sup>Astrometry is from epoch 2010.3534 and is the separation and position angle of the photocenter of the binary from HIP 79797 A.

Table 7. Candidate Companions with One Epoch of Data

Star	#	Sep (")	Sep (AU)	PA (deg)	$\Delta H$ (mag)	Epoch	Action
HD 31295	1	7.77	277	162.4	15.6	2009.0356	Sep < 7.77"
	2	8.66	309	277.1	17.5	2009.0356	
HIP 36188	1	10.64	528	352.7	14.6	2011.8384	Sep < 10.64"
HIP 40916	1	6.26	421	332.7	12.8	2009.0466	Sep < 6.26"
	2	6.95	467	131.0	12.6	2009.0466	
	3	7.65	514	60.9	7.4	2009.0466	
	4	7.67	515	90.9	8.2	2009.0466	
HD 71155	1	9.93	372	221.0	15.2	2008.9563	Sep < 9.93"
HIP 50191	1	4.11	128	257.9	15.4	2010.0110	Revert to 2008.9563 ASDI
HD 118878	1	9.21	1114	330.7	11.6	2009.1041	
	2	12.66	1532	69.2	14.9	2009.1041	
	3	12.84	1553	39.5	14.9	2009.1041	
	4	12.99	1571	145.1	13.9	2009.1041	
	5	8.81	1066	299.4	10.7	2012.2650	
	6	10.88	1317	175.8	15.0	2012.2650	
GJ 560 A	1	5.71	95	230.7	15.9	2009.1891	Sep < 5.88"
	2	5.88	97	185.6	15.8	2009.1891	
	3	6.15	102	27.5	16.3	2009.1891	
	4	6.30	104	52.6	16.1	2009.1891	
	5	6.86	114	269.0	14.6	2009.1891	
	6	7.34	122	284.4	15.0	2009.1891	
HD 131835	1	2.31	280	274.2	14.4	2009.2712	Drop
	2	5.27	638	20.2	12.3	2009.2712	
	3	5.70	689	22.7	11.5	2009.2712	
	4	6.13	741	303.2	11.4	2009.2712	
	5	8.09	979	239.8	13.8	2009.2712	
	6	8.29	1003	91.6	14.6	2009.2712	
	7	8.93	1080	100.7	13.8	2009.2712	
HD 135454	1	3.82	658	135.2	12.1	2009.1918	Drop
	2	4.96	854	205.7	14.4	2009.1918	
	3	5.32	916	26.2	14.9	2009.1918	
	4	6.01	1033	349.7	10.1	2009.1918	
	5	6.83	1174	178.2	13.2	2009.1918	
	6	7.30	1255	118.8	10.1	2009.1918	
	7	8.21	1412	82.3	12.3	2009.1918	
HD 136482	1	6.05	823	157.1	15.2	2009.1891	Sep < 6.05"
	2	8.59	1168	80.1	15.5	2009.1891	
	3	8.94	1215	280.1	13.6	2009.1891	
	4	9.24	1257	181.1	15.1	2009.1891	
	5	9.57	1302	77.7	10.3	2009.1891	
	6	10.46	1422	17.4	13.9	2009.1891	
HD 138965	1	8.34	651	97.6	13.4	2009.1151	Sep < 8.16"
	2	12.12	946	111.1	13.9	2009.1151	

Table 7—Continued

Star	#	Sep (")	Sep (AU)	PA (deg)	$\Delta H$ (mag)	Epoch	Action
	3	13.19	1029	90.8	10.6	2009.1151	
	4	8.16	636	244.6	14.7	2011.3151	
	5	10.92	852	199.7	12.4	2011.3151	
HIP 77464	1	8.83	477	31.9	12.7	2010.5671	Sep < 8.83"
HIP 79797	1	13.23	691	291.3	13.7	2011.3589	Sep < 13.232"
HIP 78106	1	3.31	202	280.9	12.4	2009.2739	Drop
	2	5.02	306	104.9	16.3	2009.2739	
	3	6.37	389	47.9	16.4	2009.2739	
	4	7.14	436	153.9	15.9	2009.2739	
	5	7.58	462	114.8	14.2	2009.2739	
	6	9.15	558	305.1	12.7	2009.2739	
HIP 81650	1	1.44	71	87.1	13.0	2010.3534	Drop
	2	1.83	91	245.7	13.8	2010.3534	
	3	2.10	104	253.1	12.5	2010.3534	
	4	2.28	112	32.4	13.2	2010.3534	
	5	2.83	140	120.2	14.1	2010.3534	
	6	2.89	143	218.4	12.0	2010.3534	
	7	2.96	146	355.1	11.9	2010.3534	
	8	3.41	168	350.0	15.1	2010.3534	
	9	3.60	178	64.6	14.1	2010.3534	
	10	3.75	185	111.0	11.6	2010.3534	
	11	3.92	194	190.3	9.6	2010.3534	
	12	3.98	197	227.4	15.0	2010.3534	
	13	4.23	209	292.8	14.9	2010.3534	
	14	4.29	212	123.2	12.7	2010.3534	
	15	4.31	213	219.6	12.3	2010.3534	
	16	4.37	216	189.7	14.7	2010.3534	
	17	4.44	219	284.8	14.8	2010.3534	
	18	4.50	222	211.8	13.8	2010.3534	
	19	4.54	224	207.6	13.9	2010.3534	
	20	4.65	230	251.1	14.6	2010.3534	
	21	5.00	247	5.6	12.5	2010.3534	
	22	5.15	254	176.6	14.5	2010.3534	
	23	5.49	271	25.0	12.9	2010.3534	
	24	5.54	274	108.9	14.8	2010.3534	
	25	5.59	276	333.3	12.5	2010.3534	
	26	5.60	277	347.2	13.9	2010.3534	
	27	5.74	284	133.7	13.6	2010.3534	
	28	5.93	293	233.4	10.8	2010.3534	
	29	6.21	307	30.4	13.9	2010.3534	
	30	6.25	309	353.9	13.8	2010.3534	
	31	6.33	313	344.2	14.6	2010.3534	
	32	6.44	318	39.7	10.8	2010.3534	
	33	6.78	335	13.6	15.1	2010.3534	

Table 7—Continued

Star	#	Sep (")	Sep (AU)	PA (deg)	$\Delta H$ (mag)	Epoch	Action
	34	6.79	335	89.8	14.5	2010.3534	
	35	7.10	351	285.4	12.6	2010.3534	
	36	7.12	352	255.7	15.0	2010.3534	
	37	7.14	353	59.1	14.3	2010.3534	
	38	7.37	364	128.0	14.3	2010.3534	
	39	7.37	364	94.6	15.5	2010.3534	
	40	7.65	378	200.1	14.5	2010.3534	
	41	7.80	386	222.8	14.6	2010.3534	
	42	7.81	386	28.3	14.9	2010.3534	
	43	8.07	398	295.3	14.3	2010.3534	
HIP 85038	1	4.26	264	156.1	13.0	2010.3562	Drop
	2	4.30	267	121.2	12.1	2010.3562	
	3	5.35	332	202.5	13.9	2010.3562	
	4	5.45	338	321.3	13.2	2010.3562	
	5	5.70	354	115.0	14.9	2010.3562	
	6	5.83	361	216.5	8.5	2010.3562	
	7	6.71	416	224.3	9.8	2010.3562	
	8	7.91	491	23.5	13.6	2010.3562	
$\gamma$ Oph	1	9.24	291	241.7	14.5	2010.2657	Sep < 9.24"
HD 176638	1	9.76	577	153.6	13.6	2011.7917	Sep < 9.76"
HIP 93805	1	3.45	131	90.9	14.5	2010.2712	Drop
	2	3.89	147	169.9	14.9	2010.2712	
	3	4.35	165	275.9	15.3	2010.2712	
	4	4.84	183	46.4	14.5	2010.2712	
	5	5.24	198	36.6	15.9	2010.2712	
	6	6.01	228	80.5	13.1	2010.2712	
	7	6.58	249	173.3	15.4	2010.2712	
	8	7.24	275	63.2	16.2	2010.2712	
HD 182681	1	4.49	314	250.1	11.2	2010.6521	Drop
	2	5.29	370	251.4	15.7	2010.6521	
	3	8.59	600	305.1	13.6	2010.6521	
	4	8.87	620	289.6	12.0	2010.6521	
	5	9.54	667	303.7	14.9	2010.6521	

Note. — Target stars with candidate companions for which we only have a single epoch of data. Since we cannot classify these as either CPM or background, we provide the properties of these candidates here and note the changes we make to the contrast curves in the Action column (see Section 5.5.1 for details). Contrast curves are edited either by reverting to a less sensitive contrast curve or restricting the contrast curve to within a given separation. For cases where we have only a single epoch and there are candidates inside the 100% coverage region for position angle, we drop the star from our analysis.

Table 8. 95% completeness  $CH_4S$  and  $H$ -band contrasts ( $\Delta\text{mag}$ )

Target	0.36''	0.5''	0.75''	1''	1.5''	2''	3''	4''	5''	7''	Cov.	9''	Cov.	12''	Cov.	14.8''	Cov.
HD 1160, $CH_4$	10.8	12.2	12.9	13.6	14.0	13.8	14.0	13.9	13.9	13.8	0.98	13.3	0.72	12.2	0.29	11.8	0.02
HD 1160, $H$ -band	7.5	9.6	11.5	13.0	14.3	14.6	14.6	14.7	14.5	14.5	0.88	14.3	0.61	13.8	0.26	13.7	0.03
HIP 2072, $H$ -band	-	-	-	13.1	14.9	16.1	17.0	17.1	17.1	16.9	0.96	16.2	0.82	15.6	0.44	15.5	0.15
49 Cet, $CH_4$	10.7	12.4	13.4	14.0	14.6	14.9	14.9	14.8	14.6	14.2	1.00	13.3	0.84	12.4	0.47	12.1	0.10
49 Cet, $H$ -band	-	-	4.0	13.2	14.8	15.9	16.8	16.9	16.8	16.6	0.89	16.3	0.66	15.8	0.32	15.3	0.07
HD 10939, $CH_4$	7.6	9.6	11.8	13.1	14.2	14.5	14.6	14.6	14.5	14.5	0.93	14.4	0.68	14.0	0.30	13.5	0.06
HIP 12394, $CH_4$	11.5	12.9	14.2	15.1	15.3	15.5	15.5	15.4	15.2	15.2	0.98	15.0	0.74	14.3	0.32	13.4	0.03
HIP 12394, $H$ -band	-	-	-	-	10.0	16.1	17.4	17.8	17.7	17.9	0.86	17.7	0.62	17.4	0.27	16.9	0.04
HIP 12413, $CH_4$	10.6	12.4	13.5	14.1	14.6	14.6	14.6	14.6	14.5	14.1	0.99	13.6	0.83	12.9	0.48	12.4	0.14
HIP 12413, $H$ -band	-	-	-	13.8	15.4	16.2	17.2	17.3	17.4	17.2	0.88	16.9	0.62	16.2	0.29	16.2	0.05
HD 17848, $CH_4$	10.5	11.8	13.0	13.8	14.5	14.8	14.9	14.9	14.8	14.7	0.99	14.4	0.76	13.8	0.32	13.3	0.06
HD 17848, $H$ -band	-	-	-	-	14.4	15.6	16.9	17.1	17.2	17.0	0.87	16.8	0.63	16.4	0.28	15.8	0.05
HIP 14146, $H$ -band	8.2	10.0	11.6	12.7	15.0	15.9	17.3	17.6	17.7	17.9	0.87	17.9	0.60	17.7	0.23	17.1	0.02
HD 21997, $CH_4$	11.5	12.7	13.4	14.1	14.3	14.3	14.2	14.1	14.0	13.6	1.00	12.4	1.00	12.0	0.57	12.5	0.12
HD 21997, $H$ -band	-	-	10.6	12.5	14.3	15.4	16.1	16.2	16.1	16.5	0.84	16.6	0.57	16.5	0.23	16.4	0.02
HD 24966, $CH_4$	11.4	12.8	13.5	13.9	14.3	14.3	14.3	14.1	13.9	13.7	1.00	12.3	0.99	11.7	0.62	11.9	0.19
HD 24966, $H$ -band	-	6.3	12.4	13.3	14.9	15.3	15.8	15.7	15.5	15.3	0.89	14.9	0.67	14.3	0.32	13.9	0.06
HD 31295, $CH_4$	11.1	12.8	13.8	14.7	15.1	15.3	15.4	15.2	15.3	15.0	0.98	14.7	0.72	13.6	0.28	13.1	0.02
HD 31295, $H$ -band	-	-	-	-	14.9	16.0	17.0	17.2	17.3	17.2	0.86	17.1	0.62	16.5	0.27	15.1	0.04
HD 32297, $CH_4$	11.2	12.5	13.1	13.6	13.9	13.9	13.9	13.9	13.9	13.7	0.97	13.3	0.70	12.1	0.27	11.9	0.04
HD 32297, $H$ -band	-	-	11.5	12.7	14.6	15.1	15.3	15.2	15.2	15.1	0.85	15.0	0.60	14.8	0.25	14.3	0.03
HIP 25280, $CH_4$	11.9	13.1	14.1	14.6	14.9	15.3	15.1	15.0	14.8	14.6	1.00	13.9	0.89	13.1	0.56	11.9	0.11
HIP 25280, $H$ -band	-	-	4.9	15.5	16.0	16.3	16.6	16.6	16.7	16.2	1.00	15.3	1.00	13.0	0.57	15.0	0.09
HD 38206, $CH_4$	11.5	12.8	13.7	14.3	14.8	14.8	14.8	14.7	14.6	14.4	1.00	13.7	0.86	13.0	0.47	12.5	0.06
HD 38206, $H$ -band	-	-	-	12.6	14.6	15.4	16.1	16.2	16.2	16.2	0.86	16.1	0.60	15.8	0.25	14.9	0.03
$\zeta$ Lep, $CH_4$	11.1	12.5	13.7	14.6	15.5	15.6	15.6	15.4	15.4	15.3	0.99	14.9	0.81	14.3	0.43	13.3	0.07
$\zeta$ Lep, $H$ -band	-	-	-	-	-	15.1	16.6	17.2	17.6	17.5	0.92	17.6	0.74	16.9	0.37	15.7	0.09
$\beta$ Pic, $CH_4$	10.8	12.2	13.4	14.3	14.9	15.0	15.0	15.0	15.0	15.0	1.00	14.6	0.96	13.9	0.60	12.8	0.17
HIP 28910, $CH_4$	10.8	12.4	13.7	14.3	15.0	15.1	15.2	15.0	14.9	14.7	1.00	14.2	0.87	13.5	0.48	13.0	0.12
HIP 28910, $H$ -band	-	-	-	13.1	14.7	15.8	17.0	17.2	17.3	17.2	0.90	17.2	0.64	16.9	0.29	16.5	0.05
HD 46190, $CH_4$	11.9	13.2	14.0	14.5	14.8	14.7	14.8	14.8	14.8	14.5	0.98	14.1	0.73	13.0	0.29	13.0	0.05
HD 46190, $H$ -band	-	5.8	12.1	13.4	15.3	15.8	16.1	16.2	16.1	16.0	0.87	15.8	0.63	15.4	0.25	14.9	0.03
HD 54341, $CH_4$	10.9	12.2	13.2	13.8	14.2	14.4	14.4	14.1	14.1	13.7	1.00	12.5	0.89	11.8	0.52	12.0	0.07
HD 54341, $H$ -band	-	-	3.5	12.4	13.9	14.9	15.6	15.7	15.5	15.3	0.89	15.0	0.67	14.6	0.32	14.2	0.06
HIP 36188, $CH_4$	11.0	12.5	14.1	14.8	15.4	15.7	15.8	15.7	15.7	15.5	0.98	15.3	0.69	15.1	0.27	14.2	0.05

Table 8—Continued

Target	0.36''	0.5''	0.75''	1''	1.5''	2''	3''	4''	5''	7''	Cov.	9''	Cov.	12''	Cov.	14.8''	Cov.
HIP 36188, $H$ -band	-	-	-	12.6	13.7	14.7	16.3	17.2	17.7	17.8	0.87	18.0	0.62	17.8	0.25	17.3	0.03
HIP 40916, $CH_4$	10.6	11.9	12.7	13.3	13.9	14.0	14.2	14.1	14.1	13.9	0.99	13.6	0.78	12.9	0.38	12.2	0.04
HIP 40916, $H$ -band	8.5	9.6	10.4	11.3	13.1	14.1	14.9	14.9	14.8	14.5	0.88	14.4	0.65	13.8	0.30	13.5	0.06
HD 71155, $CH_4$	11.8	13.3	14.6	15.4	15.8	15.8	15.7	15.8	15.8	15.7	0.98	15.2	0.74	14.4	0.31	13.9	0.04
HD 71155, $H$ -band	-	-	-	-	-	16.9	18.0	18.3	18.4	18.7	0.99	18.7	0.76	18.4	0.14	16.8	0.06
HIP 41373, $CH_4$	9.9	11.4	12.3	12.8	13.5	13.7	13.9	13.9	13.8	13.6	0.99	12.9	0.81	12.2	0.41	11.7	0.05
HIP 43121, $CH_4$	11.1	12.4	13.7	14.3	14.8	15.1	15.0	15.0	15.0	15.0	0.98	14.7	0.73	14.0	0.28	13.7	0.05
HIP 43121, $H$ -band	-	-	-	12.3	14.1	15.3	16.0	16.3	16.3	16.2	0.87	16.0	0.63	15.5	0.26	14.7	0.03
HIP 45150, $CH_4$	11.6	12.7	14.1	14.4	14.8	15.0	14.9	15.0	14.8	14.8	0.99	14.4	0.75	13.6	0.30	13.2	0.05
HIP 45150, $H$ -band	-	-	4.2	13.7	15.3	16.2	16.7	16.9	16.9	16.7	0.87	16.6	0.63	16.3	0.26	16.0	0.04
HIP 45336, $CH_4$	11.2	12.7	13.9	14.9	15.3	15.4	15.5	15.4	15.4	15.1	0.98	14.9	0.74	14.2	0.30	13.7	0.05
HIP 45336, $H$ -band	-	-	-	-	14.4	15.4	16.8	17.5	17.6	17.5	0.88	17.3	0.64	16.8	0.27	16.5	0.04
HD 85672, $CH_4$	11.3	12.8	13.5	14.0	14.5	14.4	14.4	14.3	14.3	14.3	0.99	13.9	0.73	12.1	0.25	12.5	0.03
HD 85672, $H$ -band	7.6	9.4	11.6	12.9	14.5	14.7	14.7	14.9	14.9	14.8	0.86	14.6	0.61	14.1	0.26	12.6	0.03
HIP 49669, $CH_4$	8.1	11.0	12.1	13.3	14.3	14.5	14.7	14.7	14.6	14.5	1.00	14.3	0.87	13.3	0.30	13.7	0.01
HIP 49669, $H$ -band	12.4	13.7	14.0	13.8	14.4	14.7	16.2	17.6	18.0	18.8	0.87	18.9	0.63	18.8	0.26	18.0	0.04
HIP 50191, $CH_4$	11.8	13.1	14.3	15.0	15.2	15.2	15.2	15.0	14.8	14.8	1.00	14.4	0.83	13.7	0.45	12.8	0.06
HIP 50191, $H$ -band	-	-	-	-	13.7	14.9	16.1	16.6	16.8	16.8	0.92	16.6	0.70	16.1	0.38	15.4	0.09
HIP 54688, $CH_4$	11.3	13.0	14.0	14.6	14.8	14.8	15.1	15.2	14.9	15.0	0.95	14.8	0.71	14.3	0.31	13.5	0.06
HIP 54688, $H$ -band	9.1	10.7	12.0	13.5	15.0	16.1	16.6	16.6	16.6	16.6	0.90	16.5	0.63	16.0	0.24	15.4	0.03
HIP 54872, $CH_4$	9.8	11.4	12.7	13.9	14.9	15.4	15.5	15.4	15.4	15.4	1.00	15.1	0.83	14.2	0.24	14.5	0.01
HIP 54872, $H$ -band	10.1	11.2	10.9	12.2	12.8	14.3	15.7	16.8	17.2	17.3	0.87	17.4	0.62	17.0	0.25	16.5	0.03
HIP 57328, $CH_4$	12.1	13.9	14.9	15.4	15.6	15.5	15.6	15.7	15.6	15.6	0.95	15.4	0.76	15.1	0.36	14.1	0.09
HIP 57328, $H$ -band	-	-	-	-	14.6	16.0	17.1	17.5	17.7	17.6	0.87	17.5	0.62	17.3	0.24	17.0	0.03
HD 102647, $CH_4$	-	-	13.4	14.5	15.3	15.9	16.0	16.0	16.0	15.9	0.98	15.8	0.70	15.4	0.26	14.2	0.02
HD 102647, $H$ -band	-	-	-	-	14.5	15.2	16.5	17.5	17.9	18.3	0.86	18.5	0.61	18.4	0.26	17.2	0.04
HIP 60965, $CH_4$	11.2	12.7	14.1	14.9	15.6	15.8	15.7	15.6	15.7	15.5	0.99	15.2	0.80	14.5	0.39	13.7	0.09
HIP 60965, $H$ -band	10.5	11.1	11.1	12.1	12.4	13.7	15.4	16.4	16.7	16.8	0.92	16.8	0.72	16.5	0.34	16.0	0.08
HR 4796, $CH_4$	11.6	12.6	13.6	14.0	14.8	15.0	15.0	15.1	14.8	14.8	0.99	14.7	0.78	14.0	0.34	13.6	0.07
HR 4796, $H$ -band	8.6	9.9	12.3	13.4	15.2	15.9	16.2	16.2	16.1	15.8	0.90	15.4	0.70	14.6	0.34	15.8	0.01
HD 110058, $CH_4$	11.1	12.2	12.9	13.3	13.7	13.8	13.8	13.6	13.7	13.3	0.99	12.8	0.78	11.8	0.35	11.7	0.07
HD 110058, $H$ -band	9.0	10.0	11.4	12.7	14.0	14.6	14.5	14.4	14.4	14.2	0.88	13.9	0.66	13.5	0.31	13.1	0.06
HD 110411, $CH_4$	12.1	13.4	14.4	14.9	15.7	15.6	15.8	15.6	15.4	15.4	0.98	15.2	0.74	14.6	0.28	13.8	0.05
HD 110411, $H$ -band	-	-	-	14.0	15.7	16.6	17.4	17.7	17.6	17.5	0.87	17.4	0.63	17.1	0.26	16.7	0.04
HIP 65109, $CH_4$	10.0	11.7	13.2	14.0	14.9	14.9	14.9	15.1	15.1	14.8	0.98	14.6	0.73	14.1	0.28	13.5	0.05

Table 8—Continued

Target	0.36''	0.5''	0.75''	1''	1.5''	2''	3''	4''	5''	7''	Cov.	9''	Cov.	12''	Cov.	14.8''	Cov.
HIP 65109, <i>H</i> -band	-	-	-	-	8.0	12.9	14.7	15.4	15.8	16.1	0.92	16.3	0.72	15.8	0.35	15.4	0.08
HD 118878, <i>CH</i> <sub>4</sub>	10.8	12.4	13.2	13.6	14.4	14.3	14.5	14.5	14.4	14.2	0.99	13.5	0.81	12.6	0.39	12.4	0.09
HD 118878, <i>H</i> -band	6.8	8.6	10.8	12.4	14.3	14.9	15.2	15.1	15.2	15.2	0.85	15.0	0.59	14.7	0.26	14.9	0.03
GJ 560 A, <i>CH</i> <sub>4</sub>	10.8	12.5	13.8	14.9	15.7	15.9	15.9	15.9	15.8	15.7	0.98	15.5	0.74	14.9	0.31	14.3	0.06
HD 131835, <i>CH</i> <sub>4</sub>	11.1	12.4	13.1	13.3	13.7	13.8	13.7	13.7	13.6	13.3	1.00	12.3	0.84	11.3	0.43	11.5	0.10
HD 131835, <i>H</i> -band	8.5	9.8	12.0	13.1	14.4	14.9	15.0	14.9	15.0	14.8	1.00	14.2	1.00	13.6	0.74	13.4	0.14
HD 135454, <i>CH</i> <sub>4</sub>	11.0	12.6	13.4	13.8	14.3	14.6	14.7	14.6	14.5	14.4	0.99	13.9	0.73	12.8	0.27	13.1	0.04
HD 135454, <i>H</i> -band	-	6.0	12.1	13.2	14.8	15.5	15.7	15.9	15.8	15.5	0.89	15.1	0.65	14.6	0.28	14.3	0.05
HIP 74785, <i>CH</i> <sub>4</sub>	11.8	13.1	14.5	15.0	15.6	15.6	15.6	15.5	15.6	15.3	0.98	15.0	0.80	14.5	0.39	13.5	0.10
HIP 74785, <i>H</i> -band	8.9	10.0	11.0	11.4	12.8	14.0	15.7	16.2	16.3	16.4	0.89	16.4	0.64	16.0	0.26	15.6	0.04
HIP 74824, <i>CH</i> <sub>4</sub>	11.0	12.2	13.7	14.5	15.0	15.3	15.3	15.2	15.1	15.1	0.99	14.8	0.76	14.3	0.31	13.7	0.06
HD 136482, <i>CH</i> <sub>4</sub>	11.0	12.6	13.5	14.2	14.5	14.7	14.7	14.7	14.6	14.5	1.00	14.3	0.76	13.6	0.21	12.7	0.02
HD 136482, <i>H</i> -band	9.0	10.6	12.3	13.4	14.9	15.7	15.8	15.8	15.7	15.6	0.88	15.3	0.64	14.6	0.27	14.3	0.04
HD 138965, <i>CH</i> <sub>4</sub>	10.9	12.2	13.4	13.9	14.5	14.8	14.9	14.9	15.0	14.9	1.00	13.9	0.84	12.8	0.38	13.8	0.03
HD 138965, <i>H</i> -band	5.8	7.7	9.8	11.7	13.8	14.8	14.9	15.1	15.1	15.1	0.90	14.9	0.63	14.6	0.21	14.1	0.02
HIP 77464, <i>H</i> -band	-	-	4.4	14.1	16.0	16.5	17.1	17.1	17.2	17.1	0.89	16.9	0.63	16.4	0.25	16.3	0.04
HD 141569, <i>CH</i> <sub>4</sub>	12.5	14.0	14.7	15.2	15.5	15.6	15.5	15.3	15.4	15.1	1.00	15.0	0.90	14.5	0.57	13.9	0.18
HD 141569, <i>H</i> -band	-	10.1	11.7	13.0	14.7	15.5	15.6	15.6	15.6	15.3	0.88	14.9	0.65	14.4	0.27	14.1	0.04
HIP 78106, <i>CH</i> <sub>4</sub>	10.6	12.1	13.4	14.0	14.5	14.7	14.7	14.7	14.5	14.4	1.00	14.1	0.83	13.5	0.42	12.9	0.10
HIP 78106, <i>H</i> -band	8.0	10.0	11.5	13.0	15.0	15.9	16.9	17.1	17.2	17.1	0.87	17.0	0.62	16.7	0.24	16.6	0.03
HD 145964, <i>CH</i> <sub>4</sub>	10.9	12.3	13.2	13.7	14.4	14.7	14.6	14.7	14.6	14.5	0.99	14.0	0.77	13.0	0.31	13.0	0.06
HD 145964, <i>H</i> -band	-	-	11.3	12.4	14.2	15.1	15.5	15.5	15.3	15.1	0.93	14.7	0.73	14.1	0.35	13.8	0.08
HIP 79781, <i>H</i> -band	-	-	12.2	13.8	15.5	16.3	16.9	17.0	17.0	17.0	0.88	16.8	0.61	16.5	0.25	15.5	0.03
HIP 79797, <i>CH</i> <sub>4</sub>	11.0	12.6	13.8	14.4	14.8	14.9	15.1	15.3	15.0	14.9	0.99	14.6	0.84	13.7	0.41	13.6	0.07
HIP 79797, <i>H</i> -band	-	-	4.0	13.1	14.9	15.5	16.2	16.3	16.4	16.3	0.85	16.1	0.61	15.6	0.29	14.8	0.05
HIP 79881, <i>CH</i> <sub>4</sub>	11.0	12.4	13.7	14.4	15.1	15.3	15.5	15.6	15.4	15.5	1.00	15.2	1.00	15.0	0.22	14.3	0.02
HIP 81650, <i>CH</i> <sub>4</sub>	11.1	12.7	13.7	14.2	14.7	14.7	14.9	14.8	14.7	14.7	0.95	14.4	0.73	14.0	0.31	13.1	0.07
HIP 85038, <i>CH</i> <sub>4</sub>	10.6	12.2	13.4	14.0	14.3	14.6	14.7	14.5	14.5	14.4	0.94	14.0	0.71	13.5	0.29	13.1	0.05
HIP 85340, <i>CH</i> <sub>4</sub>	11.9	13.3	14.7	15.6	16.1	16.3	16.2	16.1	16.2	16.2	0.98	16.1	0.73	15.5	0.28	14.9	0.05
HIP 85922, <i>CH</i> <sub>4</sub>	11.7	12.8	14.0	14.3	14.8	14.7	14.8	14.7	14.5	14.4	0.95	14.2	0.74	13.5	0.37	12.7	0.08
$\gamma$ Oph, <i>CH</i> <sub>4</sub>	11.3	13.0	14.3	14.8	15.3	15.5	15.5	15.5	15.4	15.3	1.00	15.1	0.79	14.5	0.29	13.9	0.04
$\gamma$ Oph, <i>H</i> -band	9.2	10.8	12.0	12.8	15.0	15.9	17.2	17.5	17.6	17.7	0.88	17.8	0.62	17.6	0.25	17.1	0.03
HD 172555, <i>CH</i> <sub>4</sub>	11.1	12.9	14.2	14.9	15.3	15.3	15.4	15.3	15.4	15.2	1.00	14.8	0.85	14.4	0.34	12.5	0.03
HD 172555, <i>H</i> -band	-	-	-	1.4	14.2	15.6	16.9	17.3	17.5	17.6	0.87	17.6	0.63	17.3	0.25	16.9	0.03
HD 176638, <i>CH</i> <sub>4</sub>	10.9	12.4	13.7	14.6	15.2	15.1	15.1	15.1	15.1	14.8	0.95	14.4	0.76	13.8	0.38	13.3	0.10

Table 8—Continued

Target	0.36''	0.5''	0.75''	1''	1.5''	2''	3''	4''	5''	7''	Cov.	9''	Cov.	12''	Cov.	14.8''	Cov.
HD 176638, <i>H</i> -band	-	-	-	13.1	15.0	16.3	17.1	17.4	17.5	17.5	0.85	17.4	0.60	17.3	0.25	17.2	0.03
HIP 93805, <i>CH</i> <sub>4</sub>	10.9	12.3	13.7	14.6	15.0	15.1	15.0	15.0	14.9	14.7	0.95	14.5	0.72	14.0	0.31	13.1	0.06
HR 7329, <i>CH</i> <sub>4</sub>	10.6	11.8	12.9	13.6	14.4	14.6	14.8	14.6	14.7	14.5	0.98	14.3	0.76	13.7	0.32	13.1	0.06
HR 7329, <i>H</i> -band	-	-	-	1.4	14.4	15.5	16.6	16.7	16.8	16.9	0.88	16.7	0.63	16.0	0.26	15.7	0.04
HD 182681, <i>H</i> -band	-	-	11.0	12.8	14.7	15.8	16.4	16.4	16.4	16.4	0.88	16.3	0.60	16.0	0.23	15.6	0.02
HIP 98495, <i>CH</i> <sub>4</sub>	8.8	10.6	12.4	13.0	13.5	13.5	13.4	13.4	13.3	13.2	0.94	13.0	0.68	12.7	0.26	11.9	0.04
HD 196544, <i>CH</i> <sub>4</sub>	10.1	12.2	13.5	14.6	15.2	15.5	15.5	15.5	15.6	15.6	0.98	15.4	0.72	14.8	0.27	14.6	0.04
HD 196544, <i>H</i> -band	-	-	4.2	14.0	15.4	16.3	17.3	17.5	17.4	17.4	0.87	17.1	0.63	16.5	0.28	15.8	0.05
HIP 104308, <i>H</i> -band	-	-	12.5	14.1	15.5	16.0	16.4	16.3	16.3	16.2	0.88	15.8	0.66	14.3	0.33	14.5	0.07
HIP 107556, <i>H</i> -band	-	-	-	-	9.3	15.0	16.5	17.3	17.8	17.9	0.90	17.8	0.66	17.5	0.30	16.6	0.06
HIP 110935, <i>H</i> -band	-	-	12.3	13.6	15.4	16.1	16.8	16.8	16.8	16.8	0.87	16.6	0.65	16.3	0.33	15.7	0.07
Fomalhaut, <i>CH</i> <sub>4</sub>	-	6.5	12.9	13.9	15.4	16.1	16.7	16.6	16.7	16.4	1.00	16.1	1.00	15.3	0.50	14.4	0.08
Fomalhaut, <i>H</i> -band	-	-	-	-	-	-	18.9	19.8	20.6	21.3	0.87	21.7	0.61	21.5	0.27	20.1	0.04
HIP 118121, <i>H</i> -band	-	-	-	12.4	14.3	15.5	16.4	16.4	16.5	16.4	0.88	16.2	0.62	15.7	0.27	14.8	0.04
Median, <i>H</i> -band	8.9	10.0	11.5	13.0	14.6	15.5	16.5	16.8	16.8	16.8	0.88	16.6	0.63	16.2	0.27	15.7	0.04
Median, <i>CH</i> <sub>4</sub>	11.0	12.5	13.6	14.3	14.8	14.9	15.0	15.0	14.9	14.8	0.99	14.4	0.76	13.7	0.32	13.1	0.06

Note. — Contrasts achieved in the *CH*<sub>4</sub>*S* and *H*-bands. For separations less than 1.5'', the *CH*<sub>4</sub> filter contrasts (obtained in ASDI mode) are usually better. For larger separations, the *H*-band contrasts (obtained in ADI mode) are usually better. Beyond 6.3'' each final image has data only at a fraction of the 360° range in position angle. This angular coverage fraction (ranging from 0 to 1) is given beside the contrast at these large separations. All the contrasts are 95% completeness contrasts, except at separations beyond 6.3'' where the nominal 5σ contrast curve is used. A constant is added to the 5σ curve so that both curves match at 6.3''.

Table 9. Stellar and Brown Dwarf Binaries to Sample Stars

Star	Projected Separation (AU)	Sp. Type	Reference	Allowable Planetary $a$ (AU)
HD 1160	81, 530	$\sim$ L0, M3.5	Nielsen et al. (2012)	$<20, >2700$
HIP 36188	1.2 <sup>1</sup>	$\sim$ A3	Jarad et al. (1989)	$>6$
HIP 49669	3900, 4200, 4800	K2, M5, M5	Dommanget & Nys (2002)	$<780$
HD 102647	720, 1100, 2600	$\sim$ M, $\sim$ M, G2	Dommanget & Nys (2002)	$<140$
HIP 60965	630	K0	Dommanget & Nys (2002)	$<130, >3200$
HR 4796 A	560, 14000	M2, M4.5	Jura et al. (1995), Kastner et al. (2008)	$<110$
GJ 560 A	260	K5	Dommanget & Nys (2002)	$<52, >1300$
HD 141569	880, 1000	M2, M4	Weinberger et al. (2000)	$<180$
HIP 78106	490	A3	Dommanget & Nys (2002)	$<99, >2500$
HIP 79797	350, 350	$\sim$ M9, $\sim$ M9	Huélamo et al. (2010), this work	$<70, >1800$
HIP 85038	580	G8	Dommanget & Nys (2002)	$<120, >2900$
HD 172555	2000	K5	Feigelson et al. (2006)	$<410$
HR 7329	200, 20000	M7-8, F6	Neuhäuser et al. (2011)	$<40, 1000 < a < 4000$
Fomalhaut	57400	K4	Mamajek (2012)	$<11000$

<sup>1</sup>Semi-major axis

Table 10. Upper Limits on Planet Fraction (95% Confidence Level)

Mass ( $M_{Jup}$ )	Planet Fraction			
	$\leq 5\%$	$\leq 10\%$	$\leq 20\%$	$\leq 50\%$
1	...	...	...	...
2	...	...	...	50 – 490 AU
4	...	...	59 – 460 AU	25 – 940 AU
10	...	38 – 650 AU	24 – 1100 AU	15 – 1800 AU

Note. — This table gives the range in semi-major axis at which a given upper limit on planet fraction is reached for a given planet mass. For example, between semi-major axis of 38 and 650 AU fewer than 10% of B and A stars can have giant planets more massive than 10  $M_{Jup}$ .